

August 2014

# Development of Novel Methods for Characterization of Complex Organic Mixtures By Liquid Chromatography and Raman Spectroscopy

Veronica Maria Marco Alvarez  
*University of Wisconsin-Milwaukee*

Follow this and additional works at: <https://dc.uwm.edu/etd>

 Part of the [Chemistry Commons](#)

---

## Recommended Citation

Marco Alvarez, Veronica Maria, "Development of Novel Methods for Characterization of Complex Organic Mixtures By Liquid Chromatography and Raman Spectroscopy" (2014). *Theses and Dissertations*. 552.  
<https://dc.uwm.edu/etd/552>

This Thesis is brought to you for free and open access by UWM Digital Commons. It has been accepted for inclusion in Theses and Dissertations by an authorized administrator of UWM Digital Commons. For more information, please contact [open-access@uwm.edu](mailto:open-access@uwm.edu).

DEVELOPMENT OF NOVEL METHODS FOR CHARACTERIZATION OF COMPLEX  
ORGANIC MIXTURES BY LIQUID CHROMATOGRAPHY AND  
RAMAN SPECTROSCOPY

by

Veronica Marco Alvarez

A Thesis Submitted in  
Partial Fulfillment of the  
Requirements for the Degree of

Master of Science  
in Chemistry

at

The University of Wisconsin-Milwaukee

August 2014

**ABSTRACT**  
**DEVELOPMENT OF NOVEL METHODS FOR CHARACTERIZATION OF COMPLEX  
ORGANIC MIXTURES BY LIQUID CHROMATOGRAPHY AND  
RAMAN SPECTROSCOPY**

by

Veronica Marco Alvarez

The University of Wisconsin-Milwaukee, 2014  
Under the Supervision of Professor Joseph H. Aldstadt III

The development of methods for the study of Humic Acids (HAs) and related substances is described. In the first part, a reversed-phase liquid chromatography (RP-LC) instrument was designed, fabricated, and a method for the separation of HAs was optimized for application as the second dimension in a two-dimensional LC (LCxLC) system. The optimized method for the RP-LC was used in the study of amino acid mixtures and HA standard solutions. The RP-LC used a monolithic disk in which the stationary phase was composed of butyl (C4) functional groups. The method had the following conditions: 100  $\mu$ L injection volume, 1.0 mL/min flow rate, 30:70 acetonitrile:water (pH = 7.00) mobile phase, and fluorescence detection ( $\lambda_{ex}$  = 257 nm,  $\lambda_{em}$  = 310 nm). Several HA fractions from solid-phase extraction separations were examined as a means to simplify the HA standard and their spectra were compared to the characteristic peaks found for HAs in the literature. The next step in this work is to integrate the RP-LC method into the LCxLC system.

In the second part of this thesis, the characterization of two natural varnishes — Linseed Oil and Chinawood Oil— was studied by accelerated ageing experiments and Fourier Transform Raman Spectroscopy (FT Raman). An ageing chamber designed in our group for a previous investigation was modified to perform the ageing experiments. Two factors were studied over a range of time periods: heat and ultraviolet light. Thermal studies were conducted from 25°C to 210°C while the time periods ranged from 2 to 170 hr.

A direct correlation was found between the changes in the vibrational bands that were observed in the FT Raman spectra and the observation of overt physical changes in the samples. Based upon these data, several reaction mechanisms for the decomposition of the varnishes were proposed. The FT Raman method may also be applied in the future to fractions collected from the LCxLC system for a more detailed off-line characterization of the molecular structures that are present.

©Copyright by Veronica Marco Alvarez, 2014  
All Rights Reserved

A mi Madre

## TABLE OF CONTENTS

CHAPTER 1. INTRODUCTION .....	1
1.1 Analysis of Coating Oils by Raman Spectroscopy.....	2
1.1.1 Background.....	2
1.1.2 Ageing of Varnishes.....	3
1.1.3 Analysis of Varnishes.....	5
1.1.4 Research Approach .....	10
1.2 Analysis of Humic Acids by Liquid Chromatography .....	10
1.2.1 Introduction to Humic Acids .....	10
1.2.2 Analysis of HS .....	12
1.2.3 Research Goals .....	17
1.3 Figures and Tables .....	18
1.4 References .....	28
CHAPTER 2. EXPERIMENTAL.....	34
2.1 Analysis of Coating Oils by Raman Spectroscopy.....	34
2.1.1 Chemical Reagents.....	34
2.1.2 Instrumentation.....	34
2.2 Analysis of Humic Acids by Liquid Chromatography .....	36
2.2.1 Chemicals Reagents.....	36
2.2.2 Buffers and Mobile Phases .....	36
2.2.3 Sample Preparation.....	37
2.2.4 Instrumentation.....	38
2.3 Figures and Tables .....	40
2.4 References .....	50
CHAPTER 3. RESULTS AND DISCUSSIONS. ....	51
3.1 Analysis of Coating Oils by Raman Spectroscopy.....	51
3.1.1 Raman Spectroscopy — An Overview of the Theory & Practice .....	51
3.1.2 Method Optimization.....	52
3.1.3 Design and Application of the Ageing Chamber .....	53
3.1.4 Characterization of Chinawood Oil and Linseed Oil .....	55
3.2 Analysis of Humic Acids by Liquid Chromatography .....	64

3.2.1 Two-Dimensional Liquid Chromatography — An Overview of the Theory & Practice.....	64
3.2.2 Fluorescence Spectroscopy — An Overview of the Theory & Practice .....	67
3.2.3 Separation of Complex Organic Mixtures .....	69
3.3 Figures and Tables .....	78
3.4 References .....	149
CHAPTER 4. CONCLUSIONS.....	154



## LIST OF FIGURES

### CHAPTER 1.

Figure 1-1. Jablonski diagram presenting Rayleigh and Raman Scattering.....	18
Figure 1-2. Polarization of a molecular bond.....	19
Figure 1-3. Schematic diagram of environmental chamber that was used for the accelerated ageing experiment.....	20
Figure 1-4. Scheme for the isolation of HS from soils.....	21
Figure 1-5. Model structure of FA.....	22
Figure 1-6. Model structure of HA.....	23

### CHAPTER 2.

Figure 2-1. Schematic diagram of the Nexus 670 FT-Raman .....	40
Figure 2-2. Schematic diagram of environmental chamber that was used for the accelerated ageing experiment.....	41
Figure 2-3. Photograph of the ageing chamber.....	42
Figure 2-4. Schematic diagram of a TCD .....	43
Figure 2-5. SPE extraction general procedure.....	44
Figure 2-6. A) Schematic diagram of the liquid chromatography system. B) Detail of the two- position valve .....	45

Figure 2-7. A) Schematic diagram of the fluorescence detector. B) Detail of the flow cell .....	46
Figure 2-8. A) Schematic diagram of the UV detector. B) Detail of the flow cell .....	47
Figure 2-9. Photograph of the RP-LC system .....	48
Figure 2-10. Schematic diagram of the Horiba FluoroLog®-3 Spectrofluorometer Model FL3-22 .....	49
CHAPTER 3.	
Figure 3-1. Spectroscopic transitions underlying several types of vibrational spectroscopy .....	78
Figure 3-2. Raman spectrum of chloroform at room temperature obtained with a 514.5 nm source .....	79
Figure 3-3. Schematic diagram of the Nexus 670 FT-Raman .....	80
Figure 3-4. Raman spectra of a solid sulfur sample .....	82
Figure 3-5. Raman spectra of a single sample of Chinawood Oil measured at different laser powers. Tests 1-4, 2 hr aged, T=100°C. ....	83
Figure 3-6. Variation of the Raman intensity of the major peak in the spectrum (~3000 cm <sup>-1</sup> ) using different laser power. Error bars (n=3) are shown at 95% confidence (two-tailed) based upon the Student t value.....	84
Figure 3-7. Schematic diagram of environmental chamber that was used for the accelerated ageing experiment.....	85
Figure 3-8. Structure of glycerol, general structure of a fatty acid, and general structure of a triglyceride .....	86

Figure 3-9. An example of the possible triglyceride structure that are present in Linseed Oil; chemical structure of the major fatty acid components that form this triglyceride.....	88
Figure 3-10. An example of the possible triglyceride structure of Chinawood Oil; chemical structures of the major fatty acid components that form this triglyceride .....	89
Figure 3-11. Formation of hydroperoxides and cross-linking reaction for a drying oil with non-conjugated double bonds.....	90
Figure 3-12. Photographs of slides with Linseed Oil and Chinawood Oil in which can be appreciated the different textures of the oils before and after the ageing process .....	91
Figure 3-13. Color development for samples of Linseed Oil aged with (a) UV light (centered at 254 nm, 15 W) and (b) Heat (90 to 210°C).....	92
Figure 3-14. FT-Raman spectrum of pristine Linseed Oil after drying .....	93
Figure 3-15. FT-Raman spectra of pristine and artificially aged samples of Linseed Oil .....	94
Figure 3-16. FT-Raman spectra of pristine and artificially aged samples of Linseed Oil. Detail of the Raman shift at 3010 $\text{cm}^{-1}$ .....	95
Figure 3-17. FT-Raman spectra of pristine and artificially aged samples of Linseed Oil. Raman shifts are noted at 1265 and 1655 $\text{cm}^{-1}$ .....	96
Figure 3-18. Photographs of: (a) NMR tubes sealed with glass, and (b) sealed NMR tubes in closed vials with the aged samples.....	97
Figure 3-19. Chromatograms obtained by GC-TCD. Data were corrected with a blank and smoothed by ensemble averaging with a 51 point "boxcar" .....	98
Figure 3-20. FT-Raman spectra of pristine Linseed Oil, Linoleic Acid and Oleic Acid after treatment at 50°C in the Ageing Chamber.....	99
Figure 3-21. FT-Raman spectra comparison of pristine Linseed Oil and Oleic Acid .....	100

Figure 3-22. FT-Raman spectra comparison of pristine Linseed Oil and Linoleic Acid .....	101
Figure 3-23. FT-Raman spectra comparison of pristine Linseed Oil and the sample aged for 100 hr at 50°C .....	103
Figure 3-24. Raman spectra comparison of Linseed Oil samples aged the same time at different temperatures.....	104
Figure 3-25. FT-Raman spectra of pristine and artificially aged samples of Linseed Oil. UV-light aged samples .....	105
Figure 3-26. FT-Raman spectra comparison of pristine Linseed Oil sample and the 170 hr, UV-light aged samples .....	106
Figure 3-27. Schematic diagram of the chromatographic separation in a RP column.....	107
Figure 3-28. Schematic diagram and microscopic detail of the structure of a monolith column. Composition and working conditions of the CIM® RP-SDVB DISK monolith column .....	109
Figure 3-29. A) Diagram of Singlet and Triplet excited states. B) Jablonski diagram .....	110
Figure 3-30. Chemical structures and characteristic absorbance and emission spectra of TRP, TYR and PHE .....	111
Figure 3-31. PHE, TRP, and TYR emission spectra obtained with $\lambda_{ex}= 257$ nm (1 mM aqueous solutions, pH = 7.00).....	113
Figure 3-32. PHE, TRP, and TYR emission spectra obtained with $\lambda_{ex}= 274$ nm (1 mM aqueous solutions, pH = 7.00).....	114
Figure 3-33. PHE, TRP, and TYR emission spectra obtained with $\lambda_{ex}= 280$ nm (1 mM aqueous solutions, pH = 7.00).....	115
Figure 3-34. Titration of a diprotic amino acid .....	117

Figure 3-35. Emission spectra of TYR at pH= 7.00 and at pH = 9.00. Forms of TYR presents at both pH values .....	121
Figure 3-36. The fluorescence of TRP varied markedly with solution pH (1 mM aqueous solutions, $\lambda_{ex}=257$ nm).....	122
Figure 3-37. Relation between intensity of fluorescence and pH for 1mM solutions of PHE, TRP, and TYR. Error bars (n=3) are shown at 95% confidence (two-tailed) based upon the Student t value .....	123
Figure 3-38. Comparison of the chromatograms obtained with amino acid mixtures in the Plackett-Burman study for two different mobile phases: 80:20 (v/v) methanol: buffer pH=4.00; and 20:80 (v/v) acetonitrile: buffer pH4.00. Injection loop = 35 $\mu$ L, flow rate = 1.0 mL/min .....	125
Figure 3-39. Comparison of the chromatograms obtained individually for PHE, TRP, and TYR (0.5 mM) with 30:70 (v/v) acetonitrile: phosphate buffer, pH=7.00. Injection loop = 35 $\mu$ L, flow rate = 1.0 mL/min. ....	126
Figure 3-40. Effect of mobile phase flow rate on retention time. Error bars (n=3) are shown at 95% confidence (two-tailed) based upon the Student t value.....	127
Figure 3-41. Effect of the mobile phase flow rate on fluorescence intensity of the solutes. . Error bars (n=3) are shown at 95% confidence (two-tailed) based upon the Student t value .....	128
Figure 3-42. Hypothetical structure of a humic acid according to Stevenson.....	129
Figure 3-43. Chromatograms of humic solutions #5 and #7 (Table VIII). $\lambda_{ex} = 350$ nm, $\lambda_{em} = 430$ nm; 30:70 (v/v) acetonitrile: phosphate buffer pH =7.00, mobile phase; 1.0 mL/min flow rate; 100 $\mu$ L injection loop.....	131
Figure 3-44. Scheme of the general procedure followed to obtain the humic acid fractions .....	132

Figure 3-45. Scheme of a displacement development.....	133
Figure 3-46. Matrix active groups present in the SPE columns.....	135
Figure 3-47. Chromatograms of humic acid fractions from LC-NH2. Fraction #1= ethylacetate, fraction #2= dimethylformamide, fraction #3 methanol. $\lambda_{ex} = 350$ nm, $\lambda_{em} = 430$ nm; acetonitrile and buffer phosphate pH=7.00 (1:2 v/v) mobile phase; 1.0 mL/min flow rate; 100 $\mu$ L injection loop.....	137
Figure 3-48. Chromatograms of humic acid fractions from ENVI-8. Fraction #1= methanol, fraction #2= dimethylformamide, fraction #3 ethylacetate. $\lambda_{ex} = 350$ nm, $\lambda_{em} = 430$ nm; acetonitrile and buffer phosphate pH=7.00 (1:2 v/v) mobile phase; 1.0 mL/min flow rate; 100 $\mu$ L injection loop.....	138
Figure 3-49. Spectrum of four humic acid dilutions from HA (1.3 mg/mL in acetonitrile and buffer phosphate pH=7 (30:70 v/v)). $\lambda_{ex} = 350$ nm.....	139
Figure 3-50. Variation of the fluorescence intensity with excitation wavelength for the HA solution of concentration 0.13 mg/mL.....	140
Figure 3-51. Spectrum of HA fractions #1, #2 and #3 from LC-Si (Normal phase, diethyl ether) .....	141
Figure 3-52. Spectrum of HA fractions #1, #2 and #3 from LC-NH2 (Normal phase, Diethyl ether) .....	142
Figure 3-53. Spectrum of HA fractions #1, #2 and #3 from ENVI-8 (pH=9) .....	143
Figure 3-54. Spectrum of HA fractions #1, #2 and #3 from DSC-18 (pH=7).....	144
Figure 3-55. Spectrum of HA fractions #1, #2 and #3 from LC-WCX (pH=7) .....	145
Figure 3-56. Spectrum of HA fractions #1, #2 and #3 from LC-SCX (pH=7).....	146
Figure 3-57. Spectrum of HA fractions #1, #2 and #3 from LC-NH2 (II) (pH=7) .....	147

## LIST OF TABLES

### CHAPTER 1.

Table I. Abundances of principal functional groups in HA (in meq/g) .....	24
Table II. Carbon, hydrogen, nitrogen and oxygen average composition in HAs (in % w/w) .....	25
Table III. Comparison of relative figures of merit for the mentioned techniques .....	26
Table IV. Comparative values for peak capacities in one dimensional system calculated with Equation 1.....	27

### CHAPTER 3.

Table I. Experimental conditions for the Raman spectrometer .....	81
Table II. Percentage fatty acid composition of Linseed Oil and Chinawood Oil .....	87
Table III. Intensities, relative intensities and retention times of the unknown volatile compounds present in the vial's headspace for both sealed and unsealed tubes .....	102
Table IV. Stationary phase ligands that are commonly used in RP-LC .....	108
Table V. Basic matrix for a seven factor Plackett-Burman design .....	112
Table VI. Absorption and emission wavelengths determined experimentally with the FluoroLog-3 Spectrofluorometer and comparison with theoretical values .....	116
Table VII. Amino acid pK <sub>a</sub> values .....	118
Table VIII. Plackett -Burman design for seven factors .....	119
Table IX. Results of Plackett-Burman study .....	120
Table X. Mobile phases used in this study (% v/v) .....	124
Table XI. Humic acid stock solutions .....	130
Table XII. SPE phases used in the preparation of the humic acid samples .....	134
Table XIII. HA samples; conditioning, washing and elution solvents used in the SPE clean-up .....	136
Table XIV. Maximum emission wavelength obtained experimentally in FluoroLog®-3 Spectrofluorometer .....	148

## ACKNOWLEDGEMENTS

Studying abroad is always a challenge not only due to the changes in customs and culture but also because of the disconnection with personal relationships, which are very difficult to build in the time it takes to complete a master degree. That was my biggest concern, and it was happily dissipated within 24 hours. Milwaukee is a quiet city with friendly, courteous and respectful people, and UWM is a reflection of the city. I would like to take the time to first, acknowledge all the people that from the first day made me feel at home.

Above all, I would like to thank my advisor, Dr. Joseph H. Aldstadt III, without whom I would not be here today. His help and guidance, and his willingness to give his time so generously have been very much appreciated.

I would like to offer my special thanks to the other members of my graduate committee, Dr. Mark Dietz and Dr. Tim Grundl. They were also a fount of knowledge throughout this process, I truly enjoyed their lectures and I sincerely thank their valuable and constructive suggestions.

I would like to express my deep gratitude to all the members of my group, from past and present: Ryan Schmeling, Dr. Lisa Kendhammer, April Grant, Marie Nider, Anahit Campbell, Janette Mamedova, Zarko Godic and Kelsey Holbert. I would also like to extend my thanks to Neal Korfhage for his amazing glassblowing work with the ageing chamber and the Raman tubes.

On a personal note, I would like to acknowledge friends and family who supported me during my time here. First and foremost I would like to thank my mother Zelmira and my parents-in-law, Sonia and Juan, for their constant love and support; and also thanks to the



rest of my dear family who were close to me every day: Alvaro, Luna, Ana Ines, Gabriel, Maria Eugenia, Juan y Enrique.

I am also lucky to have met such a varied group of friends from different parts of the globe here in Milwaukee. I would like to thank to all of them. Especially, I would like to thank Sandra Simon, I could not finish my work without her support and sincerely friendship.

I would like to thank all my priceless friends in Uruguay.

Finally, I would like to thank my husband German, my motivation to start, succeed and finish.

*“The most exciting phrase to hear in science,  
the one that heralds new discoveries,  
is not “Eureka!” but “That’s funny...”*

Isaac Asimov

## CHAPTER 1. INTRODUCTION

People are exposed to a tremendous variety of complex mixtures in their everyday lives. This exposure can range from the benign to the insidious, such as from the mixture of sucrose, flavors, and aroma precursors, the alkaloid trigonelline, and the many organic acids that are present in roasted coffee, to fruits contaminated with various pesticide residues, to the thousands of compounds that may be present in the air.<sup>1</sup>

Complex mixtures occur naturally such as oils, organic acids and atmospheric organic aerosols; or those created artificially, such as biopolymers, pharmaceutical products and agrochemicals. Moreover, complex mixtures can be either collections of dissimilar chemicals, like factory smoke, or collections of a family of particular compounds, like polychlorinated biphenyls (PCBs).<sup>2</sup> Yet another added layer of complexity is that these complex mixtures can become even more complex because of reactions that occur among the components of a given mixture, this creates new compounds that can react further with the environment as a result of processes such as hydrolysis, photolysis, and biodegradation. Although there is a limit on the ability of current techniques to address this task, it has sparked innovative scientific and technical research to face this challenge.

In the work presented herein, two different methods for analyzing and characterizing natural organic complex mixtures are described. The mixtures under examination are Humic Acids (HAs) and varnishes. Methods for characterizing these two sample types based upon the techniques of Liquid Chromatography and Raman Spectroscopy, respectively, were investigated in this research.

## 1.1 Analysis of Coating Oils by Raman Spectroscopy

### 1.1.1 Background

Paintings can be classified based upon the types of materials used, primarily the pigments, binding media, and varnishes.<sup>3</sup> On the one hand, the binding media in which the pigment is dissolved or suspended can be used to identify different types of paintings. Different media — such as water, oil, wax, or synthetic polymers — determine characteristics such as viscosity, drying time, and texture of the painting. On the other hand, the type of pigments used by the artist can be used to define a particular painting, classified according to their origin in vegetable, animal, mineral, or synthetic sources.<sup>4</sup> Another important part of a painting is the varnish. The surface of the painting is varnished primarily for protection but also for several other important functions. Varnishes are responsible for the pigment tone change (usually pigment darkening feature) and for the creation of image depth and perspective, more saturated colors, and gloss.<sup>5-7</sup> Not all artists use varnishes; in fact, there have been some movements in art history, such as the Impressionists, that preferred not to use them at all.<sup>5</sup> The types of varnishes used over the last few centuries have ranged from the very early use of egg whites as a surface coating, to recipes for natural oil varnishes<sup>7</sup> and resins that are soluble in turpentine.<sup>4</sup> Nowadays, painters also are using synthetic resins, which are more versatile and have better long-term stability.<sup>4,6</sup> Some examples of substances utilized as varnishes include: Linseed Oil, Poppy Seed Oil, Pine Oil, Chinawood Oil, Mastic resin (in Turpentine), Dammar resin (in Turpentine), and synthetic resins of high and low molecular weight (*e.g.*, Pentaerythritol ester; Acryloid B72).<sup>5,7,8</sup>

### 1.1.2 Ageing of Varnishes

When paintings, furniture, sculptures and other artistic objects are exhibited and stored, they are exposed, to a greater or lesser extent, to the effects of various environmental agents that can modify one or more of their components.<sup>9</sup> The deterioration of an artistic object is proportional to the concentration of these agents and to the exposure time.<sup>9</sup> It is for these reasons that in storage and exposition places like museums and art galleries, efforts are focused on minimizing these effects including prohibiting the use of flash cameras, avoiding intense lighting (including exposure to sunlight), avoiding extreme temperature and humidity levels<sup>10</sup>, and minimizing exposure to deleterious atmospheric substances by the use of sophisticated ambient air filtration systems,<sup>11-13</sup> In some of these places, there are other more elaborate protection methods such as glass display boxes or picture frames with controlled atmospheres and UV protection as well.

In general, the most evident change with ageing is the darkening of the artistic object.<sup>9</sup> The varnish and constituent pigments typically degrade and react with the binder (in which they are dissolved).<sup>4</sup> For a painting (as an example of an artistic object), the object as a whole responds differently to climatic changes in the environment, causing discolorations, peelings, and more delicate areas to crack under stress (a process called "crazing").

The most common restoration method that is used in art conservation is the application of a swab soaked in an organic solvent in which the varnish is soluble to remove the varnish and then put on a new varnish layer. This method must be used cautiously because it could potentially affect the color layer that rests below the varnish.<sup>14</sup> Furthermore, given the wide range of mixtures of substances used as varnishes in the past, studies must be performed to find a suitable extraction solvent for every particular case.<sup>14, 15</sup>

There are other more-modern restoration methods that do not use solvents. For instance, high-resolution cameras can be used to provide a complete digital record of the piece in great detail (sub-millimeter resolution) and with these detailed images, laser ablation can then be used to remove the deteriorated varnish, then the painting can be corrected if there is any pigment discoloration because of the laser application.<sup>4</sup> Finally, another restoration approach that is used is the application of a solution containing an enzyme (*e.g.*, lipase) to catalytically remove the aged varnish.<sup>16</sup>

After the varnish is removed, the painting conservator will add a new varnish layer. Unfortunately, for the majority of artistic objects (especially the older ones), varnish-composition records are rarely available.<sup>8</sup> Facing this issue, some conservators have opted to add a modern synthetic varnish which is completely distinct from the original varnish that had been used. In this case, the solubility of the varnish in a given organic solvent is known, so that in its subsequent restoration it can be easily removed with negligible effects to the original painting.<sup>5</sup> To preserve masterpieces, some conservators will even apply a varnish layer to objects that originally did not include one. This procedure has generated controversy and firm protests from artists such as Picasso, for instance.<sup>17</sup> Because the varnish not only provides protection of the object but also affects its appearance, color, and conveys the artist's message, restoration by using a varnish which is identical to the original is the goal of art conservators. Thus the task of finding the perfect restoration material is far from trivial. To respect the artist's vision, ideally one should try to determine the original composition of the varnish. If this is not possible, one should work with varnishes that are soluble in other solvents but with properties such as refractive index and layer thickness, similar to the original one.<sup>5,6</sup>

### 1.1.3 Analysis of Varnishes

Over the past decade, analytical chemistry has become more commonly applied in art conservation laboratories to help conservators address the challenges of various restoration efforts. The problem facing scientists in the field of art conservation is that they do not have the original sample to analyze and reference materials are unavailable. To figure out the original composition of the sample, scientists have to begin with an aged sample and work backwards. The question they face is not "What *is* it?" but rather "What *was* it?" Furthermore, in paintings dating 100 years or more, it is generally impossible to identify the specific environmental agents to which the artistic object was exposed, let alone the times of exposure. Also, in the majority of instances there are few if any records of previous restoration efforts, so the restoration scientist is confronted with the problem that the layer of original varnish may be buried beneath multiple layers of unknown restored varnishes.

Restoration scientists have increasingly focused on employing modern chemical analysis tools to try to better understand the chemistry of varnishes. The primarily qualitative goal is to elucidate the molecular structures that arise during the ageing of a varnish. One promising approach is to "artificially age" the varnish by subjecting varnish samples to varying degrees of accelerated treatments. These experiments are based upon the variation of key factors that affect ageing, including: temperature, humidity, light exposure, and atmospheric composition.<sup>9</sup>

Nowadays, in the production of coating materials for the art world as well as other applications, detailed studies are performed to determine all the factors that could potentially affect the stability of the material under different conditions.<sup>9</sup> Depending on the environmental requirements, the coating design varies.<sup>9</sup> One of the most important tests is

the accelerated ageing test in which the materials are exposed to different agents to cause artificial ageing. This gives manufacturers a better idea about the lifetime and overall stability of the product during use.<sup>9, 18</sup> For modern synthetic varnishes, abundant information exists in this regard.<sup>18</sup> Several standard test methods have been developed by the International Organization for Standardization (ISO) and the American Society for Testing & Materials (ASTM) for modern varnishes that allow for the accelerated testing of polymers.<sup>18</sup> Examples of the ISO and ASTM testing procedures include thermal stability test, liquid absorption test, environmental stress cracking (ESC), weathering test methods and chemical resistance tests.<sup>18</sup>

The chemical characterization of varnishes has been studied by several authors using mainly non-destructive techniques. Mignani *et al.* worked with optical fibers sensors to monitor temperature effects on the refractive index of the varnish.<sup>19</sup> Optical Coherence Tomography (OCT) is another non-destructive technique that allows three-dimensional imaging with a micrometer-scale resolution and has been used to measure the thickness of varnish layers, the number of layers and the presence of filler particles in varnishes from different surfaces (*e.g.*, musical instruments and paintings).<sup>20, 21</sup> Gas Chromatography – Mass Spectrometry (GC/MS) has been reported in the literature the characterization of lipids, waxes, resins, proteins, and polymers.<sup>22, 23</sup> Sample collection in this case is the most important disadvantage of the technique because the sample requires a previous derivatization (sample have to be volatile). A more direct approach to study varnishes has been the application of UV-fluorescence spectroscopy because it provides information about the homogeneity of the varnish layers.<sup>24</sup> UV flash lamps coupled to CCD cameras can be used to obtain color images of the fluorescence in a painting<sup>24</sup>; and Fluorescence Lifetime Imaging (FLIM) has been used to measure differences in composition based upon the lifetimes of fluorescent emissions.<sup>25</sup> Fourier Transform Infrared Spectroscopy (FT-IR)



and micro-Raman spectroscopy are also valuable methods in characterizing organic-binding media and varnishes.<sup>4, 26-28</sup>

### **Raman Spectroscopy**

The Raman Effect was discovered by K. S. Krishnan and C. V. Raman in 1928. Raman obtained the 1931 Nobel Prize in Physics for his discovery and investigations in the field.<sup>29</sup> Until the mid 1970's, analytical applications of Raman spectroscopy were relatively uncommon because of several inherent practical difficulties, foremost of which being the difficulty in obtaining intense monochromatic light sources.<sup>30</sup> There were many instrumental factors that needed to be addressed, for instance, weak Raman intensity, fluorescence interference, inefficient light collection, and low detector sensitivity.<sup>30</sup> The introduction of Fourier Transform (FT)-Raman and near-infrared lasers in the last ~40 years have made Raman a more practical analytical technique. Additionally, with the introduction of fiber optics and miniaturization, Raman spectroscopy became one of the preferred techniques for in situ investigations in many fields, including art conservation.<sup>31-33</sup>

In an FT Raman experiment, an intense monochromatic beam of energy ( $h\nu_{\text{ex}}$ ) irradiates the sample molecule in either a ground vibrational level ( $\nu=0$ ) or an excited vibrational level ( $\nu=1$ ) of the ground electronic state. The molecule absorbs a photon of energy  $h\nu_{\text{ex}}$  and then reaches an excited so-called "virtual" electronic state (*i.e.*, not a specific electronic state) and then relaxes by emission of a photon of different energy ( $h\nu_{\text{em}}$ ). If a molecule originally in  $\nu=0$  emits a photon with energy equal to the frequency of the source ( $h\nu_{\text{ex}}$ ), the radiation is termed Rayleigh scattering; if the energy of the emitted photon is ( $h\nu_{\text{ex}} - h\nu_0$ ) it is a Raman signal called Stokes scattering. Molecules in the vibrational excited

state ( $\nu = 1$ ) can also scatter radiation with energy ( $h\nu_{\text{ex}} + h\nu_0$ ), a Raman signal that is termed anti-Stokes scattering (Figure 1).<sup>29, 30, 33, 34</sup>

### Polarizability

The scattering of light is the redirection of light that takes place when an electromagnetic wave (*e.g.*, from the source laser beam) interacts with matter (*i.e.*, molecule of sample).<sup>29, 30, 34</sup> The electric field (E) of the electromagnetic wave fluctuates with time (t) sinusoidally, and can be described with Equation 1.0<sup>29</sup>:

$$\mathbf{E} = \mathbf{E}_0 \cos(2\pi\nu t) \quad \text{Eq. 1.0}$$

where

- $E_0$  is the amplitude of the wave
- $\nu$  is the frequency of the source

The electromagnetic wave induces a polarization in the molecule (separation of charges) and this induced dipole moment change is proportional to the strength of the electric field:

$$\mathbf{m} = \alpha \mathbf{E} \quad \text{Eq. 1.1}$$

where

- $m$  is the induced dipole moment
- $\alpha$  is the polarizability constant
- $E$  is the magnitude of the electric field

Combining Equation 1.0 and 1.1 yields:

$$\mathbf{m} = \alpha \mathbf{E}_0 \cos(2\pi\nu t) \quad \text{Eq. 1.2}$$

The polarizability varies as a function of the distance between nuclei according to Equation 1.3 and as schematically depicted in Figure 2:

$$\alpha = \alpha_0 + (d\alpha/dr)r_m \cos(2\pi\nu_{\text{vib}}t) \quad \text{Eq. 1.3}$$

where

- $\alpha_0$  is the polarizability when the atoms of the molecule are in their equilibrium positions
- $r_m$  is the maximum internuclear separation

Combining Equations 1.2 and 1.3 yield:

$$\mathbf{m} = \alpha_0 \mathbf{E}_0 \cos(2\pi\nu_{\text{EXT}}t) + \mathbf{E}_0 r_m (d\alpha/dr) \cos(2\pi\nu_{\text{vib}}t) \cos(2\pi\nu_{\text{EXT}}t) \quad \text{Eq. 1.4}$$

Because:

$$\cos(x) \cdot \cos(y) = \frac{1}{2} [\cos(x+y) + \cos(x-y)]$$

Therefore:

$$\begin{aligned} \mathbf{m} = & \alpha_0 \mathbf{E}_0 \cos(2\pi\nu_{\text{EXT}}t) + \\ & \frac{1}{2} \mathbf{E}_0 r_m (d\alpha/dr) \cos[2\pi(\nu_{\text{EXT}} - \nu_{\text{vib}})t] \\ & + \frac{1}{2} \mathbf{E}_0 r_m (d\alpha/dr) \cos[2\pi(\nu_{\text{EXT}} + \nu_{\text{vib}})t] \end{aligned}$$

Eq. 1.5

The first term in the Equation 1.5 represents Rayleigh scattering and the second and third terms correspond to Raman scattering (Stokes and anti-Stokes), respectively.<sup>29</sup>

### 1.1.4 Research Approach

In a previous collaboration with the Conservation Laboratory at the Milwaukee Art Museum (MAM), an ageing chamber was designed, fabricated, and tested for artificially ageing samples in a controlled environment. The ageing chamber was directly incorporated into a GC to allow for the precise control of ageing conditions (Figure 3). In this thesis, characterization of two natural varnishes — Linseed Oil and Chinawood Oil— was studied by accelerated ageing experiments, with analysis of the aged varnishes by FT-Raman Spectroscopy.

## 1.2 Analysis of Humic Acids by Liquid Chromatography

### 1.2.1 Introduction to Humic Acids

Humus, the predominant part of natural organic matter (NOM) in soils, consist of two groups of compounds: non-humic and humic substances (HS).<sup>35</sup> Both groups derive from partially decomposed biological material and metabolic products of living organisms excreted into the environment. The chemistry of the formation of HS through various decomposition pathways is by no means fully understood, as a wide variety of mechanisms in soils and sediments are at work.<sup>36,37</sup> Up to 70–80% of NOM in surface soils is composed of HS.<sup>38</sup>

Non-humic substances are organic compounds that belong to a recognizable class in biochemistry (*e.g.*, proteins, lipids, nucleic acids, carbohydrates, etc.).<sup>36</sup> HS are colored, (ranging from yellow to black), refractory, and do not fall into a specific biochemical category. HS are ubiquitous in terrestrial and aquatic environments (and their associated sediments). They can be extracted from natural sources such as groundwater, soil, ores (*e.g.*,

lignite, leonardite), lake water, peat, sea water, etc., but despite their different sources they display a remarkable uniformity in their properties.<sup>36, 39-42</sup> There are three types of HS: Humic, Fulvic Acids (FAs), and Humic Acids (HAs). These fractions are classified according to their different solubilities as a function of pH (Figure 4). The Humic fraction is insoluble in both basic and acidic conditions. FAs are soluble at all pH values and are the most hydrophilic of these three fractions, which is why they are found in large proportions in water. FAs range from 500 to 2000 Da in size (Figure 2). HA are soluble in alkali solutions but precipitate in acidic conditions. This fraction of HS is composed of macromolecules of indeterminate and variable molecular weight, between 2,000 and 100,000 Da, and where structural determination has not yet been successful (Figure 3).<sup>36</sup>

There are many proposed structures for HS molecules, as some authors have proposed the existence of macromolecules with the presence of functional groups including hydroxyls, aldehydes, ketones, amines, acids, phenols, and quinones distributed in these structures; others present an aggregate model in which small to medium sized molecules with different functional groups are held together by hydrogen bonds.<sup>36, 38, 43-47</sup> To date, however, the structures of only a handful of HS compounds have been determined. The abundance of the principal oxygenated groups in HA are presented in Table I.<sup>36</sup> Elemental analysis of HA shows that C, H, O, and N generally are by far the predominant elements (Table II).<sup>48</sup>

HAs ubiquitousness, and the wide variety of functional groups found within their structures, allows for the HAs to react in the environment in different ways. Though the structure is sought after as a way to understand the many possible reactions that take place, the underlying goal is to eventually apply and manipulate the ecologically beneficial reactions. Examples of these reactions are, for instance, that HAs act like root growth promoter<sup>49</sup>; also favorably affect the quantity of nitrogen, phosphates, iron, and ammonia in

soils, which encourage germination in seeds<sup>50, 51</sup>, and HAs present good characteristics to being use as biodegradable plasticizers.<sup>52</sup> Oxidation-reduction (redox) reactions of HAs have an important role in the environment. Within the HA structure, some functional groups such as quinones or quinone-like moieties possess reversible redox activity. Other groups, such as sulfur species and metallo-organic species also can affect the redox properties of the system by acting as a mediator for redox reactions of pollutants. One application of HAs that has been studied extensively is the ability for the HA to complex with heavy metals such Cu, Pb, and Zn.<sup>53-56</sup>

### 1.2.2 Analysis of HS

HAs have been studied since the end of the eighteenth century and the first comprehensive study of the origin and chemical structure of HAs was realized in 1826 by Sprengel.<sup>36</sup> His major contribution was studying the acidic nature of HAs.<sup>36</sup> The “practical definition” of HAs, is attributed to Waksman in 1925 and has persisted to the present time.<sup>57</sup> Since the time of Sprengel, different techniques have been used in an attempt to separate and characterize the acids from soils and aquatic environments.

One method used for many years to separate HS is the method of varying the pH of the mixture and then centrifuging it.<sup>58</sup> However this method has been criticized because the extraction conditions are rather extreme, and are not conditions found in nature, and as such it may present an unrealistic view to the quantities found in nature.<sup>42, 59</sup> Other scientists also argue that by centrifuging the mixture molecules are created that do not exist in nature because of the forceful contact they experience and as such yield a false distribution of molecular weights.<sup>35</sup> Because of these critiques, other methods have come to

be used such as aqueous and organic extractions, reverse osmosis, size exclusion chromatography, reversed-phase liquid chromatography, and others.<sup>42, 58, 60-67</sup>

Size exclusion chromatography (SEC) is the most widely used technique to characterize humic substances. The separation of the molecules is based on size. A sample containing different size molecules is poured into a column, and the elution order is such that the bigger size molecules are eluted first and the smaller ones are retained. The apparent molecular weight distribution (AMW) can be represented by the number-averaged ( $M_n$ ), the weight-averaged ( $M_w$ ), and the polydispersity ( $p$ ). The molecular size distribution of aquatic humic substances, HAs and FAs from peat, soil, and compost were determined by several authors.<sup>68-71</sup>

The characterization of HS has been attempted by virtually every analytical technique. Molecular absorption spectroscopy has been and continues to be used to analyze natural organic matter (NOM) samples. Chin *et al.* correlated the molecular weight and the percent aromaticity of aquatic humic substances by measuring the molar absorptivity at  $\lambda = 280$  nm.<sup>70</sup> Peuravuori and Pihlaja, determined the molar absorptivity using the same wavelength than Chin *et al.* to calculate the aromaticity and the averages molecular weights of humic substances with different relations.<sup>69</sup> It was found a relation between the ratio of absorbances at 250 nm and 365 nm ( $E_2/E_3$ ) and the absorptivity at 280 nm. In addition, Swietlik and Sikorska, using the specific UV absorbance (SUVA) at  $\lambda=254$ nm, determined a quantitative measure of aromatic content per unit concentration of organic carbon.<sup>68</sup> Moreover, Johnson *et al.* determined the relationship of the molecular weight of NOM and SUVA.<sup>72</sup>

Within molecular absorption spectroscopy, Fourier Transform Infra-Red (FT-IR) was used to analyze NOM samples. For example, Gonzalez Perez *et al.* used this method to

identify the functional groups and determine their relative distribution in HA found in soils.<sup>73</sup> Prashob and Nair, and Sierra *et al.*, studied the functional group composition of sediments from a subtropical and a tropical zone respectively. Both research groups found signals corresponding to hydroxyl, methyl, methylene, carbonyl, carboxyl, phenol, alcohol, and amide groups, in different proportions according to the origin of the sample.<sup>74, 75</sup>

In addition to molecular absorption techniques, molecular emission (Fluorescence) techniques have been applied extensively in an attempt to characterize and classify HS. This method not only can be utilized to discern NOM compounds of various sources but to distinguish between the composition and functional properties of the NOM's subcomponents. Researchers like Miano and Senesi, and Peuravuori *et al.*, used synchronous excitation fluorescence to characterize soils and aquatic humic substances, respectively.<sup>76, 77</sup> Swietlik *et al.* and Chen *et al.* used fluorescence to study the relationship between molecular size, aromatic content, and the wavelength shifts in HA samples.<sup>68, 78</sup>

Nuclear magnetic resonance (NMR) spectroscopy, especially <sup>13</sup>C-NMR and <sup>1</sup>H-NMR were also used for the elucidation of HS's structure. For example, Gonzalez Perez *et al.* found the relation between the concentration of aromatic carbons and compositions of HAS in cultivated and non-cultivated soils.<sup>73</sup> Prashob *et al.* using H-NMR and C<sup>13</sup>-NMR demonstrate the plant origin of the HAs in a mud bank<sup>74</sup>; Peuravuori worked with one-dimensional <sup>13</sup>C and <sup>1</sup>H-NMR experiments to support the opinion that humic molecules are supramolecular associations of smaller molecules with similar functionalities.<sup>79</sup> Peuravuori found a base to follow the investigation of the structure of HAs and FAs with two dimensional NMR. Table III shown a comparison of relative figures of merit for the mentioned techniques.



HS are a very complex mixtures and even after various fractionation methods are applied, the complexity is usually still of a high degree. The insufficient ability of conventional chromatographic techniques to separate complex mixtures such as HS continues to be a challenge in separation science. One approach that has been successfully applied to some degree over the past decade or so is two-dimensional (2D) chromatography.<sup>80 81-86</sup>

In 2D chromatography, the sample is subjected to two different separation mechanisms.<sup>81</sup> The eluent from the first column is injected into the second column. It is essential that the two systems be as different as possible because if the selectivity of the mechanisms are different, the probability to obtain co-elution of two or more components of the sample at the end of the second column is minimized. When the separation systems are un-correlated, one refer to this separation as “orthogonal”.<sup>87</sup> Complete orthogonality is difficult to achieve, because this property not only depends on the separation mechanisms, but also on the properties and origin of the sample.<sup>81</sup> Giddings and Davis studied the statistical-overlap theory to describe the overlapping of the signals in a separation (resolution) and related that to the peak capacity.<sup>88, 89</sup> Giddings, who defined the term “peak capacity” in 1967<sup>90</sup>, found, with Davis, that to resolve the 98% of the components of a sample, the peak capacity of the separation method has to be 100 times greater than the number of components.<sup>88, 89</sup> Technically, if one analyzes a complex mixture (>300 components), with a single chromatography method it is not possible to get that peak capacity (Table IV). The most important advantage of combining two separation mechanisms is the increase of peak capacity to be able to resolve the mixture.

Peak capacity for a one-dimensional separation is the maximum number of peaks separable in a specific region of space<sup>90</sup>; but for a two-dimensional separation is equal,

theoretically, to the product of the one-dimensional peak capacities of the two-dimensions (Equations 1.6 and 1.7).<sup>91</sup>

$$n_c = 1 + [N^{(1/2)}/4] \times \ln (t_r / t_m) \quad \text{Equation 1.6}$$

$$(n_c)_{2D} = (n_c)_1 \times (n_c)_2 \quad \text{Equation 1.7}$$

Practically, this is not real, because the peak capacity depends on the orthogonality of the methods, if the orthogonality decreases the peak capacity also decreases.

For a LC-LC system one can have an off-line LC-LC or an on-line LC-LC. The off-line LC-LC is probably the most applied LC-LC approach because it is simple. Fractions from a first separation (“dimension”) are collected and injected in the second column (“second dimension”). This operation can be done in different ways, for instance collect all the samples and then inject all or a representative number in the second column. Moreover, fractions can be concentrated or modified in another way before the second dimension (*e.g.*, change the pH of the samples).

In an on-line LC-LC system the columns in the two dimensions are connected *via* an interface. One can have an on-line LC-LC in which only part of the eluent is directed to the second dimension, or an on-line LC-LC in which all the effluent from the first dimension is analyzed in the second dimension (“comprehensive”).

It is important to notice that only a few publications about the application of off-line LCxLC to the analysis of HS's are available in literature.<sup>66, 92</sup> Moreover, it is surprising to note that no investigations have been done about on-line LC-LC for the study of HS.

### 1.2.3 Research Goals

Our ultimate goal is to design, fabricate and optimize a comprehensive on-line LCxLC instrument for the separation of HA samples by interfacing columns with orthogonal selectivities in such a way that the system is capable of obtaining very high peak capacities. For the first dimension, we plan to use an ion-exchange (IC) LC method, while for the second dimension, as explored in this thesis, the development of an RP-LC method that balances the need for efficient separation against the limitation imposed in sampling the first dimension.

### 1.3 Figures and Tables.

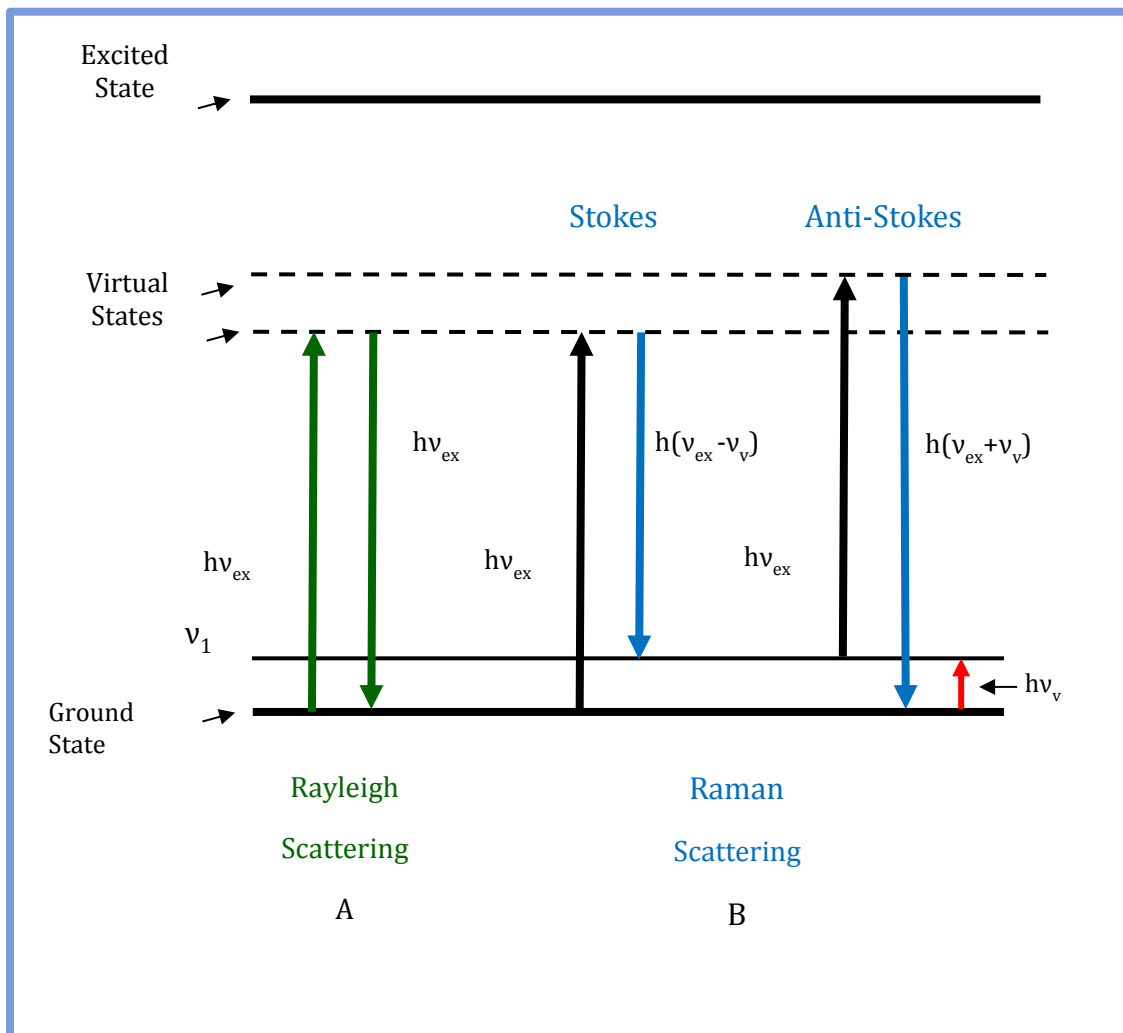
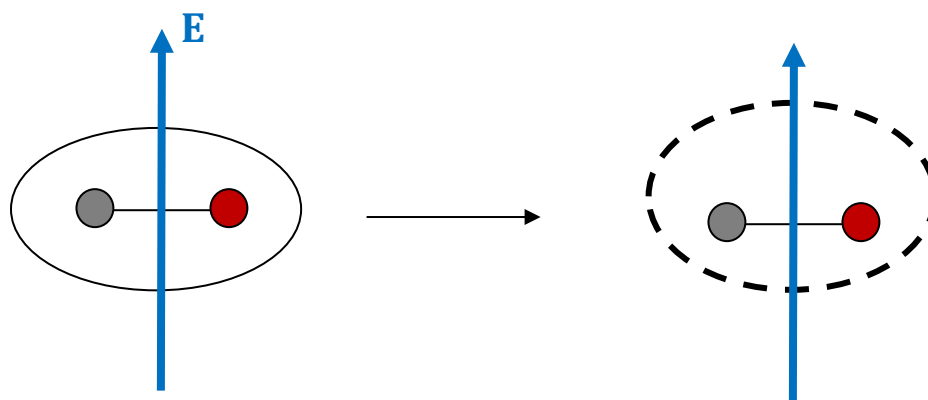
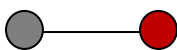


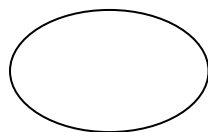
Figure 1-1. Jablonski diagram presenting Rayleigh and Raman Scattering. Adapted from Skoog et al.<sup>29</sup>



Molecule



Electronic cloud



Electric Field



(In this case E is perpendicular to the molecular bond)

**Figure 1-2.** Polarization of a molecular bond.

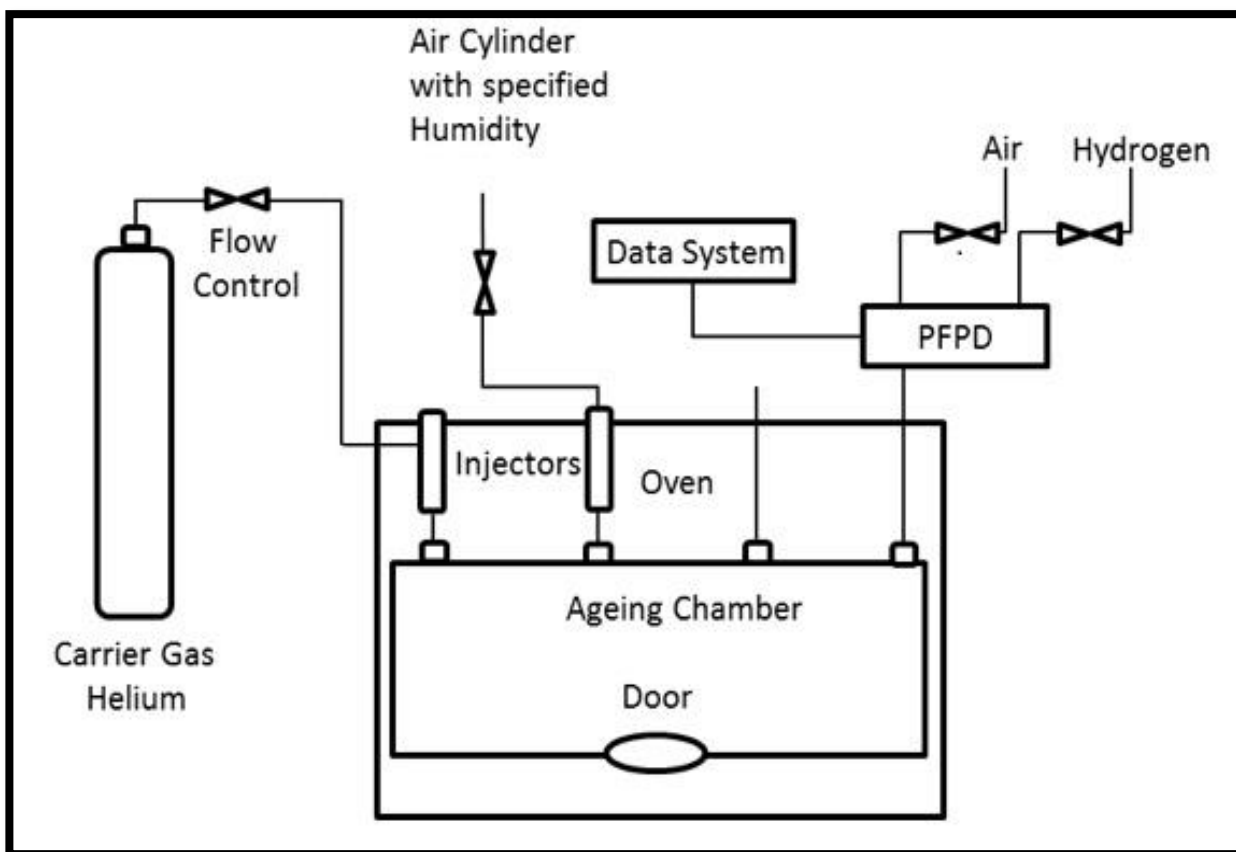


**Figure 1-3.** Schematic diagram of environmental chamber that was used for the accelerated ageing experiment.<sup>93</sup>

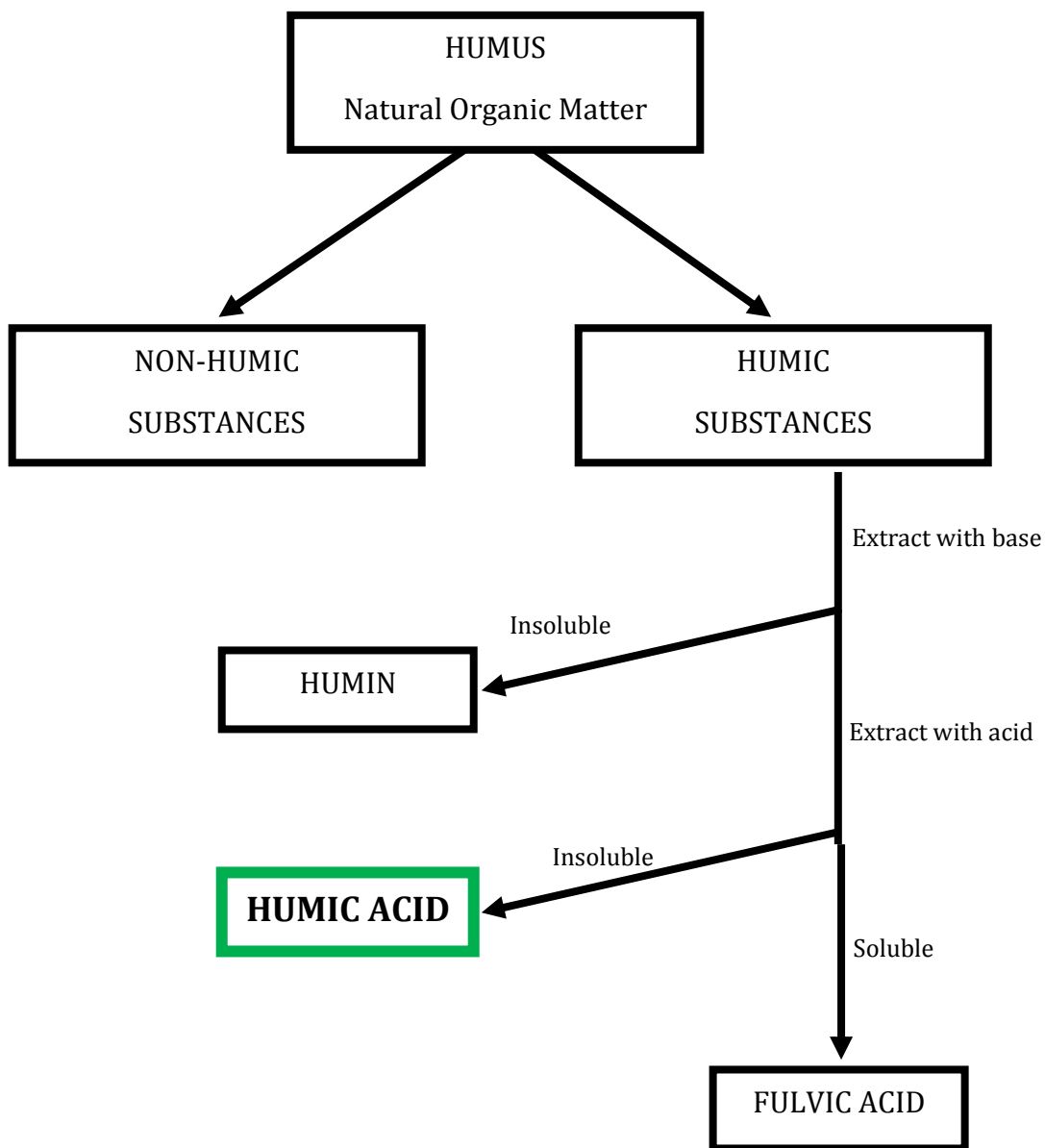


**Figure 1-4.** Scheme for the isolation of HS from soils. Adapted from Essington et al.<sup>39</sup>

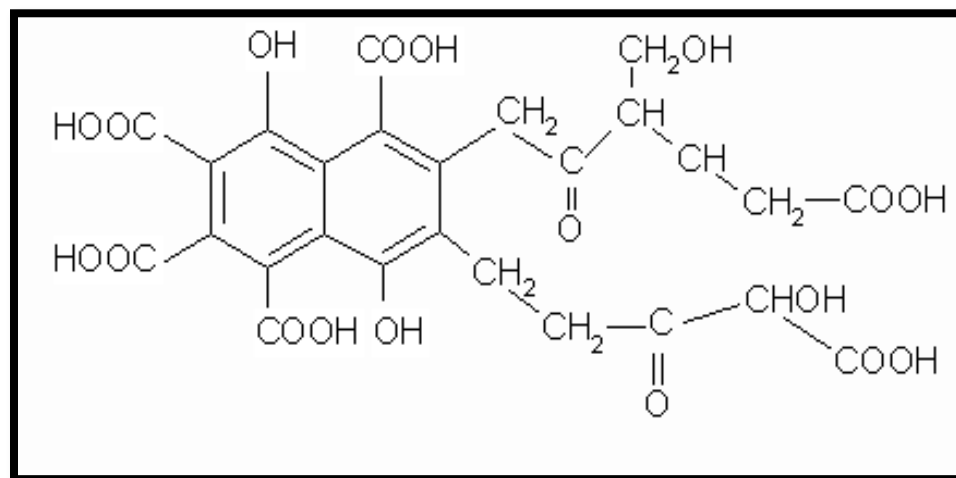


Figure 1-5. Model structure of FA.<sup>36</sup>



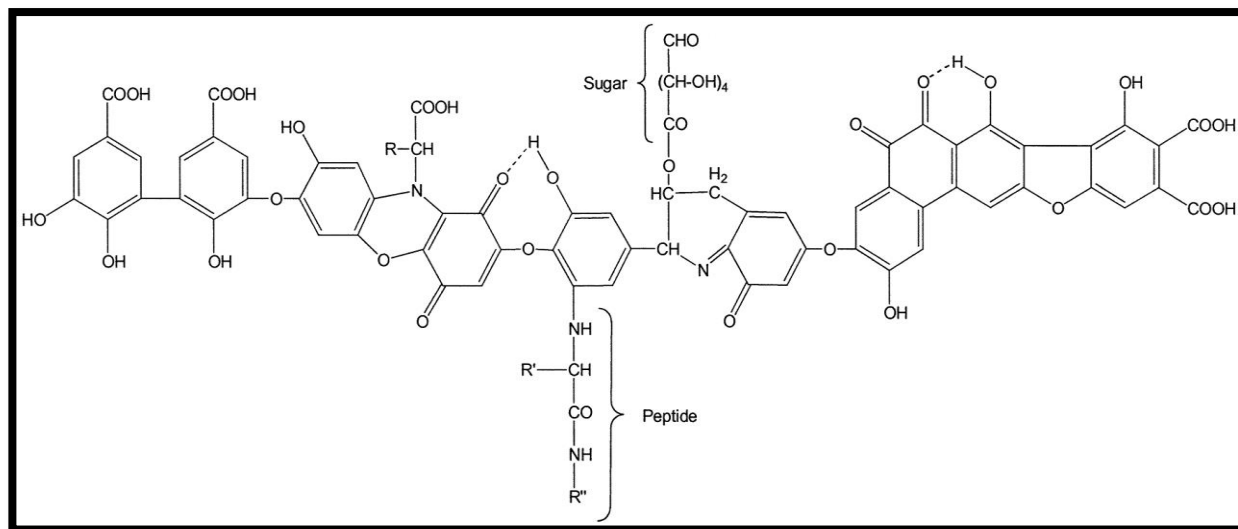


Figure 1-6. Model structure of HA.<sup>36</sup>

**Table I.** Abundances of principal functional groups in HA (in meq/g).<sup>36</sup>

Functional group	(meq/g)
Acid (-COOH-)	4.8
Methoxyl (-C-O-CH <sub>3</sub> )	0.3-0.8
Phenolic(-OH)	3.3

**Table II.** Carbon, hydrogen, nitrogen and oxygen average composition in HAs (in % w/w).<sup>48</sup>

<b>Elemental composition</b>	<b>(% ± absolute standard deviation)</b>
<b>C</b>	55.1 ±5.0
<b>H</b>	5.0 ±1.1
<b>O</b>	35.6 ±5.8
<b>N</b>	3.5 ±1.5

**Table III.** Comparison of relative figures of merit for the analytical techniques that have been used to study HAs.

	Sample	Range of concentration	RSD (%)	Ref.
UV	Water	20-30 mg/L (OC)	7%	69
	Soil & water	30-50 mg/L (OC)	N.R.	70
	Water	5 mg/L	N.R.	68
	Sediment	0.05-5 g/L	N.R.	72
IR	Soil	1 mg/100mg (KBr)	N.R.	73
	Soil	N.R.	0.5%	75
	Soil & water	N.R.	N.R.	68
	sediment	N.R.	N.R.	74
Fluorescence	water	5 mg/L	N.R.	68
	Soil	20-30 mg/L (OC)	N.R.	76
	Water & soil	20-30 mg/L (OC)	N.R.	78
	Water	20-30 mg/L (OC)	10%	77
NMR	Water	8 -40 mg/L	N.R.	74
	Soil	N.R.	6%	73
	Sediment	1 mg/mL	N.R.	75
	Soil & water	N.R.	N.R.	75
SEC & RP-LC	Water	20-30 mg/L (OC)	N.R.	69
	Soil & water	30-50 mg/L (OC)	N.R.	70
	Water	5 mg/L	10%	71
	Water	3.8-6.5 g/L	N.R.	93
	Soil	N.R.	N.R.	93
	soil	3 mg/mL	0.12-0.36%	94

\*N.R.: None reported. \*\*OC: Organic carbon.

**Table IV.** Comparative values for peak capacities in one dimension system calculated with Equation 1. Equation 2, peak capacity for a two dimensional system.<sup>90</sup>

**Table I. Comparative Peak Capacity of Gel Filtration and Other Columns for Given Numbers of Theoretical Plates**

Theoretical plates, $N$	Peak capacities, $n$		
	Gel methods	Gas chromatog.	Liquid chromatog.
100	3	11	7
400	5	21	13
1000	7	33	20
2500	11	51	31
10000	21	101	61

$$n_c = 1 + 0.2 N^{1/2} \quad \text{Equation 1}$$

$$n_{c,2D} = (1D n_c) \times (2D n_c) \quad \text{Equation 2}$$

## 1.4 References

1. Wei, F.; Furihata, K.; Hu, F.; Miyakawa, T.; Tanokura, M., Complex mixture analysis of organic compounds in green coffee bean extract by two-dimensional NMR spectroscopy. *Magn. Reson. Chem.* **2010**, *48* (11), 857-865.
2. Vouk, V. B.; Chemicals, S. G. o. M. f. t. S. E. o.; Environment, I. C. o. S. U. S. C. o. P. o. t.; Safety, I. P. o. C., *Methods for assessing the effects of mixtures of chemicals*. Published on behalf of the Scientific Committee on Problems of the Environment (SCOPE) of the International Council of Scientific Unions (ICSU), and the International Program on Chemical Safety (IPCS) of the World Health Organization (WHO), the United Nations Environment Programme (UNEP) and the International Labour Organization (ILO) by Wiley: 1987.
3. Gombrich, E. H., *The story of art*. Phaidon Press, Ltd.: 1995.
4. Dawson, T. L., Examination, conservation and restoration of painted art. *Color. Technol.* **2007**, *123* (5), 281-292.
5. McGlinchey, C. W. In *Paintings conservation varnish*, CRC Press LLC: 2006; pp 88/1-88/3.
6. Elias, M.; de la Rie, E. R.; Delaney, J. K.; Charron, E.; Morales, K. M., Modification of the surface state of rough substrates by two different varnishes and influence on the reflected light. *Opt. Commun.* **2006**, *266* (2), 586-591.
7. Soucek, M. D., <2013 soucek.pdf>. *RadTech* **2013**, (2).
8. Rie, E. R. d. l., Old Master Paintings: A Study of the Varnish Problem. *Analytical Chemistry* **1989**, *61* (21), 1228A-1240A.
9. Feller, R. L., *Accelerated aging: photochemical and thermal aspects*. Getty Conservation Institute: 1994.
10. Peters, D., Our Environment Ruined? Environmental Control Reconsidered as a Strategy for Conservation. *Journal of Conservation and Museum Studies* **1996**, *1*, 6-10.
11. Zumbuhl, S.; Wuelfert, S., Chemical aspects of the bookkeeper deacidification of cellulosic materials: the influence of surfactants. *Stud. Conserv.* **2001**, *46* (3), 169-180.
12. Lin, L.-D.; Hsieh, C.-M.; Chiang, B.-H.; Tsai, M.-J., Modified atmosphere and humidity packages for conservation of paper antiques. *J. Wood Sci.* **2007**, *53* (2), 121-126.
13. Blades, N., *Guidelines on Pollution Control in Museum Buildings*. Museums Association: 2000.
14. *New insights into the cleaning of paintings : proceedings from the Cleaning 2010 International Conference, Universidad Politecnica de Valencia and Museum Conservation Institute*. Smithsonian Institution Scholarly Press: Washington, D.C., 2013.
15. Phenix, A., The Swelling of Artists' Paints in Organic Solvents. Part 2, Comparative Swelling Powers of Selected Organic Solvents and Solvent Mixtures. *Journal of the American Institute for Conservation* **2002**, *41* (1), 61-90.

16. Bellucci, R.; Cremonesi, P.; Pignagnoli, G., A Preliminary Note on the Use of Enzymes in Conservation: The Removal of Aged Acrylic Resin Coatings with Lipase. *Studies in Conservation* **1999**, *44* (4), 278-281.
17. Price, N. S.; Talley, M. K.; Vaccaro, A. M., *Historical and Philosophical Issues in the Conservation of Cultural Heritage*. Getty Conservation Institute: 1996.
18. Maxwell, A. S. B., W.R.; Dean, G.; Sims, G. D., Review of Accelerated Ageing Method and Lifetime Prediction Techniques for Polymeric Materials. *NPL Report* **2005**, 84.
19. Mignani, A. G.; Bacci, M.; Trono, C.; Mencaglia, A. A. In *Optical fibers for monitoring the effects of temperature on picture varnishes*, SPIE: 1997; pp 154-158.
20. Arecchi, T.; Bellini, M.; Corsi, C.; Fontana, R.; Materazzi, M.; Pezzati, L.; Tortora, A. In *Optical coherence tomography for painting diagnostics*, SPIE: 2005; pp 58570Z-58570Z-5.
21. Latour, G.; Georges, G.; Siozade, L.; Deumié, C.; Echard, J.-P. In *Study of varnish layers with optical coherence tomography in both visible and infrared domains*, SPIE: 2009; pp 73910J-73910J-7.
22. Lluveras, A.; Bonaduce, I.; Andreotti, A.; Colombini, M. P., GC/MS Analytical Procedure for the Characterization of Glycerolipids, Natural Waxes, Terpenoid Resins, Proteinaceous and Polysaccharide Materials in the Same Paint Microsample Avoiding Interferences from Inorganic Media. *Anal. Chem. (Washington, DC, U. S.)* **2010**, *82* (1), 376-386.
23. Wei, S.; Pintus, V.; Schreiner, M., Photochemical degradation study of polyvinyl acetate paints used in artworks by Py-GC/MS. *Journal of Analytical and Applied Pyrolysis* **2012**, *97* (0), 158-163.
24. Thoury, M.; Elias, M.; Frigerio, J. M.; Barthou, C. In *Non-destructive identification of varnishes by UV fluorescence spectroscopy*, SPIE: 2005; pp 58570J-58570J-11.
25. Elias, M.; Magnain, C.; Barthou, C.; Nevin, A.; Comelli, D.; Valentini, G. In *UV-fluorescence spectroscopy for identification of varnishes in works of art: influence of the underlayer on the emission spectrum*, SPIE: 2009; pp 739104-739104-12.
26. Marengo, E.; Liparota, M. C.; Robotti, E.; Bobba, M.; Gennaro, M. C., Monitoring of pigmented surfaces in accelerated ageing process by ATR-FT-IR spectroscopy and multivariate control charts. *Talanta* **2005**, *66* (5), 1158-1167.
27. Schoenemann, A.; Edwards, H. G. M., Raman and FTIR microspectroscopic study of the alteration of Chinese tung oil and related drying oils during ageing. *Anal. Bioanal. Chem.* **2011**, *400* (4), 1173-1180.
28. Vandenabeele, P.; Wehling, B.; Moens, L.; Edwards, H.; De Reu, M.; Van Hooydonk, G., Analysis with micro-Raman spectroscopy of natural organic binding media and varnishes used in art. *Anal. Chim. Acta* **2000**, *407* (1-2), 261-274.
29. Skoog, D. A.; Holler, F. J.; Crouch, S. R., *Principles of Instrumental Analysis*. Thomson Brooks/Cole: 2007.
30. McCreery, R. L., *Raman Spectroscopy for Chemical Analysis*. Wiley: 2005.
31. Vandenabeele, P.; Edwards, H. G. M.; Moens, L., A Decade of Raman Spectroscopy in Art and Archaeology. *Chem. Rev. (Washington, DC, U. S.)* **2007**, *107* (3), 675-686.
32. Gerrard, D. L., Raman Spectroscopy. *Anal. Chem.* **1994**, *66* (12), 547R-57R.

33. Laane, J., *Frontiers of Molecular Spectroscopy*. Elsevier Science: 2011.
34. Ferraro, J. R., *Introductory Raman Spectroscopy*. Elsevier Science: 2003.
35. Stevenson, F. J., *Humus Chemistry: Genesis, Composition, Reactions*. Wiley: 1994.
36. Stevenson, F. J., *Humus Chemistry: Genesis, Composition, Reactions*. Wiley: 1982.
37. Adani, F.; Spagnol, M.; Genevini, P., Biochemical Origin and Refractory Properties of Humic Acid Extracted from the Maize Plant. *Biogeochemistry* **2006**, *78* (1), 85-96.
38. Piccolo, A., The supramolecular structure of humic substances: A novel understanding of humus chemistry and implications in soil science. *Adv. Agron.* **2002**, *75*, 57-134.
39. Essington, M. E., *Soil and Water Chemistry: An Integrative Approach*. Taylor & Francis: 2004.
40. Khan, S. U. S., M., *Soil Organic Matter*. Elsevier Science: 1975.
41. Ghabbour, E. A.; Davies, G.; Chemistry, R. S. o., *Humic Substances: Structures, Models and Functions*. Royal Society of Chemistry: 2001.
42. Tipping, E., *Cation Binding by Humic Substances*. Cambridge University Press: 2002.
43. Wershaw, R. L., Application of a membrane model to the sorptive interactions of humic substances. *Environ. Health Perspect.* **1989**, *83*, 191-203.
44. Wershaw, R., Model for Humus in Soils and Sediments. *Environmental Science & Technology* **1993**, *27* (5), 814-816.
45. Šmejkalová, D.; Piccolo, A., Aggregation and Disaggregation of Humic Supramolecular Assemblies by NMR Diffusion Ordered Spectroscopy (DOSY-NMR). *Environmental Science & Technology* **2007**, *42* (3), 699-706.
46. Leenheer, J. A., Progression from model structures to molecular structures of natural organic matter components. *Ann. Environ. Sci.* **2007**, *1*, 57-68.
47. Baalousha, M.; Motelica-Heino, M.; Galaup, S.; Le, C. P., Supramolecular structure of humic acids by TEM with improved sample preparation and staining. *Microsc Res Tech* **2005**, *66* (6), 299-306.
48. MacCarthy, P., The principles of humic substances: an introduction to the first principle. *Spec. Publ. - R. Soc. Chem.* **2001**, *273* (Humic Substances), 19-30.
49. Busato, J. G.; Zandonadi, D. B.; Dobbss, L. B.; Facanha, A. R.; Canellas, L. P., Humic substances isolated from residues of sugar cane industry as root growth promoter. *Sci. Agric. (Piracicaba, Braz.)* **2010**, *67* (2), 206-212.
50. Pare, T.; Saharinen, M.; Tudoret, M. J.; Dinel, H.; Schnitzer, M.; Ozdoba, D., Response of alfalfa to calcium lignite fertilizer. *Spec. Publ. - R. Soc. Chem.* **2001**, *273* (Humic Substances), 345-353.
51. Seyedbagheri, M.-M.; Torell, J. M., Effects of humic acids and nitrogen mineralization on crop production in field trials. *Spec. Publ. - R. Soc. Chem.* **2001**, *273* (Humic Substances), 355-359.
52. Lai, Y.-S.; Chen, C.-S.; Chen, S., Adsorption and Desorption of Plasticizers with Humic-Fraction-Immobilized Silica Gel in Hexane: A Facile Approach to Pre-concentration. *J. Agric. Food Chem.* **2013**, *61* (22), 5286-5290.



53. Nakashima, S., Complexation and reduction of uranium by lignite. *Sci. Total Environ.* **1992**, 117-118, 425-37.
54. Lemeé, L.; Pinard, L.; Beauchet, R.; Kpogbemabou, D., Evaluation of humic fractions potential to produce bio-oil through catalytic hydroliquefaction. *Bioresour. Technol.* **2013**, 149, 465-469.
55. Ferrara, G.; Loffredo, E.; Senesi, N., Antimutagenic and antitoxic actions of humic substances on seedlings of monocotyledon and dicotyledon plants. *Spec. Publ. - R. Soc. Chem.* **2001**, 273 (Humic Substances), 361-371.
56. Macalady, D.L. and Walton-Day, K. "Redox Chemistry and Natural Organic Matter (NOM): Geochemists' Dream, Analytical Chemists' Nightmare" in *Aquatic Redox Chemistry*, P.G. Tratnyet, T.J. Grundl, and S.B. Haderlein (Eds.), ACS Symposium Series (No. 1071), American Chemical Society, Washington, D.C., **2012**.
57. Waksman, S. A., What is humus? *Proc. Natl. Acad. Sci. U. S. A.* **1925**, 11, 463-8.
58. Thurman, E. M.; Malcolm, R. L., Preparative isolation of aquatic humic substances. *Environ. Sci. Technol.* **1981**, 15 (4), 463-6.
59. De Haan, H., Impacts of environmental changes on the biogeochemistry of aquatic humic substances. *Hydrobiologia* **1992**, 229, 59-71.
60. Song, G.; Hayes, M. H. B.; Novotny, E. H.; Simpson, A. J., Isolation and fractionation of soil humin using alkaline urea and dimethylsulphoxide plus sulphuric acid. *Naturwissenschaften* **2011**, 98 (1), 7-13.
61. Rocha, J. C.; Rosa, A. H.; Furlan, M., An Alternative Methodology for the Extraction of Humic Substances from Organic Soils. *Journal of the Brazilian Chemical Society* **1998**, 9, 51-56.
62. Leenheer, J. A., Comprehensive approach to preparative isolation and fractionation of dissolved organic carbon from natural waters and wastewaters. *Environ Sci Technol* **1981**, 15 (5), 578-87.
63. Trubetskaya, O.; Trubetskoy, O.; Richard, C., Hydrophobicity of electrophoretic fractions of different soil humic acids. *J. Soils Sediments* **2014**, 14 (2), 292-297.
64. Gora, R.; Hutta, M.; Roharik, P., Characterization and analysis of soil humic acids by off-line combination of wide-pore octadecylsilica column reverse phase high performance liquid chromatography with narrow bore column size-exclusion chromatography and fluorescence detection. *J. Chromatogr. A* **2012**, 1220, 44-49.
65. Roba, C. A.; Jimenez, C.; Baciu, C.; Beldean-Galea, S.; Levei, E.; Cordoş, E., Assessment of different sorbents efficiency for solid phase extraction of aquatic humic acids. *Central European Journal of Chemistry* **2011**, 9 (4), 598-604.
66. Hutta, M.; Gora, R.; Halko, R.; Chalanyova, M., Some theoretical and practical aspects in the separation of humic substances by combined liquid chromatography methods. *J. Chromatogr. A* **2011**, 1218 (49), 8946-8957.
67. Huber, S. A.; Balz, A.; Abert, M.; Pronk, W., Characterisation of aquatic humic and non-humic matter with size-exclusion chromatography - organic carbon detection - organic nitrogen detection (LC-OCD-OND). *Water Res.* **2011**, 45 (2), 879-885.
68. Świetlik, J.; Sikorska, E., Characterization of Natural Organic Matter Fractions by High Pressure Size-Exclusion Chromatography, Specific UV Absorbance and Total

- Luminescence Spectroscopy. *Polish Journal of Environmental Studies* **2006**, *15* (1), 145-153.
69. Peuravuori, J.; Pihlaja, K., Molecular size distribution and spectroscopic properties of aquatic humic substances. *Anal. Chim. Acta* **1997**, *337* (2), 133-150.
70. Chin, Y.-P.; Aiken, G.; O'Loughlin, E., Molecular Weight, Polydispersity, and Spectroscopic Properties of Aquatic Humic Substances. *Environmental Science & Technology* **1994**, *28* (11), 1853-1858.
71. Yan, M.; Korshin, G.; Wang, D.; Cai, Z., Characterization of dissolved organic matter using high-performance liquid chromatography (HPLC)-size exclusion chromatography (SEC) with a multiple wavelength absorbance detector. *Chemosphere* **2012**, *87* (8), 879-885.
72. Johnson, W. P.; Bao, G.; John, W. W., Specific UV Absorbance of Aldrich Humic Acid: Changes during Transport in Aquifer Sediment. *Environmental Science & Technology* **2002**, *36* (4), 608-616.
73. González Pérez, M.; Martin-Neto, L.; Saab, S. C.; Novotny, E. H.; Milori, D. M. B. P.; Bagnato, V. S.; Colnago, L. A.; Melo, W. J.; Knicker, H., Characterization of humic acids from a Brazilian Oxisol under different tillage systems by EPR, <sup>13</sup>C NMR, FTIR and fluorescence spectroscopy. *Geoderma* **2004**, *118* (3-4), 181-190.
74. Prashob, P. K. J.; Nair, S. M., Genesis of structural features of humic acids from the sediments of a high productive coastal zone. *Geochem. J.* **2014**, *48* (3), 247-258.
75. Sierra, M. M. D.; Giovanella, M.; Parlanti, E.; Esteves, V. I.; Duarte, A. C.; Fransozo, A.; Soriano-Sierra, E. J., Structural Description of Humic Substances from Subtropical Coastal Environments using Elemental Analysis, FT-IR and <sup>13</sup>C-Solid State NMR Data. *Journal of Coastal Research* **2005**, 370-382.
76. Miano, T. M.; Senesi, N., Synchronous excitation fluorescence spectroscopy applied to soil humic substances chemistry. *Science of The Total Environment* **1992**, *117-118* (0), 41-51.
77. Peuravuori, J.; Koivikko, R.; Pihlaja, K., Characterization, differentiation and classification of aquatic humic matter separated with different sorbents: synchronous scanning fluorescence spectroscopy. *Water Research* **2002**, *36* (18), 4552-4562.
78. Chen, J.; LeBoeuf, E. J.; Dai, S.; Gu, B., Fluorescence spectroscopic studies of natural organic matter fractions. *Chemosphere* **2003**, *50* (5), 639-647.
79. Peuravuori, J., NMR spectroscopy study of freshwater humic material in light of supramolecular assembly. *Environ. Sci. Technol.* **2005**, *39* (15), 5541-5549.
80. Le Masle, A.; Angot, D.; Gouin, C.; D'Attoma, A.; Ponthus, J.; Quignard, A.; Heinisch, S., Development of on-line comprehensive two-dimensional liquid chromatography method for the separation of biomass compounds. *J. Chromatogr. A* **2014**, *1340*, 90-98.
81. François, I.; Sandra, K.; Sandra, P., Comprehensive liquid chromatography: Fundamental aspects and practical considerations—A review. *Analytica chimica acta* **2009**, *641* (1-2), 14-31.
82. Ahn, S.; Lee, H.; Lee, S.; Chang, T., Characterization of Branched Polymers by Comprehensive Two-Dimensional Liquid Chromatography with Triple Detection. *Macromolecules (Washington, DC, U. S.)* **2012**, *45* (8), 3550-3556.

83. Elsner, V.; Laun, S.; Melchior, D.; Koehler, M.; Schmitz, O. J., Analysis of fatty alcohol derivatives with comprehensive two-dimensional liquid chromatography coupled with mass spectrometry. *J. Chromatogr. A* **2012**, *1268*, 22-28.
84. Gilar, M.; Olivova, P.; Daly, A. E.; Gebler, J. C., Orthogonality of Separation in Two-Dimensional Liquid Chromatography. *Anal. Chem.* **2005**, *77* (19), 6426-6434.
85. Li, X.; Carr, P. W., Effects of first dimension eluent composition in two-dimensional liquid chromatography. *Journal of chromatography. A* **2011**, *1218* (16), 2214-21.
86. Murphy, R. E.; Schure, M. R.; Foley, J. P., Effect of Sampling Rate on Resolution in Comprehensive Two-Dimensional Liquid Chromatography. *Anal. Chem.* **1998**, *70* (8), 1585-1594.
87. Cohen, S. A.; Schure, M. R.; Editors, *Multidimensional Liquid Chromatography; Theory and Application in Industrial Chemistry and the Life Sciences*. John Wiley & Sons, Inc.: 2008; p 456 pp.
88. Giddings, J. C., Sample dimensionality: A predictor of order-disorder in component peak distribution in multidimensional separation. *Journal of Chromatography A* **1995**, *703* (1-2), 3-15.
89. Davis, J. M.; Giddings, J. C., Statistical theory of component overlap in multicomponent chromatograms. *Analytical Chemistry* **1983**, *55* (3), 418-424.
90. Giddings, J. C., Maximum number of components resolvable by gel filtration and other elution chromatographic methods. *Analytical Chemistry* **1967**, *39* (8), 1027-1028.
91. Guiochon, G.; Beaver, L. A.; Gonnord, M. F.; Siouffi, A. M.; Zakaria, M., Theoretical investigation of the potentialities of the use of a multidimensional column in chromatography. *Journal of Chromatography A* **1983**, *255* (0), 415-437.
92. Whelan, T.-J.; Shalliker, R. A.; McIntyre, C.; Wilson, M. A., Development of a Multidimensional High-Performance Liquid Chromatography (HPLC) Separation for Bayer Humic Substances. *Ind. Eng. Chem. Res.* **2005**, *44* (9), 3229-3237.
93. Trubetskoj, O. A.; Richard, C.; Guyot, G.; Voyard, G.; Trubetskaya, O. E., Analysis of electrophoretic soil humic acids fractions by reversed-phase high performance liquid chromatography with on-line absorbance and fluorescence detection. *J. Chromatogr. A* **2012**, *1243*, 62-68.
94. Hutta, M.; Gora, R., Novel stepwise gradient reversed-phase liquid chromatography separations of humic substances, air particulate humic-like substances and lignins. *J. Chromatogr. A* **2003**, *1012* (1), 67-79.

## **CHAPTER 2. EXPERIMENTAL**

### **2.1 Analysis of Coating Oils by Raman Spectroscopy**

#### **2.1.1 Chemical Reagents**

Analytical reagent grade (or higher) solvents were used without further purification. Linseed Oil was obtained from Sigma Aldrich; Chinawood oil was purchased from Hope's (The Hope Company. Inc., Bridgeton, MO, USA). Linoleic acid 99% (v/v) and Oleic acid 97% (v/v) were obtained from ACROS Organics (Pittsburgh, PA, USA).

#### **2.1.2 Instrumentation**

##### **Raman Spectroscopy System**

Spectra were collected on a Fourier Transform Infrared Spectrometer (FT-IR) /Raman system (Nexus 670, Nicolet, Madison, WI, USA). The Raman spectrometer uses an Nd: YAG LASER (1064 nm, 1.5 W) with adjustable laser power and InGaAs detector. A schematic diagram of the Nexus 670 FT-IR/Raman system is shown in Figure 1.

The instrument control and data acquisition were performed on a Pentium III personal computer (Dell OptiPlex GX1, Round Rock, TX, USA) using OMNIC software version 6.02 (Thermo Scientific, Madison, WI, USA).

##### **Ageing Chamber**

For artificial (accelerated) ageing studies, a Varian Model 3800 (Varian Inc., Palo Alto, CA, USA) gas chromatograph (GC) was employed. A schematic diagram of the system is shown in Figure 2. Instrument control was performed by a Pentium II personal computer (Dell OptiPlex GX1) using Saturn software version 5.52 (Varian. Inc.).

A quartz reaction chamber (Figure 3) was designed to fit inside the oven of the GC to more precisely control the reaction temperature. The chamber has a door to allow entry of the sample and four tubes to facilitate the entrance of other reagents. Two of the tubes have keys to control the pressure inside the chamber while the other two tubes have stainless steel fittings which can be connected to the to the GC injectors. A UV Germicidal Lamp (254 nm, Osram Sylvania, G15T8, 15 W, 55 V) was attached inside the oven.

The aged samples were characterized off-line by FT-Raman spectroscopy.

### **Gas Chromatography System**

The aged samples were analyzed to determine if volatile compounds leaked during the ageing process using a GC system with a thermal conductivity detector (TCD). A schematic diagram of the system is shown in Figure 4.

Was used a GC Agilent (Palo Alto, CA, USA) Model 6890 system, consisting of:

- Stationary phase: SPB-1 column (100 (v/v) PDMS), 30 m x 0.32 micrometers, 1.0 micrometer film thickness (Supelco, Bellefonte, PA, USA)
- Mobile phase: ultra-high purity (99.999% (v/v) Helium (Airgas, Milwaukee, WI, USA)
- Mobile phase flow rate: 2.0 mL/min (constant, 40.0 cm/s)
- Injector temperature: 225°C
- Sample volume (splitless): 1.0 µL
- Oven program: isothermal at 25°C for 10 min (then stepped to 225°C to prepare for next sample)
- Detector temperature: 225°C
- Flow rate of reference gas (He): 2.0 mL/min
- Flow rate of makeup gas (He): 5.0 mL/min
- Data acquisition rate: 20 Hz

## 2.2 Analysis of Humic Acids by Liquid Chromatography

### 2.2.1 Chemicals Reagents

Analytical reagent grade (or higher) solvents were used without further purification. Methanol and ethyl acetate were obtained from Sigma Aldrich (Milwaukee, WI, USA), acetonitrile, 2-propanol, hexane and dimethylformamide were purchased from Fisher Scientific (Pittsburgh, PA, USA).

Sulfuric acid, hydrochloric acid and nitric acid were purchased from Fisher Scientific; salicylic acid and benzoic were obtained from Sigma Aldrich (Milwaukee, WI, USA).

Potassium chloride was purchased from Fisher Scientific; 2-naphtol was obtained from Sigma Aldrich; sodium hydroxide, disodium hydrogen phosphate and sodium acetate tri-hydrate were purchased from EMD Chemicals (Billerica, MA, USA).

L-tyrosine, L-tryptophan and L-phenylalanine were purchased from Acros Organics (Pittsburgh, PA, USA); L-tryptophan benzyl ester and humic acid (sodium salt) were purchased from Sigma Aldrich.

Reagent water (18 M $\Omega$ -cm) was obtained by using a water purification system (*Nanopure™ Barnstead* Waltham, MA, USA).

### 2.2.2 Buffers and Mobile Phases

Two different mixtures of acetic acid (0.1 M) and sodium acetate tri-hydrate (0.1 M) were prepared to obtain acetate buffer solutions with pH=3.00 ( $\pm 0.01$ ) and pH=5.00 ( $\pm 0.01$ ). Two different mixtures of disodium hydrogen phosphate (0.1 M) and hydrochloric acid (0.1 M) were used to prepare buffer solutions with pH=7.00 ( $\pm 0.01$ ) and pH=9.00

( $\pm 0.01$ ). A phosphate buffer at pH=11.00 ( $\pm 0.01$ ) was prepared with disodium hydrogen phosphate (0.1 M) and sodium hydroxide (0.1 M). The final pH was adjusted by the use of a pH Meter (Delta 320, Mettler Toledo, Columbus, OH, USA) with a glass "combination" pH electrode (Accumet™, Fisher Scientific).

### 2.2.3 Sample Preparation

Stock solutions 0.1 M of 2-naphtol, salicylic acid, benzoic acid, L-tyrosine, L-tryptophan and L-phenylalanine were prepared with 18 M $\Omega$ -cm water. Stock solutions 0.1 M of L-tyrosine, L-tryptophan and L-phenylalanine were prepared in four buffer solutions with pH=3.00, pH=5.00, pH=7.00 and pH=9.00. The samples were stored at room temperature in glass bottles. Before injection into the LC, they were filtered by PTFE 0.45  $\mu$ m membrane filters (Corning™, Fisher Scientific).

A 2.0 mg/mL stock solution of humic acid (sodium salt) was prepared with 18 M $\Omega$ -cm water. Nine stock solutions of the humic acid sodium salt were prepared in organic and aqueous solvents. The humic acid samples (1.00 mL, filtered by 0.45  $\mu$ m membrane filter) were loaded onto Solid Phase Extraction (SPE) columns, previously conditioned with the appropriate solvent (according to the sorbent), to obtain fractions for further study. Eight types of sorbents were tested: two normal phase, three reversed phase and three ion-exchange resins. All the fractions obtained were stored at room temperature in amber glass vials (20 mL, Aldrich, Milwaukee, WI, USA), and filtered through a 0.45  $\mu$ m membrane filter before they were injected into the LC. A diagram of the general procedure followed to obtain the humic acid fractions is shown in the Figure 5.



## 2.2.4 Instrumentation

### Liquid Chromatography System

The optimized configuration of the liquid chromatography system (LC) used in the separation of the complex organic mixtures is shown schematically in Figure 6(A). The instrument had the following components: a six port two-position injection valve (E-60, Valco Instruments Co. Inc., Houston, TX, USA) equipped with Polytetrafluoroethylene (PTFE) tubing ( 0.5 mm i.d., VICI), and polyether ether ketone (PEEK) fittings (Cheminert, VICI) (Figure 6B). The sample loops were made in three sizes (with the same tubing and fittings mentioned above): 35  $\mu$ L, 50  $\mu$ L and 100  $\mu$ L. The valve was connected to a peristaltic pump (Alitea XV, FIA Lab, Seattle, WA, USA) fitted with Accu-Rated PVC tubes ( 1.42 mm i.d.; two-stop – 40 cm; Fisher Scientific ). A reversed phase (RP) monolithic column (Model CIM® RP-SDVB DISK, BIA Separations, Wilmington, DE, USA) was used instead of a traditional HPLC column. The proprietary stationary phase is based upon polystyrene-co-divinylbenzene. An on-line fluorescence spectrometer (Model F1000, Hitachi, Schaumburg, IL, USA) equipped with 150W xenon lamp, a 12  $\mu$ L flow cell and a photomultiplier tube (PMT) (Figure 7A and B); and an on-line absorption spectrometer (Model USB4000, Ocean Optics, Dunedin, FL, USA) with a CCD detector and a pulsed xenon source (Ocean Optics, Dunedin, FL, USA), were used to identify solutes(Figure 8 A and B). A photograph of the RP-LC system is shown in Figure 9.

The system control and data acquisition for the LC were performed on a Pentium II personal computer (Dell OptiPlex GX1, Round Rock, TX, USA) using LabVIEW software version 7.1 (National Instruments, Austin, TX, USA).



### **Spectrofluorometer**

For obtaining high-resolution fluorescence spectra, a FluoroLog®-3 Spectrofluorimeter (Model FL3-22, Horiba Scientific, Irvine, CA, USA) was used to optimize the excitation and emission wavelengths in different solvents. The spectrofluorimeter design was based upon a double-grating excitation monochromator and a double-grating emission monochromator. The instrument has a 450W Xenon lamp and a photomultiplier tube as detector. A schematic diagram of the spectrofluorimeter is shown in Figure 10.

Instrument control was performed on a personal computer Pentium III (Dell, Round Rock, TX, USA) with the software SpectrAcq version 4.13 (Instrument Control Center, Version 2.2.9.1, Jobin Yvon, Inc., Edison, NJ, USA). The data acquisition were performed on a personal computer Pentium 4 (Dell, Round Rock, TX, USA) using the software DataMax version 2.20 for Windows® (Instrument s SA. Inc., Jobin Yvon Inc., Edison, NJ, USA).

## 2.3 Figures and Tables

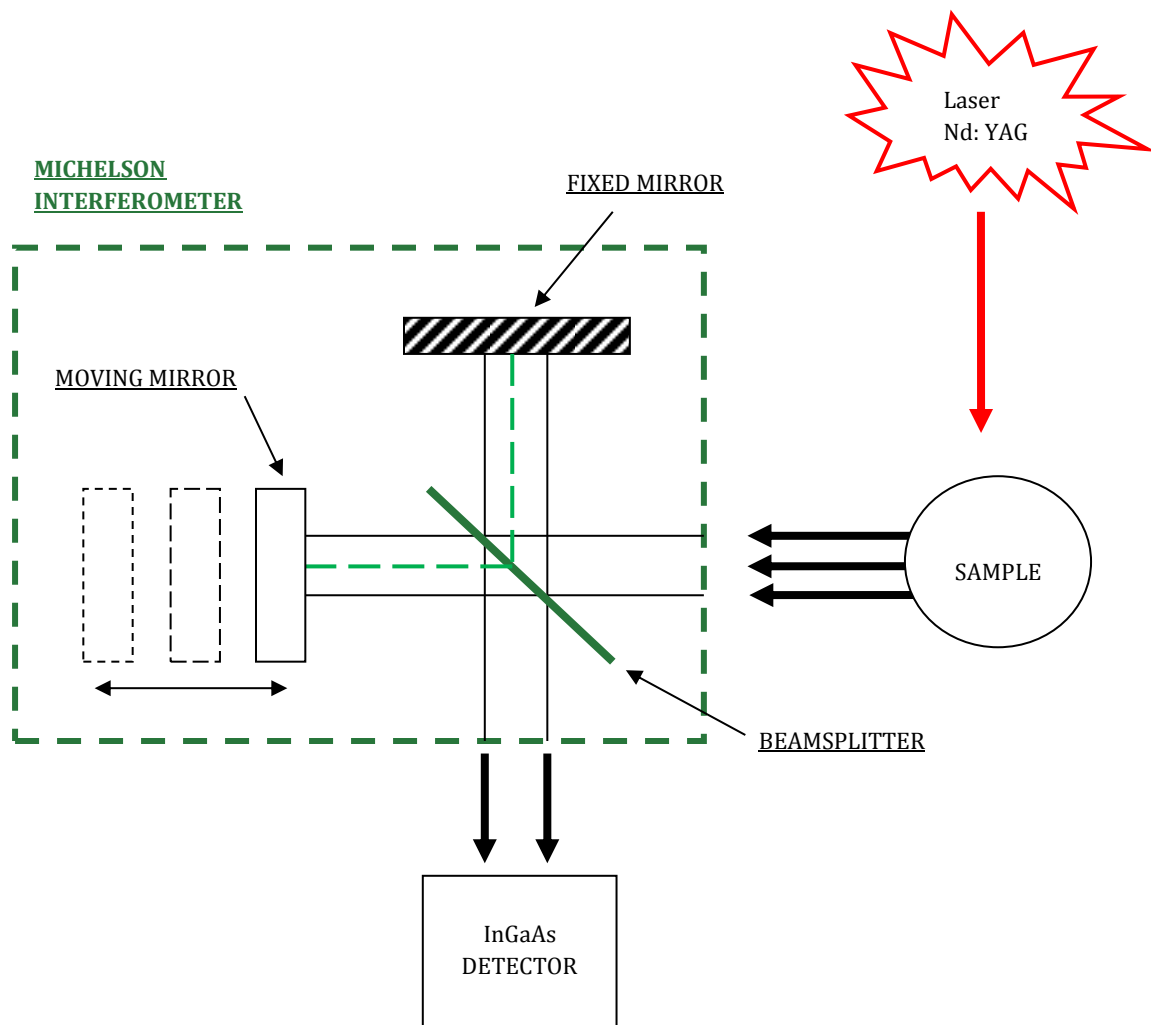


**Figure 2-1.** Schematic diagram of the Nexus 670 FT-Raman. (Adapted from FT-Raman Module User's Guide).<sup>5</sup>

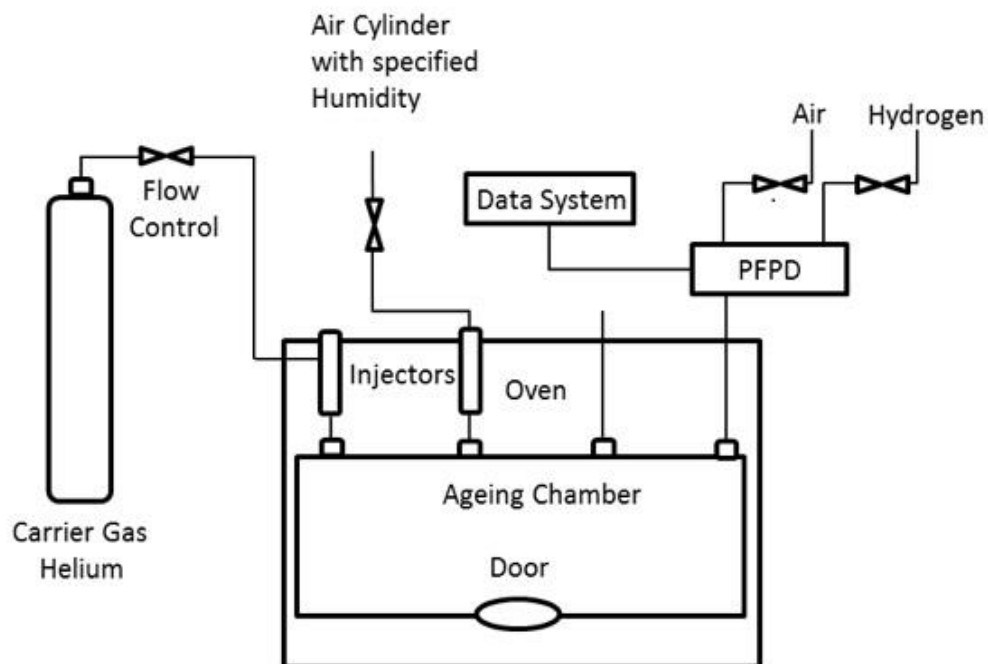


**Figure 2-2.** Schematic diagram of environmental chamber that was used for the accelerated ageing experiment.<sup>6</sup>



**Figure 2-3.** Photograph of the ageing chamber.

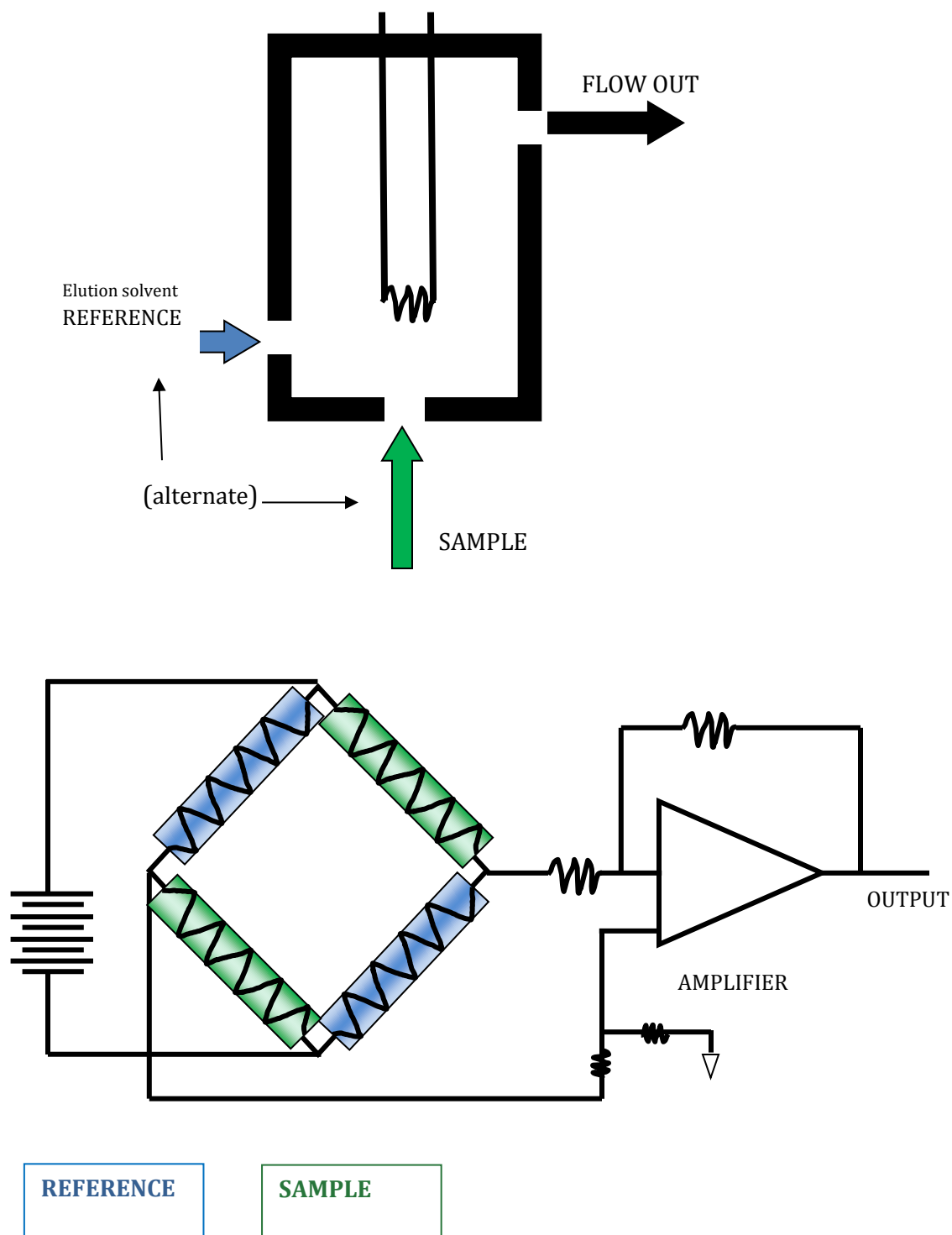
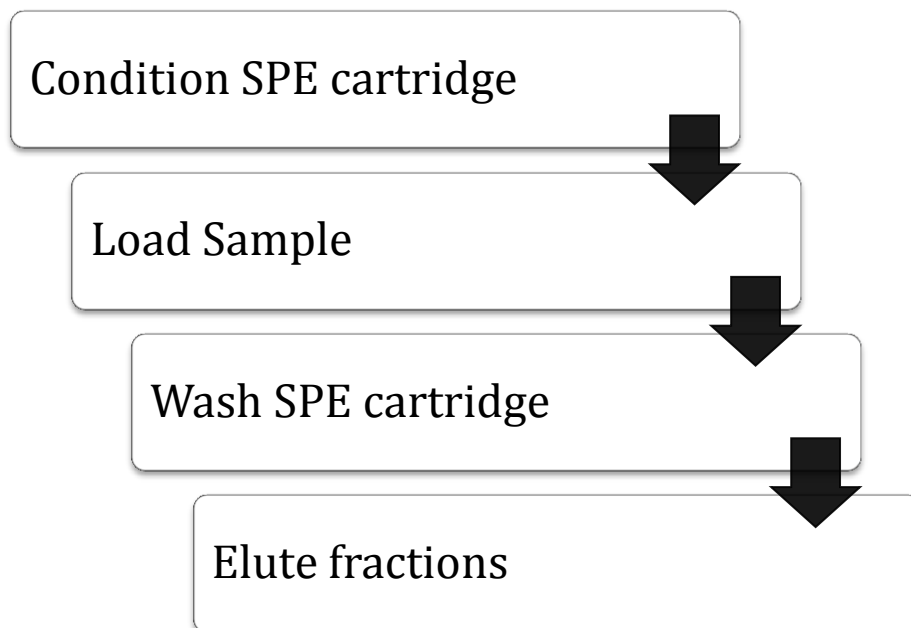
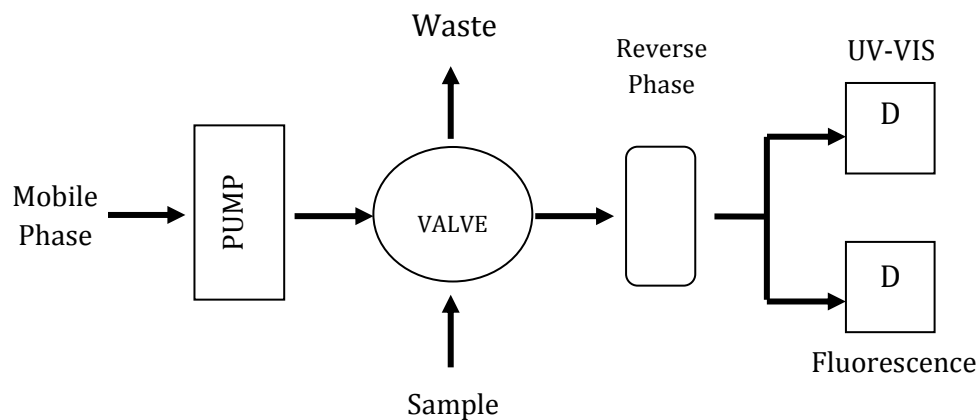


Figure 2-4. Schematic diagram of a TCD detector. Adapted from Skoog *et al.*, 2007.<sup>7</sup>



**Figure 2-5.** SPE extraction general procedure.

A)



B)

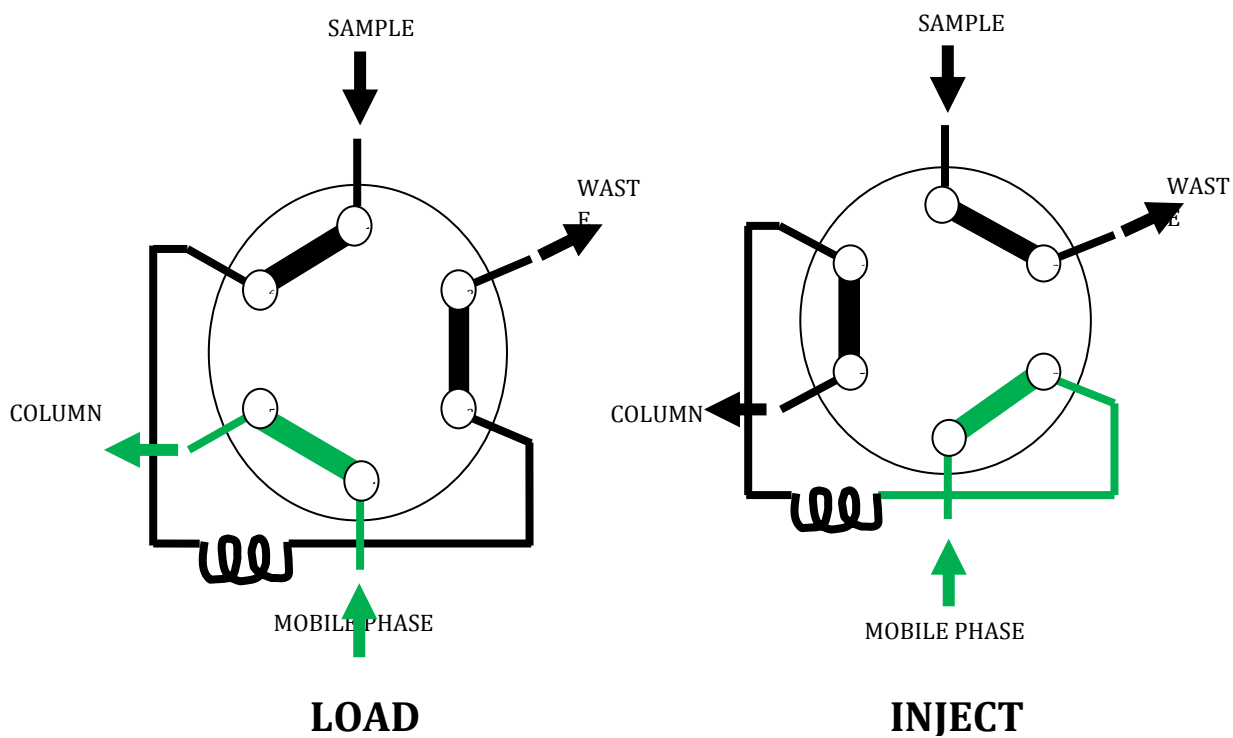


**Figure 2-6.** A) Schematic diagram of the liquid chromatography system. B) Detail of the six-port/ two-position valve. Adapted from Valco Instruments Co. Inc.<sup>1</sup>

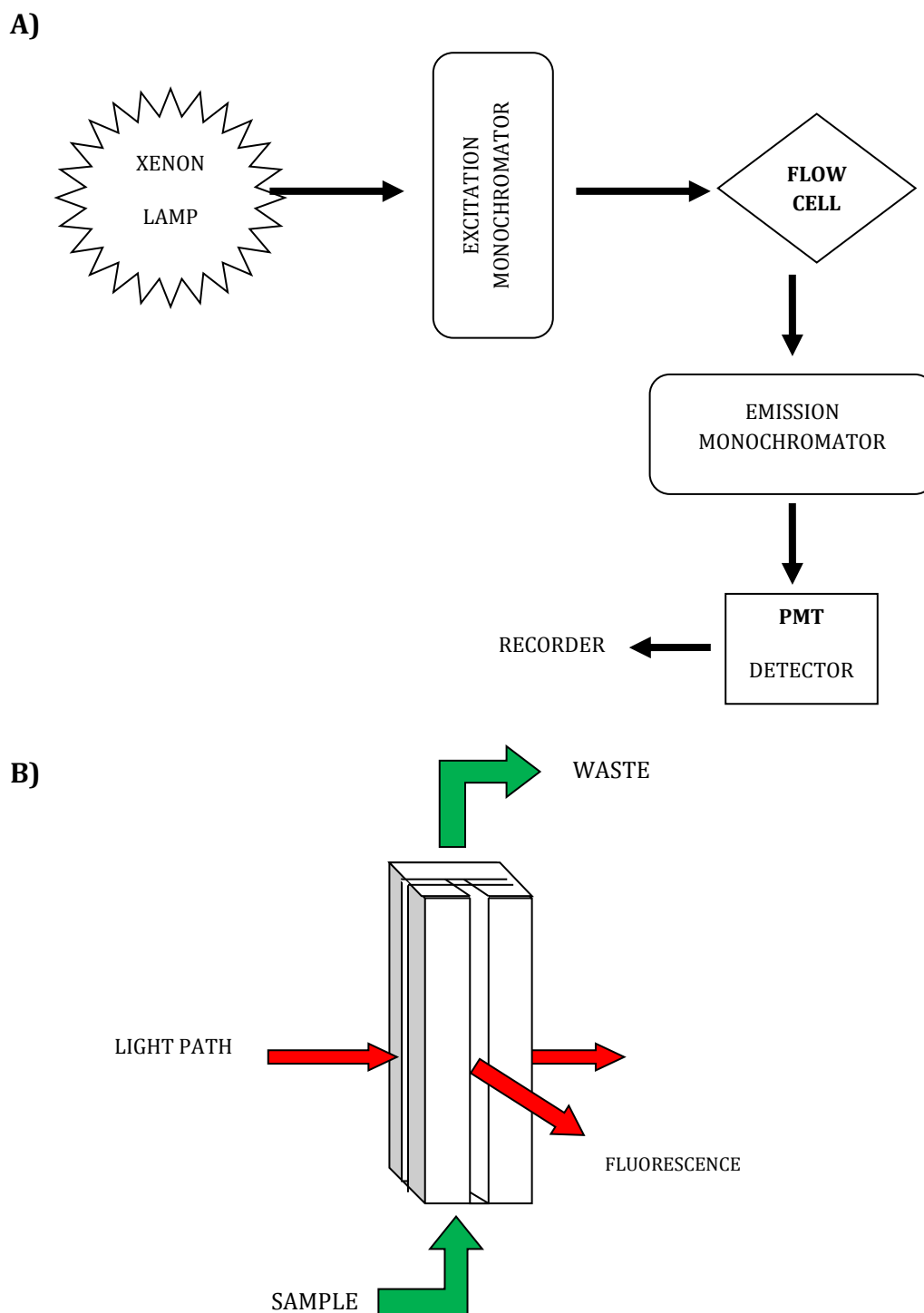


**Figure 2-7.** A) Schematic diagram of the fluorescence detector. B) Detail of the flow cell (Adapted from Hitachi Instruction Manual for F-1300 Fluorescence spectrometer).<sup>2</sup>



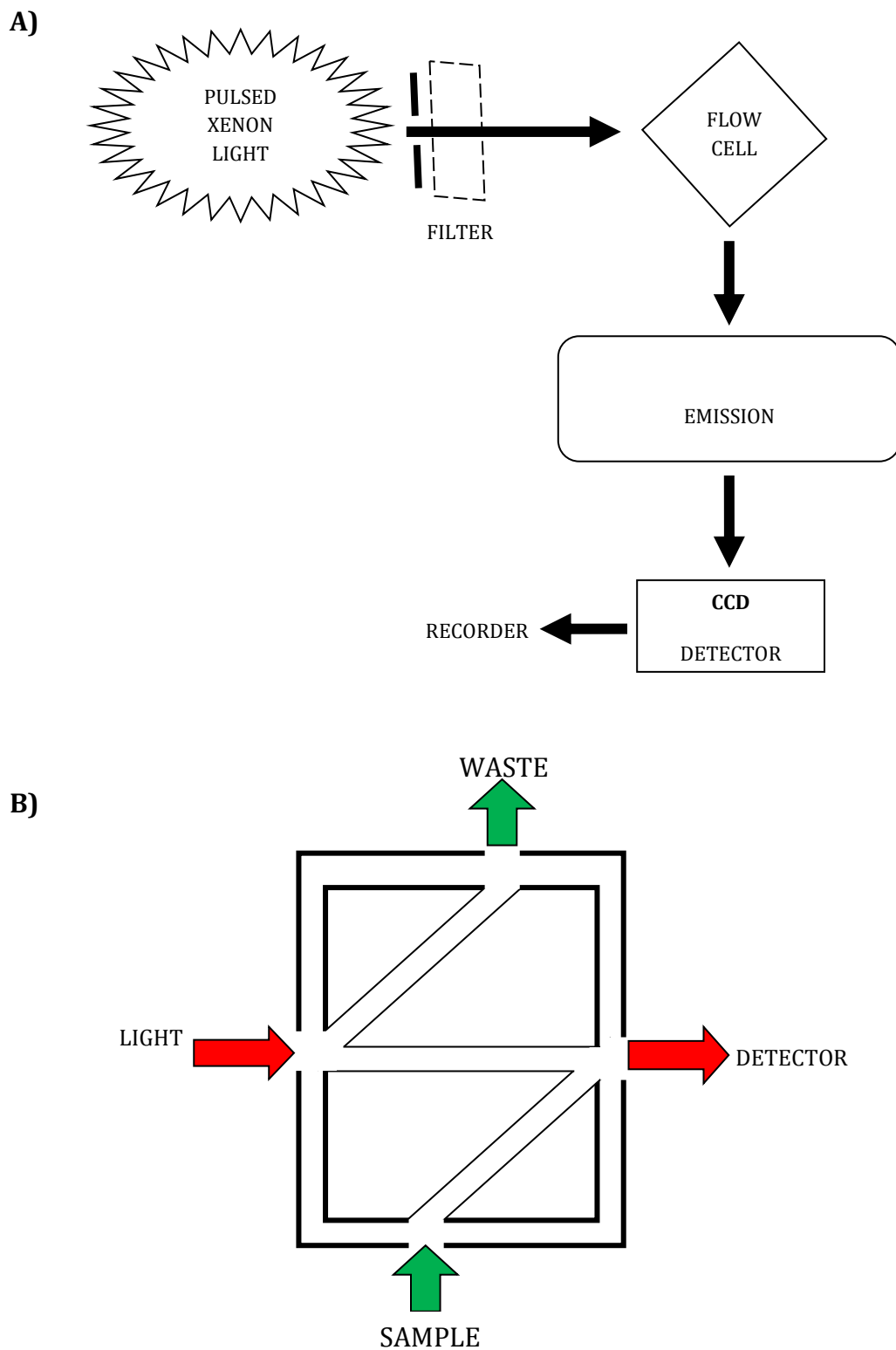


**Figure 2-8.** A) Schematic diagram of the UV detector. (Adapted from USB4000 Fiber Optic Spectrometer Installation and Operation Manual).3 B) Detail of the flow cell.



Figure 2-9. Photograph of the RP-LC system.

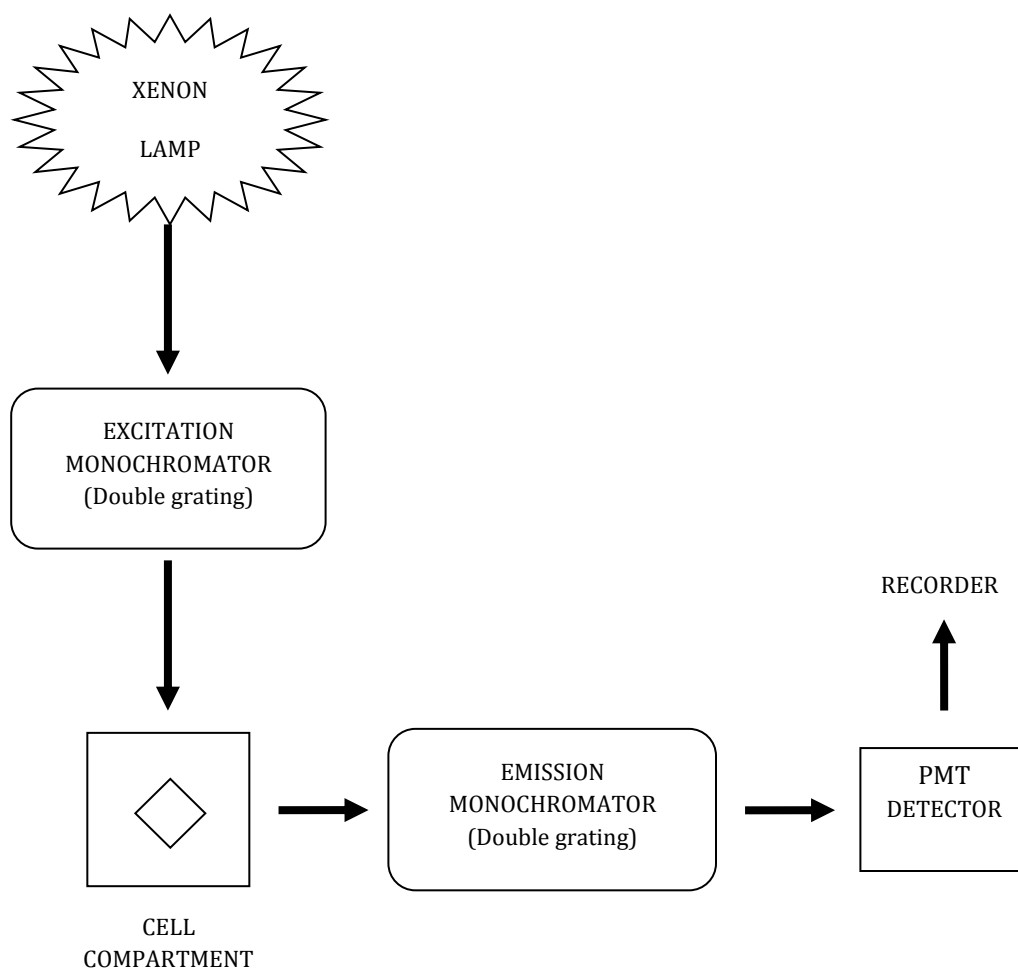


**Figure 2-10.** Schematic diagram of the Horiba FluoroLog®-3 Spectrofluorometer Model FL3-22.(Adapted from FluoroLog®-3 Operation Manual).<sup>4</sup>

## 2.4 References

1. VICI, Valco Instrument Co. Inc. [www.vici.com](http://www.vici.com) (Accessed July **2014**).
2. Hitachi., Instruction Manual for Model 1030 Fluorescence Spectrophotometer, 1985.
3. Ocean Optics Inc. USB4000 Operating Manual.
4. Jobin Yvon Inc. Fluorog 3 Manual. **2002**.
5. Guide, F.-R. M. U. s., FT-Raman Module User's Guide. *Thermo Nicolet Corporation, Madison, WI, USA 1999*.
6. Skoog, D. A.; Holler, F. J.; Crouch, S. R., *Principles of Instrumental Analysis*. Thomson Brooks/Cole: 2007.

## CHAPTER 3. RESULTS AND DISCUSSION

### 3.1 Analysis of Coating Oils by Raman Spectroscopy

#### 3.1.1 Raman Spectroscopy — An Overview of the Theory & Practice

The Raman Effect occurs when monochromatic light of energy ( $h\nu_{\text{ex}}$ ) interacts with the electron cloud of a molecule. As the incident photon distorts the molecule, the polarization of the molecule is affected, the molecule is excited from the electronic ground state to a so-called “virtual” state, and when the molecule relaxes one can observe and measure the scattered light. The scattered light consists of two types: (a) Rayleigh scattering (elastic scattering), which is strong and has the same frequency as the incident beam ( $\nu_{\text{ex}}$ ), and (b) Raman scattering (inelastic scattering), which is very weak ( $\leq 10^{-5}$  of the incident beam) and has transition frequencies ( $\nu_{\text{ex}} \pm \nu_{\text{v}}$ ), where  $\nu_{\text{v}}$  is a vibrational frequency of the molecule (Figure 1).<sup>1-3</sup> The “virtual state” is not a quantized electronic energy level, rather it can be considered as a distortion of the electron cloud caused by the electric field vector of the incident light. In Raman scattering, the incident radiation causes excitation to the virtual level and emission of a photon of lower or higher energy. The lower-frequency emissions ( $\nu_{\text{ex}} - \nu_{\text{v}}$ ) are called Stokes scattering and the higher-frequency emissions ( $\nu_{\text{ex}} + \nu_{\text{v}}$ ) are called anti-Stokes scattering.<sup>3</sup> The Stokes and anti-Stokes Raman peaks are symmetrically positioned about the Rayleigh peak but their intensities are very different (Figure 2).<sup>2</sup> Usually, the vibrational level in the electronic ground state is more highly populated, so the Stokes lines are more intense than the anti-Stokes lines.<sup>2, 3</sup> By convention, in Raman spectra, only the Stokes shifts are shown (as absolute values).<sup>2, 3</sup>

### 3.1.2 Method Optimization

A schematic diagram of the Raman system and the optimized conditions to obtain the Raman spectra are shown in Figure 3 and Table I respectively.

The spectrometer was stabilized for 20 min before turning on the laser source. To stabilize the laser before running the samples, the laser power was turned on 60 min in advance. The alignment was calibrated daily with a solid sulfur standard sample. The sulfur sample was re-prepared monthly (Figure 4).

To control the reliability of our results, the impact of the laser power was tested with a Chinawood Oil sample (which had been artificially aged at 100°C for 2 hr) (Figure 5). The sample was measured (n=3) at four different laser powers to optimize the source intensity. The difference between the intensities of the major peak in the spectra was substantial (Figure 6). For the following experiments the laser power was then adjusted to  $2.0 \pm 0.2$  W and monitored for each sample to control small fluctuations.

A standard “pristine” sample (*i.e.*, one that had not been subjected to ageing treatment) of both Linseed Oil and Chinawood Oil were stored at room temperature in amber glass bottles, within a vacuum desiccator, under a nitrogen atmosphere.

After the ageing treatments had been performed, the samples were loaded directly as neat solutions, into NMR tubes (glass, 0.3 mm i.d., Thermo Scientific, Madison, WI, USA) without any further preparation. Some samples were aged on glass slides (1.5 cm x 2.0 cm x 0.2 mm) and others were aged directly in the NMR tubes. NMR tubes were cut to a 2.00 cm length to better fit into the Ageing Chamber and to thereby eliminate having to transfer the sample from the glass slides into the tubes.

Because some samples were difficult to transfer from the slides to the Raman tubes, the sample size was adjusted to an average of  $0.100 \pm 0.020$  g. The spectral resolution was

adjusted to  $8 \text{ cm}^{-1}$ , and the optimal slit aperture was set automatically by the instrument software based upon the resolution value. Thus samples which had a low Raman scattering intensity could be measured at higher source intensities. Also, the scan number was set to 128 to obtain higher spectral resolution and improved signal-to-noise ratios. The gain for the InGaAs detector was chosen (setting=8) to optimize the sensitivity.

### 3.1.3 Design and Application of the Ageing Chamber

In the last three decades, extensive reports have appeared in the literature regarding accelerated ageing experiments applied to artistic media. These studies have provided new insights into the chemical changes that are ultimately responsible for the physical disintegration and failure of materials used in works of art.<sup>4-14</sup>

The ageing of varnishes that have been applied to paintings is a major concern in art conservation, and accelerated ageing tests have been carried out to study the chemical stability and physical durability of the materials.<sup>9</sup> This is done to obtain a better understanding of the chemical reactions involved in the degradation process.<sup>9</sup> To aid efforts in restoring these works of art, it is crucial to understand the nature of the ageing process, given that the composition of the original varnish as well as subsequent restoration(s) is seldom known.

The objective of this area of investigation is the development of techniques that can monitor the extent of degradation and understand the patterns of deterioration in artistic varnishes.<sup>9</sup> To validate the methods that are used to study artistic materials, a standard reference material (SRM) is needed. However, because of the plethora of materials used in art conservation as well as the myriad environmental conditions to which artistic objects are subjected a practical SRM does not exist.<sup>15</sup> Therefore, in the present study accelerated-

ageing tests were performed as a means to provide experimental data to support the development of an SRM. The goal of this study is to develop through the artificial ageing approach an SRM varnish that closely resembles naturally aged varnishes.<sup>15</sup>

The mechanisms of degradation processes were studied as a function of key environmental factors (*e.g.*, ambient heat, light, moisture, etc.) These factors cause the varnish layer to yellow, crack, and flake and present other consequences that harm not only the appearance of the work, but also the stability of the work itself. A quartz reaction chamber for precisely controlling these factors was designed, fabricated, and tested.<sup>16</sup> The chamber fits inside the oven of a conventional gas chromatograph (GC), thereby facilitating precise control of temperature and introduction and regulation of gases. The design of the chamber allows for the samples to be easily inserted for exposure to the environmental conditions that are set for a specific experiment (Figure 7). The stainless steel to quartz fittings permit connection to the GC injection ports for the introduction of specific gas phase mixtures (*i.e.*, humidity and oxygen levels) to create the atmosphere to which the sample is exposed within the chamber. A UV Lamp (254 nm, 15 W) was incorporated within the GC oven to expose the samples to UV radiation in the same controlled environment. The accelerated ageing experiments were conducted using common triglycerides fatty acids, and two complex mixtures thereof (Linseed Oil and Chinawood Oil) subjected to time-course experiments in which temperature, light, and the atmospheric gases were varied. The aged varnish samples were then characterized off-line by FT-Raman spectroscopy. The Raman spectra that were collected for the time-course studies and the possible mechanisms that are happening during the ageing process are described in the following pages.



### 3.1.4 Characterization of Chinawood Oil and Linseed Oil

#### Structure and Reactivity

Natural binders and varnishes can be classified into four groups according to their constitution: (a) proteinaceous media, (b) polysaccharide media, (c) fatty acid-containing media and (d) resinous media. The fatty acid-containing media group consists of drying oils and waxes.<sup>4</sup>

The drying oils by definition are triglycerides of natural origin (Figure 8) which are capable of reacting with atmospheric oxygen (auto-oxidation). Two examples of drying oils are Linseed Oil and Chinawood Oil (also known as Tung Oil).<sup>17, 18</sup> Linseed Oil and Chinawood Oil are triglycerides primarily containing unsaturated fatty acids (Table II). Probable structures with major components of Linseed Oil and Chinawood Oil are shown in Figures 9 and 10.

The mechanisms of the auto-oxidation of drying oils are different depending on the structure of the fatty acids that constitute the triglyceride. Fatty acids with non-conjugated double bonds, for example Linolenic Acid or Oleic Acid (the main components of the Linseed Oil), react with molecular oxygen to form hydroperoxides. Fatty acids with conjugated double bonds, for example eleostearic acid (the main component of Chinawood Oil), react differently by producing cyclic peroxides.<sup>17-21</sup> This auto-oxidation reaction for both oils proceeds via a free radical mechanism.<sup>22, 23</sup> During the film formation many different products are formed because other reactions such as isomerization are happening in parallel.<sup>18, 24, 25</sup> Hydroperoxides decompose into many products: epoxides, alcohols, diols, ketones, carboxylic acids, aldehydes, and various isomerization and polymerization products.<sup>17</sup>

Considering for example the auto-oxidation of a non-conjugated fatty acid, the mechanism has an induction period during which free radicals are formed. This mechanism is initiated by light, heat or a compound that generates free radicals (*e.g.*, peroxides) (Figure 11). The olefin radical formed subsequently isomerizes, and the isomerization process leads to conjugated hydroperoxides.<sup>17, 18, 22-25</sup> The obtained hydroperoxide (-OOH) is quite unstable and undergoes heterolytic cleavage between the two oxygens (-O—OH), producing an oxygen free radical (O·). That radical initiates a reaction with a double bond in another chain and forms an oxygen-carbon bond. The cross-linking process generates still another free radical, a carbon free radical, which can react with yet another double bond in a new chain, forming a carbon-carbon bond. This process continues until all (or almost all) of the carbon-carbon double bonds are cross-linked.<sup>18</sup> For Chinawood Oil the mechanism of auto-oxidation and cross-linking is similar to that observed for Linseed Oil, again showing that conjugated double bonds favor these reactions and the film will therefore dry faster.<sup>21-23</sup> Moreover, the resultant film is intended to be thinner and smoother for aesthetic reasons. Sims reported that there is a difference in kinetic order between the polymerization of non-conjugated and conjugated oils.<sup>26</sup> Linseed Oil has a first-order behavior, while second-order kinetics is observed for Chinawood Oil polymerization. This is of course evidence that the mechanisms of reaction for both oils are different.<sup>26</sup>

This difference in reactivity was observed during this work. Glass plates (1.0 cm width, 1.5 cm length, 2.0 mm thickness) containing approximately 0.200 g of sample were initially studied. Slides were well-suited for Linseed Oil samples because it is viscous and thus forms a thick film. However, compared to Chinawood Oil, the slide will thus contain a higher quantity of Linseed Oil per cm<sup>2</sup>. A Chinawood Oil film is easier to remove and transferred to a NMR tube than Linseed Oil film, which has a gel-like consistency in ageing experiments performed under mild conditions (*vide infra*). The solution to this problem was

to work with NMR tubes of 2.0 cm length because those fit easily into the Ageing Chamber, thus permitting the same mass to be applied for both analytes (Figure 12).

A “yellowing” reaction is a chemical change that occurs in films that contain fatty acids with isolated double bonds. The yellowing is caused by formation of colored polyenes or quinone structures, starting from conjugated unsaturated hydroperoxides via ketones as intermediates. The formed 1,4-diketones may also react with nitrogen to yield substituted pyrroles that can form colored products by oxidation. Linseed Oil presents fatty acids with non-conjugated bonds so *a priori* a yellow color is expected. Naturally Linseed Oil will yellow in the dark but the yellowing will largely disappear if the film is exposed to light. Irreversible yellowing takes place if films of Linseed Oil and related products are aged or baked at higher temperatures (Figure 13).<sup>17-19, 27, 28</sup>

## **Experiments**

### **Experiment A: Short Heating Exposure Time (up to 14 hr) at 100°C (with previous drying of sample)**

Samples of Linseed Oil and Chinawood Oil were applied to glass slides and dried for 100 hr in a specially conditioned fume hood (25°C). Pristine samples of Linseed Oil and Chinawood Oil were also dried under the same conditions as controls. After this period of time the samples were introduced into the Ageing Chamber and exposed to a constant temperature of 100°C for variable amounts of time (at 2 hr intervals up to 14 hr). The samples were prepared in duplicate. After the artificial ageing process was finished, Raman spectra were collected (also in duplicate) (Figures 14 – 17).

In Figure 14 the spectra for the pristine sample of Linseed Oil including the corresponding Raman shifts is shown. It is evident that the spectrum of the pristine sample has the same features as those found in the literature.<sup>11</sup>

For drying oils the assignment of the Raman shifts are very well studied:<sup>4, 5, 7, 8, 11</sup>

- The symmetric =C-H stretching vibration of cis double bonds (H-C=C-H) can be found around 3010 cm<sup>-1</sup>.
- The region between 3010 and 2980 cm<sup>-1</sup> is characteristic of C-H stretching vibrations.
- The symmetric and antisymmetric C-H stretching vibrations of methyl (-CH<sub>3</sub>) and methylene (-CH<sub>2</sub>-) groups appear in the region between 2850 and 2980cm<sup>-1</sup>.
- The region between 1800 and 2600 cm<sup>-1</sup> did not contain any significant bands.
- The ester stretching  $\nu(\text{C}=\text{O})$  can be found at 1747cm<sup>-1</sup>, and the cis double bond stretching  $\nu(\text{C}=\text{C})$  appears at 1655 cm<sup>-1</sup>.
- Under 1500cm<sup>-1</sup> appear three signals: the symmetric rock in cis double bond  $r(=\text{C}-\text{H})$  at 1265 cm<sup>-1</sup>; the in-phase methylene(CH<sub>2</sub>) twist at 1302 cm<sup>-1</sup>; and at 1442 cm<sup>-1</sup> the scissoring mode of methylene  $\delta(\text{CH}_2)$  was observed.<sup>4, 5, 7, 8, 11</sup>

Experimental results for the sample of Linseed Oil fit very well with the values found in the literature. The major differences between the spectra for the different oil media are located for the bands at 1265, 1657 and 3011 cm<sup>-1</sup>, which correspond to vibrations in *cis* double bonds. As many unsaturated bonds are present, the intensities of these signals are correspondingly larger. This fact can be corroborated with the comparison of the corresponding Raman spectra for Chinawood and Linseed Oil. Even though in this case both oils are highly unsaturated and the difference is not as evident as if a wax and a drying oil were compared.<sup>11</sup>

As seen in Figures 15, 16 and 17, with continued ageing the peaks in the Raman spectra reveal in general an increase in intensity and also broadening and distortion. The bands in the region between 0 and 800  $\text{cm}^{-1}$  are not very helpful because the signals become weaker and broader as the ageing experiment progresses. If we compare the spectra before and after ageing, the main effect of the drying process is the loss of the bands at 1265  $\text{cm}^{-1}$ , 1657  $\text{cm}^{-1}$  and 3010  $\text{cm}^{-1}$  because of the loss of cis double bonds (Figures 16 and 17). In addition, the increase of the intensity for peaks at 1298  $\text{cm}^{-1}$  and at 1444  $\text{cm}^{-1}$  can be attributed to the methylene deformation that is happening during the polymerization process. The development of a peak at 1737  $\text{cm}^{-1}$  occurs because of the formation of carbonylic compounds as a result of the auto-oxidation reaction. Finally, polymerization also shows effects on the intensities of the alkyl bands at 2856, 2910 and 2914  $\text{cm}^{-1}$ .

#### **Experiment B: Tube Sealing Integrity Test**

The experiments were performed on glass slides or in NMR tubes. At 100°C some issues arose when working with tubes because as the samples were being heated, they were ejected toward the walls of the Ageing Chamber. To solve this problem, different methods for securely closing the end of the tube were tested. A key requirement for the closure methods was to avoid any modification of the sample within the NMR tube. Glass wool caps and Teflon caps were made but were not effective in avoiding spillage of the sample because they were removed by the increasing pressure inside the tube. Finally the method of choice for sealing the tubes was to melt the end of the tube (Figure 18). At 100 °C, nevertheless, some pressure-induced spillage was still present. However, the glass ceiling method was effective in performing the experiment at 50 °C.

As a way to determine if the glass-melted sealed tubes were leaking, and also, to investigate what type of compounds were being ejected from the sample, the following experiment was performed: samples of Linseed Oil were exposed to 50 °C in NMR glass tubes sealed with melted glass and put inside a transparent vial (Figure 18). At the same time, together with the other samples, a control sample in which the NMR tube was not sealed was introduced into the chamber. This was done to check the amount of volatile compounds that were lost from the sealed tubes during the experiment (Figure 19).

The vials were introduced into the Ageing Chamber and exposed to a constant temperature of 50°C for 100 hr. Samples were analyzed by a GC with thermal conductivity detection (DB-1, 0.25 mm film, 30 m, splitless).

The results showed clearly that in the headspace of all the sealed-tube vials several compounds were present at significant levels (up to nearly 20%). Simply by comparing the peak areas and taking into account that the same amount of sample was initially present in each tube, it was possible to conclude that the loss through the glass seal ranged from 4-18% for the solutes that we observed in the chromatogram (Table II). According to the literature<sup>29,30</sup> the volatile organic compounds (VOC) could be: Hexanal, Pentanal, Heptanal as well as a myriad of other aldehydes, ketones and carboxylic acids. Juita *et al.* demonstrated that the concentration of propanal, hexanal, 2-pentenal, 1-penten-3-ol, 2,4-heptadienal, 2,4-decadienal, 3,5-octadien-2-one, ethanoic acid, and hexanoic acid in the oil increased during the first six hours of oil oxidation.<sup>29</sup> For oils rich in non-conjugated fatty acids, such as Linseed Oil, the main VOC is hexanal.

### **Experiment C: Short Heating Exposure Time (up to 16 hrs) at 50°C**

In another experiment, samples of Linseed Oil, Linolenic Acid and Oleic Acid were exposed to high temperature conditions (50 and 100°C) for variable amounts of time (2-16 hr at 2 hr intervals) in the Ageing Chamber. The samples did not need to be dried in the fume hood because they were prepared in NMR tubes (2 cm long). The resulting Raman spectra for the temperature study at 50°C are shown in Figures 20-22.

It is interesting in this case to compare the sample spectra because Linolenic Acid and Oleic Acid are components of the Linseed Oil. Because of the fatty acid percentage present in the triglyceride (48 % for Linolenic Acid; 23% Oleic Acid) and their saturation grade, it is logical to assume *a priori* that the Linolenic Acid spectrum has to resemble that of the Linseed Oil, which was confirmed (Figure 20 and 22). In Figure 21, it is possible to observe clearly the differences in the Linseed Oil versus Oleic Acid spectra in the following shifts: peaks at 1264  $\text{cm}^{-1}$  and 1743  $\text{cm}^{-1}$  are not present in the Oleic Acid spectrum; and peaks at 1439  $\text{cm}^{-1}$ , 1656  $\text{cm}^{-1}$  and 3010  $\text{cm}^{-1}$  are much less intense in the oleic acid spectrum. In Figure 22 it is possible to observe the similarity between the spectra, of Linseed Oil and Linoleic Acid, only the peak at 1743 $\text{cm}^{-1}$  is absent in the Linoleic acid spectrum. According to the literature, the signal at 1744  $\text{cm}^{-1}$  is the result of the presence of the ester carbonyl groups in the triglyceride.<sup>4</sup>

The differences between Oleic Acid and Linoleic Acid are the result of their different saturation grades (Iodine Values equal to 90 and 274 respectively).<sup>31</sup>

**Experiment D: Long Heating Exposure Time (100 hrs) at 50°C**

The FT-Raman spectra of the samples from Experiment B were obtained and compared to those obtained in Experiment A. In both experiments the pristine sample had been aged for 100 hr, but in the latter at low temperature (25°C) and in the former at high temperature (50°C). Figure 23 shows that a drastic change in peak intensities was observed.

**Experiment E: Short Heating Exposure Time (2 hr) with Variable Temperature (60 to 210°C)**

Samples of Linseed Oil and Chinawood Oil were exposed for a constant amount of time (two hr) at variable temperatures (60 to 210°C). With increasing temperature, peak broadening in the range of 0 to 2000  $\text{cm}^{-1}$  was observed. The yellowing processes that are reversible at ambient temperature appear to be irreversible at high temperatures. By observation of degree of "yellowing" in the sample, one can conclude that at temperatures below 90°C the yellowing is reversible (Figure 12(b)). Thermal treatment (unlike photochemical) acts as a catalyst for the polymerization reactions that contribute to "yellowing". Thus, a "threshold temperature" will force the equilibrium to move irreversibly toward the oxidized products. This effect is clearer for Chinawood Oil than for Linseed Oil because of the conjugated double bonds that are present in Chinawood Oil, making the polymerization reactions occur much faster. At much higher temperatures than ambient temperature, the oil is literally baked, which implies that other chemical reactions occur that are different from the "yellowing" ones (Figure 24).



**Experiment F: Short UV-light Radiation Exposure Time (up to 14hrs) at 25°C**

Another experiment was performed at constant temperature in which samples of Linseed Oil were exposed to 25°C for variable amounts of time inside the Ageing Chamber but under UV light. The time interval was 2 hr, the exposure time varied from zero to 14 hr, and the samples were in the NMR tubes.

It is important to note that drastic changes in the color of the samples were observed during thermal ageing experiments, but not with the UV light ageing experiments (Figure 12(a)). Only very subtle differences between the aged and pristine samples were observed (Figure 25). Clearly the thermal and photochemical ageing mechanisms are quite different.

**Experiment G: Long UV-light Radiation Exposure Time (170 hr) at 25°C**

In this experiment the exposition time to UV light was extended to 170 hr (25°C), as a means to determine the upper limit at which oxidation commences. In this case, stark changes between the aged and the pristine sample were observed (Figure 26).

## 3.2 Analysis of Humic Acids by Liquid Chromatography

### 3.2.1 Two-Dimensional Liquid Chromatography — An Overview of the Theory & Practice

Chromatographic methods are powerful and versatile tools for separating and determining a wide variety of atomic and molecular species. However, it can be a difficult task such as in the case of HAs given that they are very complex mixtures, numbering thousands of solutes. To efficiently separate these compounds, our research group is developing a two-dimensional liquid chromatography system (LCxLC). LCxLC systems have been used for many years to characterize and separate complex mixtures.<sup>32-37</sup> LCxLC systems subject the sample to consecutive, on-line chromatographic separations using orthogonal retention mechanisms, thereby providing a separation efficiency that is in theory the product of the individual peak capacities.<sup>38-44</sup>

There are two general types of LCxLC instrument designs: In "Comprehensive" LCxLC instruments, the entire first dimension is sampled and injected as aliquots into the second dimension, whereas "Heart-Cutting" instruments "slice" specific zones from the first dimension.<sup>38</sup> A variety of interfaces for the two columns have been studied over the past two decades, as reviewed by Jorgenson.<sup>45</sup> The most common way for one to perform an LCxLC separation is for the first-dimensional separation to be relatively slow, with a typical analysis time of one hour or longer. The fractions of the effluent from the first-dimension column are collected and injected onto the second column, which provides a much faster separation, typically with an analysis time of  $\sim 1/50$ th of the first dimension. The separations employ mechanisms that are as different as possible to maximize selectivity (termed "orthogonality").<sup>38</sup> The total analysis time is determined by the speed of the first

dimension whereas the overall efficiency is primarily a function of the speed of the second dimension. Optimization of multidimensional separation systems requires that one understand the relationship between chromatographic resolution and the number of second dimension samples that are found within a (typical) peak in the first dimension. LCxLC is not truly comprehensive in that one has to periodically sample the first dimension because only a small volume is needed in the second dimension. To obtain minimal two-dimensional resolution, the sampling frequency should be no more than one-third of the standard deviation of the narrowest peak in the first dimension.<sup>42</sup>

LCxLC potentially has the peak capacity and the selectivity to separate mixtures of humic substances. Humic substances are complex, amorphous mixtures of highly heterogeneous, chemically reactive yet refractory molecules that are produced during the decay of biological material.<sup>46-48</sup> Humic substances are formed ubiquitously in the environment via processes involving chemical reactions of species randomly chosen from a pool of diverse molecules and through random chemical alteration of precursor molecules.<sup>49</sup>

There are many combinations of separation techniques that one can use in LCxLC to achieve "orthogonality". In our work for the first dimension, we studied an ion-exchange high-pressure liquid chromatography (HPLC) method (IEX-HPLC or, more commonly, simply "IC"). This approach is well-suited to humic compounds because humic substances contain numerous carboxylic acid ( $-COOH$ ) functional groups. For the second dimension, we studied a reversed-phase (RP) low-pressure liquid chromatography (RP-LC) method with molecular fluorescence and absorption (UV-VIS) spectroscopies as the methods of detection. Because we are employing a conventional anion-exchange IC method, our work focused on developing the RP-LC method for the second dimension.

### **Reversed-Phase Liquid Chromatography (RP-LC)**

In RP-LC a molecule with hydrophobic regions interacts with the immobilized hydrophobic molecule (ligand) that constitutes the stationary phase and is retained as a function of its relative hydrophobicity. The sample is applied to the column as an aqueous solution, and the solutes are transported in a mobile phase that is primarily aqueous, though modified with an organic solvent. Elution can proceed either by isocratic conditions, where the composition of the mobile phase is constant, or by gradient elution, where the composition of the mobile phase changes during the development of the chromatogram. The amount of organic modifier is varied to optimize the efficiency of the separation.<sup>3, 50</sup> Generally, the solutes elute in order of increasing molecular hydrophobicity. The type and concentration of organic modifier in the mobile phase generally leads to greater retention so separations can be optimized by changing the organic modifier.<sup>3, 51</sup> A schematic diagram of this process is shown in Figure 27.

The best known ligands used for RP-LC are *n*-butyl (C4), *n*-octyl (C8) and *n*-octadecyl (C18), and they are covalently attached to a silicone support.<sup>51-54</sup> To improve the separation of compounds with similar hydrophobicity, one can use different ligands that provide a secondary interaction in addition to a hydrophobic interaction, such as a phenyl ligand, which provides a  $\pi$ - $\pi$  interaction with the analyte, or a tri-phenyl ligand which provides a  $\pi$ - $\pi$  interaction and stereo-selectivity (Table IV).<sup>53</sup> These columns can be prepared with a stationary phase support that is based on either silica or a polymer (*e.g.*, polystyrene).

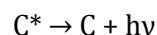
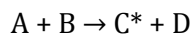
LC columns can be classified based upon their physical structure into two general types: particle or monolithic. The manufacturing processes to obtain these two groups of columns are different because one group of columns is formed with discrete porous

particles, which have to be synthesized, characterized, and packed in a multi-step process, whereas the other group of columns is formed by a single mass of very porous stationary phase with a simpler (one step) *in situ* preparation.<sup>52, 55-57</sup> In a column that is packed with particles, the accessibility of solutes to the stationary phase ligands is a function of the size of the pores within the stationary phase and the size of the particles. A monolithic column does not contain inter-particle spaces, so the mobile phase flows through a network of pores (Figure 28) that vary from ~10 nm to >1 μm in diameter (known as “micropores” and “mesopores”, respectively).<sup>52, 58</sup> The surface area of monolithic columns is larger than for a packed column, and because of course all of the mobile phase flows through the stationary phase, one has higher efficiency for the monolith, and observes a relative increase in the speed of the separation. A C4 monolithic disk made with poly (glycidyl methacrylate-co-ethylene dimethacrylate-co-butyl methacrylate) (Figure 28) was used for the research described herein.

### 3.2.2 Fluorescence Spectroscopy — An Overview of the Theory & Practice

Luminescence is the emission of light from a molecule and occurs from electronically excited states. Luminescence is divided into Chemiluminescence and Photoluminescence.

Chemiluminescence is produced when the product of a chemical reaction (in an excited electronic state) emits light as it returns to its ground state:



Chemiluminescence reactions are common in several biological systems, where the process is called bioluminescence. Many organisms have evolved to produce light for example, some deep sea organisms and the firefly.<sup>3</sup>

Photoluminescence is formally divided into two categories—fluorescence and phosphorescence—depending on the nature of the excited state. In Fluorescence, one has excited singlet states so the electron in the excited orbital is paired (*i.e.*, opposite in spin) with the electron in the ground state (Figure 29a), and the emission of light occurs fast because it is “spin allowed”.<sup>59</sup> The processes that occur between the absorption and emission of light are illustrated by the Jablonski diagram. A typical Jablonski diagram is shown in Figure 29b.<sup>59</sup>

In the diagram one can recognize the singlet ground state  $S_0$  and its higher electronic energy levels, which can be singlet ( $S_1, S_2, S_1$ ) or triplet ( $T_1$ ). Triplet states are those in which the excited state electron is unpaired (*i.e.*, same spin) as the ground state. Within each of these electronic energy levels occur a variable number of vibrational energy levels ( $V_0, V_1 \dots V_n$ ). When the sample is irradiated by a high energy light source such as a Xenon lamp, electrons can absorb energy and be promoted to a higher energy level (*e.g.*,  $S_1$  or  $S_2$ ) depending on the quanta of energy absorbed. Relaxation of the excited initially occurs by the dissipation of heat from higher vibrational levels within the excited electronic state to the lowest vibrational level (*e.g.*, denoted as  $S_1, V_0$ ). The emission of light from the electronic excited singlet level to the ground state is called fluorescence. Alternatively, certain molecules in the  $S_1, V_0$  state can undergo a spin conversion to the first triplet excited state  $T_1$  in a process called “intersystem crossing”<sup>59</sup>. Emission from  $T_1$  is called phosphorescence, and is found at longer wavelengths (lower energy) relative to fluorescence.

The rate of photon absorption is very rapid and takes place in about  $10^{-14}$  to  $10^{-15}$  s. Fluorescence typical lifetime is near 10 ns ( $10^{-8}$  s). In phosphorescence the transitions to the ground state are spin forbidden and the emission rates are slower, so phosphorescence lifetimes can be seconds.

Fluorophores can be divided into two main classes — intrinsic and extrinsic.<sup>59</sup> Intrinsic fluorophores are those that occur naturally, such as found in the aromatic amino acids; extrinsic fluorophores are covalently bound to the sample molecule to provide fluorescence when the molecule doesn't fluoresce (or has low fluorescence yield). Many factors affect the fluorescence yield including temperature, pH, polarity of the solvent, the presence of fluorescence quenchers and inner filtering effects.<sup>3, 59</sup>

### 3.2.3 Separation of Complex Organic Mixtures

#### Amino Acid Model

There have been numerous fluorescence studies about the presence of protein-like substances in water and soils.<sup>60-62</sup> Aromatic amino acids were studied herein because they are natural fluorophores present in humic matter.<sup>60</sup> Although the characteristic emission bands of protein-like substances in soils and waters sample are not in the same region as the emission bands of humic-like substances, for simplicity, we initially studied fluorescent amino acids tryptophan, tyrosine, and phenylalanine.<sup>54, 55</sup> The indole groups of tryptophan (TRP) residues are the dominant chromophores for molecular absorption and emission (fluorescence) in proteins.<sup>59</sup> Tyrosine (TYR) has an emission spectrum more narrowly distributed on the wavelength scale, and phenylalanine (PHE) has the weakest emission in presence of tryptophan and tyrosine (Figure 30).<sup>59</sup>

The goal of this work was three-fold: (1) develop a fluorescence detection approach for the three aromatic amino acids; (2) optimize the separation of the amino acids by using a monolithic column; (3) study the separation of HA mixtures using the three amino acids as standards for quantitation.

### **Characterization of the Amino Acid Standards**

Using the emission wavelength values for TYR, TRP, and PHE found in the literature<sup>59</sup>, the excitation and emission wavelength values for these samples were determined experimentally with a high-resolution spectrofluorimeter, the FluoroLog®-3 system. The spectra were obtained in the range of 200 to 600 nm with entrance and exit slit bandpasses equal to 2.0 nm. The absorption and emission wavelengths that were observed for the individual amino acids correlated well with the literature values (Table VI).<sup>59</sup> The three amino acids were then evaluated by studying their emission intensity using all their individuals' excitation wavelengths. The intensity of the signal for all amino acids with  $\lambda_{ex} = 257$  nm (excitation wavelength for PHE) varied between  $3 \times 10^4$  and  $1 \times 10^5$ , and a clear signal was observed for each of the amino acids (Figure 31). Using  $\lambda_{ex} = 274$  and 280 nm (excitation wavelengths for TRP and TYR, respectively) the results were poor because the intensities of the signals were too dissimilar. The signal for TYR was comparatively very large; and this could thus lead to difficulties in distinguishing a mixture of the three amino acids (Figures 32 and 33). On the other hand, at the optimal emission wavelength (310 nm), a clear signal was observed for each of the three amino acids (Figure 31). Therefore the excitation and emission wavelengths chosen for a mixture of the three amino acids were  $\lambda_{ex} = 257$  nm and  $\lambda_{em} = 310$  nm.

To perform the chromatographic optimization, instead of using a univariate ("one-factor-at-a-time") approach, we applied a two-level screening design based upon a Plackett-



Burman model for seven factors.<sup>63</sup>

Usually the conventional method to optimize a process is by studying one factor at a time, *i.e.*, while holding all other factors constant. This is a time-consuming, inefficient approach because the interactions between different factors will not be observed. In the multivariate approach, multiple factors are changed simultaneously so that the effects of different factors at different levels can be determined to identify which factors are most significant.

To determine which factors are most significant and interacting with one another, so-called "screening designs" are used. The most effective screening design was proposed by Plackett and Burman in 1946.<sup>63</sup> Plackett and Burman proposed a series of basic designs based on balanced incomplete blocks. Each design of N experiments is used for studying up to (N - 1) variables. The original Plackett-Burman theory suggested basic designs for N = 8, 12, 16 and 20, up to 100 experiments.<sup>63</sup> In this approach, a matrix is constructed, defining a fixed first row with the remainder of the matrix generated by shifting the first row cyclically one place (N - 2) times and then adding a final row of minus signs.<sup>64</sup> The result is a matrix containing N rows and N - 1 columns (Table V).

For example, the first row of the Plackett-Burman design for N = 8 and 7 factors is: (+++-+--) <sup>63</sup> The factor's effect is calculated using the response obtained for all the experiments. The general formula is:

$$\text{Effect} = [\sum (Y^{(+)}) - \sum (Y^{(-)})]/N$$

For example, the effect for the factor A ( $E_A$ ) in a seven factor study is:

$$E_A = [(Y_{1+} + Y_{4+} + Y_{6+} + Y_{7-}) - (Y_{2-} + Y_{3-} + Y_{5-} + Y_{5-})]/8$$

One difficulty with the Plackett-Burman approach is that the main effects are sometimes confounded with two-factor interactions. To remove this confounding a "foldover" design is used. This design is a reflection of the original design. For a seven factor Plackett-Burman the foldover matrix contains 16 experiments in which the last eight experiments are a reflection of the first eight. The calculation of the effect of the factors is the same but with  $N = 16$ .

The factors chosen for screening in this study were: amino acid concentration, injection loop volume, mobile phase flow rate, type of organic modifier, percentage of organic modifier, mobile phase pH, and a "dummy factor" (whether ultrasonic de-gassing of the mobile phase had been done), *i.e.*, to have a total of seven factors so that the Plackett-Burman matrix could be completed.

The mobile phase was composed of an organic modifier combined with high purity (18 M $\Omega$ -cm) water (hereafter referred to as "reagent water"). The organic solvents most commonly used as RP-LC mobile phases are acetonitrile and methanol.<sup>50</sup> Acetonitrile was chosen for this work because it has a lower UV cut-off (~190 nm). Furthermore, it is less viscous than methanol, thus causing less fluctuation in pressure in the column. Methanol was nevertheless compared to acetonitrile as a factor in the Plackett-Burman design as a means to compare two different levels (*i.e.*, "mobile phase type").

The pH was chosen based upon the different pK<sub>a</sub> values of the aromatic amino acids (Table VII) and the consequent structures present in the mixture (Figure 34). Depending upon solution conditions, amino acids can exist in various forms: cations, anions or as zwitterions (in which the net charge is zero) (Figure 34). Because the stationary phase in the monolithic column was reversed-phase, the zwitterionic species would intuitively seem to be the more retained of the various forms.

The matrix for the Plackett -Burman study for the seven factors is shown in Table VIII. Results are presented in Table IX. The study showed that, in decreasing order, factors #6 (pH), #4 (type of organic solvent) and #5 (percentage of organic solvent) were most significant.

To understand the effect of pH, the variation of the fluorescence intensity, as a function of pH, was studied. The absorbance and emission wavelengths presented in Table VI were determined at pH=7.00.<sup>59</sup> At pH=7.00 the dominant species is the zwitterionic form. In addition, it is seen that when one varies the pH, the emission wavelength for the amino acids is notably affected (Figure 35).<sup>59</sup> The observed signal intensities for the three amino acids were almost constant for pH values between 3.00 and 9.00, so the examination of a sample containing a mixture of these amino acids is possible in this range (Figures 36 and 37).

To find the optimal mobile phase composition, different mixtures of the amino acid stock solutions in two solvents were studied (Table X). For mixtures that included methanol, low fluorescence intensities were observed in the chromatogram and the amino acids could not be resolved (Figure 38); for mixtures with acetonitrile, larger fluorescence intensities were obtained and the resolution of the signals for the mixture depended upon the proportion of acetonitrile (Figures 38 and 39).

To find the optimal mobile phase flow rate, a range between 0.5 and 2.5 mL/min was studied. Figure 40 shows that when the flow rate was increased, the retention time was reduced. However, the change in the total run time is not as important as the increase in pressure of the system. At a flow rate of 2.5 mL/min, an increase in the diameter of the tubing, in the pump, was observed. The intensity of the peaks at a flow rate of 0.5 mL/min was very low, because of their broadness, while the intensities of the peaks for the other flow rates were comparable (Figure 41).

The optimal RP-LC system conditions chosen for the model mixture of amino acids were: 30:70 (% v/v) acetonitrile: phosphate buffer, pH 7.00; 1.0 mL/min; 100  $\mu$ L sample volume; excitation wavelength = 257 nm and emission wavelength = 310 nm.

### **Separation of Humic Acids**

Fluorescence techniques have been used widely in the study of humic substances because it provides important information on the chemical nature of the humic substances. Soil HAs have molecular masses ranging from several hundred to several hundred thousand Daltons. Because an array of different chemical functional groups is present in the humic macromolecules (Figure 42), the observed fluorescence spectra are complex. The position and intensity of the peaks can be correlated to structural information such as type of functional groups and degree of aromaticity.<sup>65-71</sup> Some general behaviors may be described.<sup>60, 67, 72-74</sup>

- When the molecular size of the humic macromolecule increases, the fluorescence intensity decreases.
- Electron-withdrawing groups decrease and electron-donating groups increase the fluorescence intensity in aromatic compounds.
- Carbonyl, hydroxyl, alkoxy, and amino groups tend to shift fluorescence maxima to longer wavelengths (bathochromic or red-shift).
- A reduction in the number of aromatic rings or a reduction in the number of conjugated bonds in a chain structure tends to shift fluorescence maxima to shorter wavelengths (hypsochromic or blue-shift).

Several standard solutions of HAs in organic solvents (heptane, hexane, cyclohexane and diethyl ether) and in buffer solutions (pH 3.00, 5.00, 7.00 and 9.00) were prepared

(Table XI). Their behavior was studied with the monolithic C4 column using a 350 nm excitation wavelength and a 430 nm emission wavelengths.<sup>75</sup> The other experimental conditions were those that had been optimized for the amino acid study. However, poor separation of individual solutes in the chromatograms was observed, and the intensities were lower than expected considering that the solutions injected were relatively concentrated (~1.5 mg/mL) (Figure 43).

### **Solid Phase Extraction**

To simplify the standard HA mixtures as a means to study individual solutes, the HA standard was subjected to Solid-Phase Extraction (SPE) (Figure 44) and the subsequent fractions were then examined by the RP-LC method described above.

SPE is a displacement chromatography technique. In this mode the sample is applied to the column and the higher-affinity solutes are preferentially retained near the head of the column while the other components migrate through the column. Then an eluent phase, chosen to selectively elute the retained species, is added and the solutes are eluted. In displacement chromatography, the steps found in the chromatogram represent pure components (Figure 45).<sup>76</sup>

Seven different types of SPE stationary phases were examined as a means to determine the optimal separation conditions given the different functional groups that may be present in a given HA sample (Table XII, Figure 46).

The goal of the SPE work was to obtain ~10 fractions for study by RP-LC as "simplified" HA mixtures. The elution solvents were chosen according the Hildebrand solubility parameters (Table XIII).<sup>19</sup>

The ENVI-8 and LC-NH<sub>2</sub> columns proved to be the most useful of the SPE approaches (Figure 47 and 48). For a normal phase (LC-NH<sub>2</sub>) experiment, a small signal from the first

fraction, extracted with acetonitrile, was detected ( $t_r = 47$  s), *i.e.*, the most hydrophilic of the fractions. In contrast, a peak was detected in the most hydrophobic fractions that were eluted with acetonitrile from the RP SPE column (ENVI-8) ( $t_r = 16$  s). Clearly these two fractions met the goal of the SPE study in that they are clearly different in polarity and fluorescence properties so that they will be useful as "simplified" HA standards for further monolithic RP-LC work.

### **Fluorescence Spectra of HA**

Each of the fractions prepared for the SPE study were studied by spectrofluorimetry to find the optimal concentration. Solution #7 was diluted (1:2, 1:4, 1:10, 1:20, and 1:50) to obtain solutions with the following concentrations: 0.650, 0.325, 0.130, 0.065 and 0.026 mg/mL, respectively. The solutions were filtered by 0.45  $\mu$ m cellulose acetate membrane filter to avoid problems caused by particles in the system.

Experiments revealed that the concentration of the HA was not directly proportional to the intensity of the peaks (Figure 49), apparently because of self-absorption of the radiation. For lower concentrations one expects to observe lower fluorescence but for dilutions 1:2 (0.65 M) and 1:4 (0.325 M), the self-absorption effect was at work. Two solutions that were intermediate in concentration, 0.130 mg/mL and 0.065 mg/mL, appeared to be unaffected and presented an acceptable emission intensity level.

The next step was to find the optimal wavelength for excitation. The wavelengths chosen for the optimization procedure were: 220, 240, 260, 280, 300, 320, 340, 350, and 370 nm (Figure 50). At 350 nm strong fluorescence intensity was obtained that is well separated from the emission spectra. Therefore, using  $\lambda_{ex}=350$  nm, all of the HA fractions from the SPE separation were examined and their spectra were compared to the characteristic peaks found for HA. The full spectra were obtained in the range of 200 to 600

nm with an exit/entrance slit bandpass equal to 2.0 nm (Figure 51 - 57). Buffers were analyzed too, and all the measurements were corrected with the corresponding buffer solution.

As seen in Figures 51 through 57, the presence of the characteristic broad peak for HA is corroborated in several fractions obtained from the different SPE columns. A maximum emission wavelength was identified for each of the SPE phases (Table XIV).

The optimized conditions found for the analysis of the SPE-separated fractions in the monolithic RP-LC were: (30:70 (% v/v) acetonitrile : phosphate buffer at pH=7.00; 1.0 mL/min; 100  $\mu$ L sample volume;  $\lambda_{ex}$  = 350 nm and  $\lambda_{em}$  adjusted according to Table XIV.

### 3.3 Figures and Tables

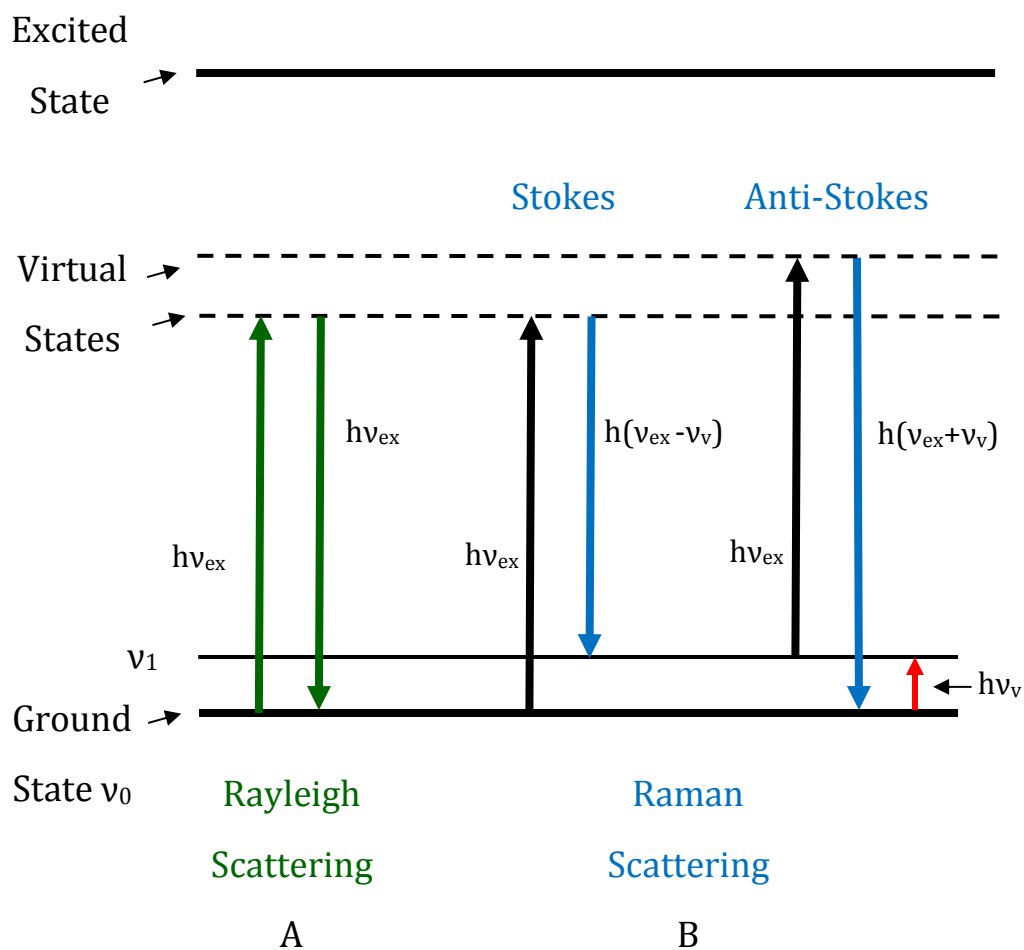


**Figure 3-1.** Spectroscopic transitions underlying several types of vibrational spectroscopy. Adapted from Skoog *et al.*, 2007.<sup>7</sup>



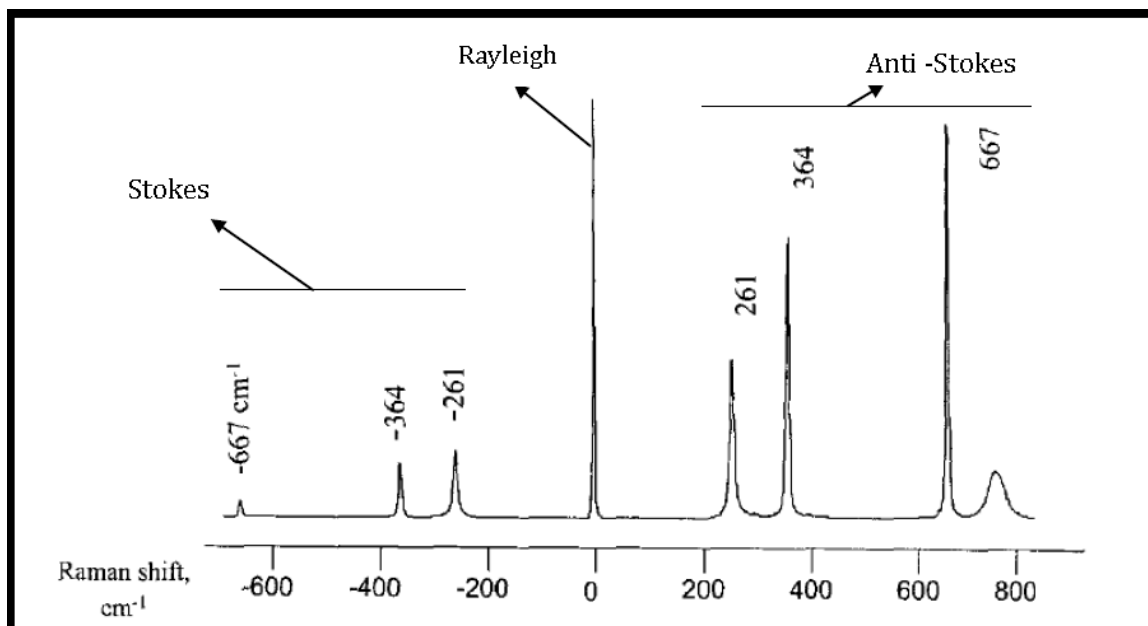


**Figure 3-2.** Raman spectrum of chloroform at room temperature obtained with a 514.5 nm source. Rayleigh scattering (at zero Raman shift) is heavily attenuated by a band reject filter (is actually several orders of magnitude more intense than the Raman scattering).<sup>9</sup>

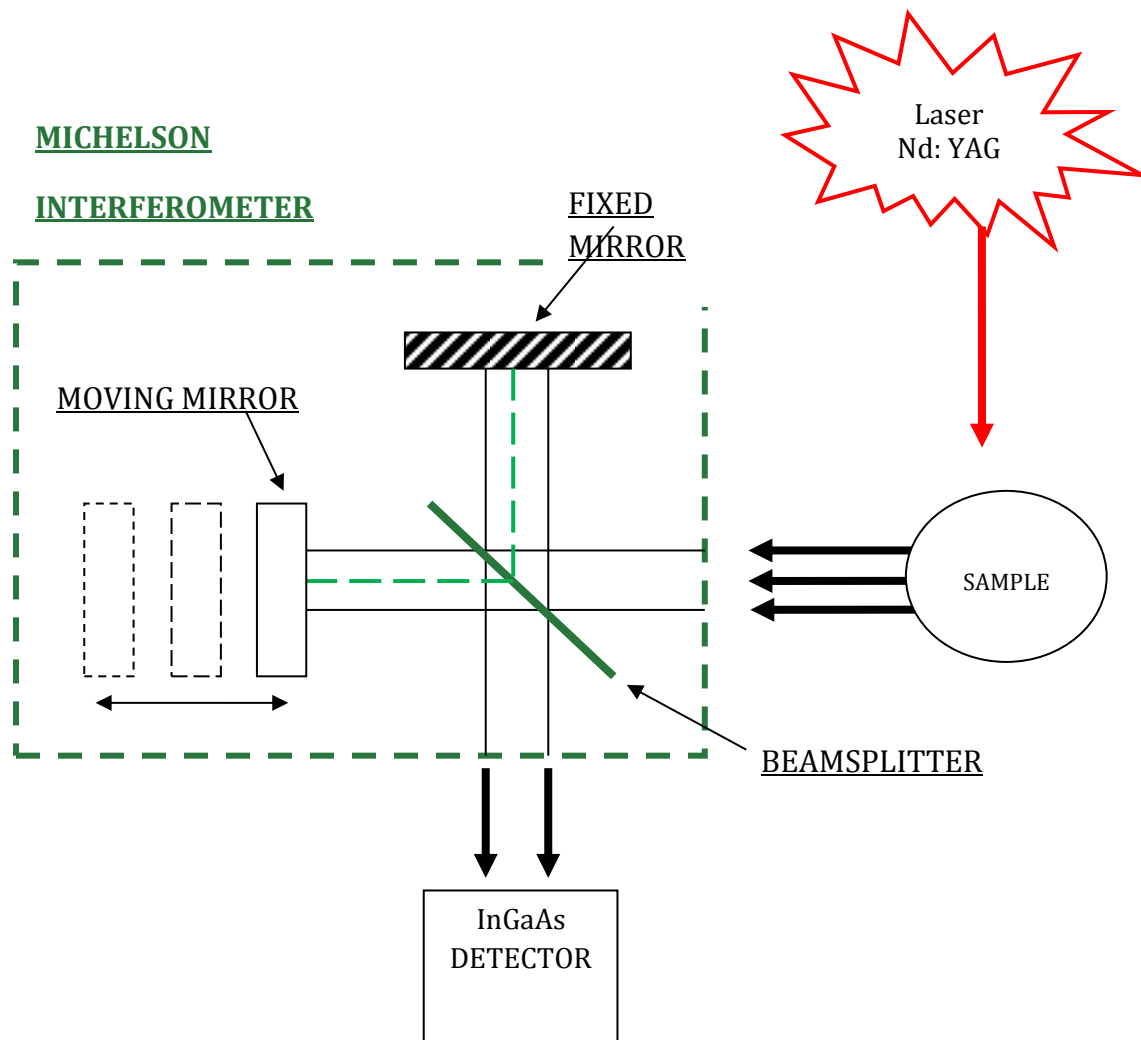


**Figure 3-3.** Schematic diagram of the Nexus 670 FT-Raman. (Adapted from FT-Raman Module User's Guide).<sup>5</sup>

**Table I.** Experimental conditions for the Raman spectrometer.**Factors**

<b>Warm up time</b>	60 min
<b>Number of scans</b>	128
<b>Resolution</b>	8 cm <sup>-1</sup>
<b>Aperture</b>	100 %
<b>Detector Gain</b>	8
<b>Laser Power (average)</b>	2.0 W
<b>Sample size</b>	1.0 g
<b>Spectral range</b>	3600-100 cm <sup>-1</sup> (Stokes)

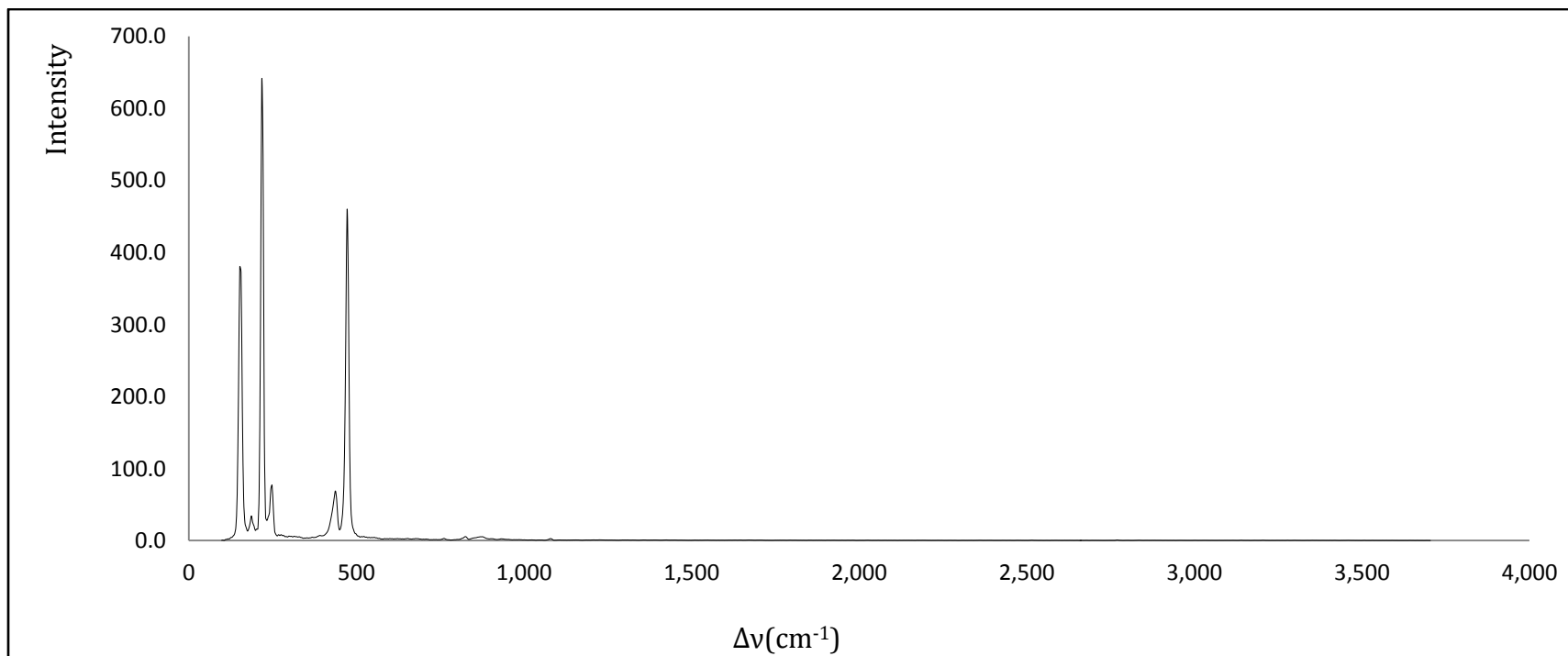


Figure 3-4. Raman spectra of a solid sulfur sample.

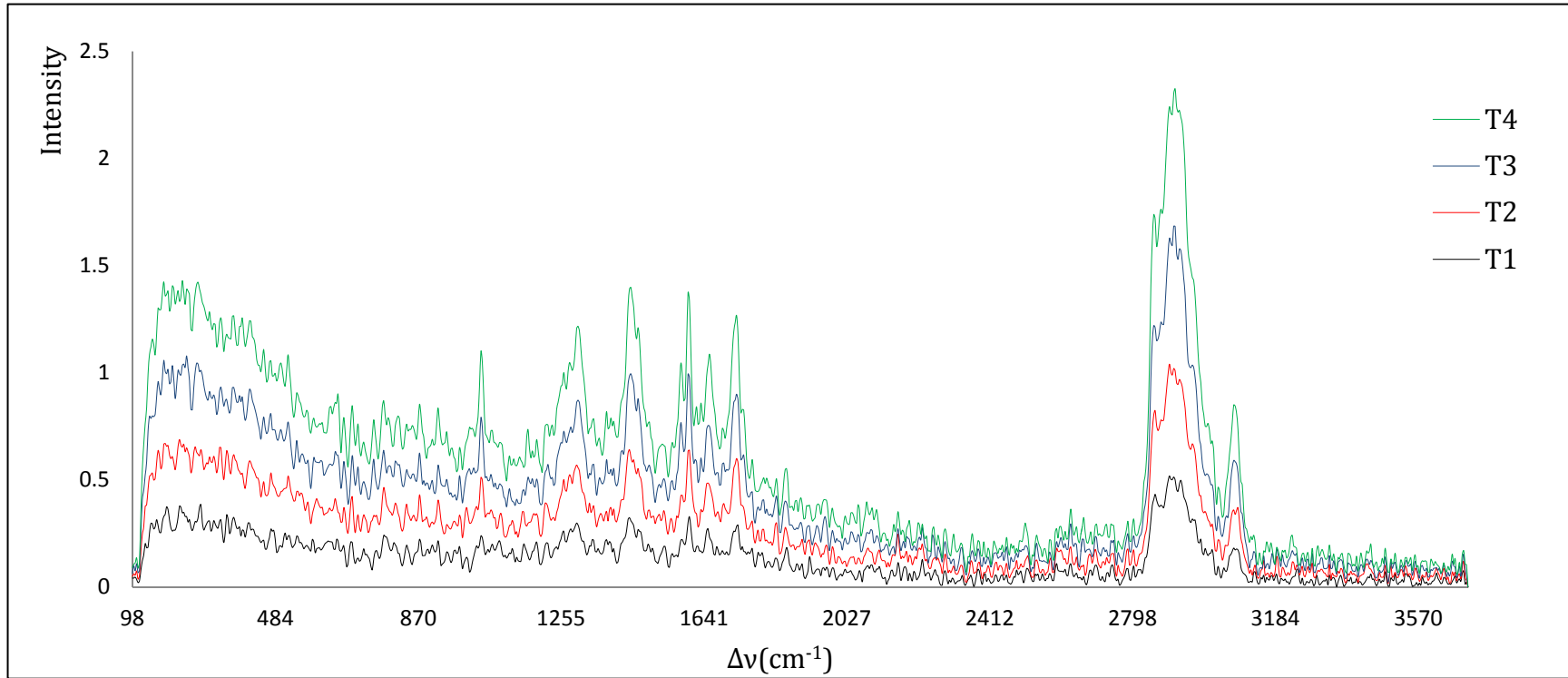
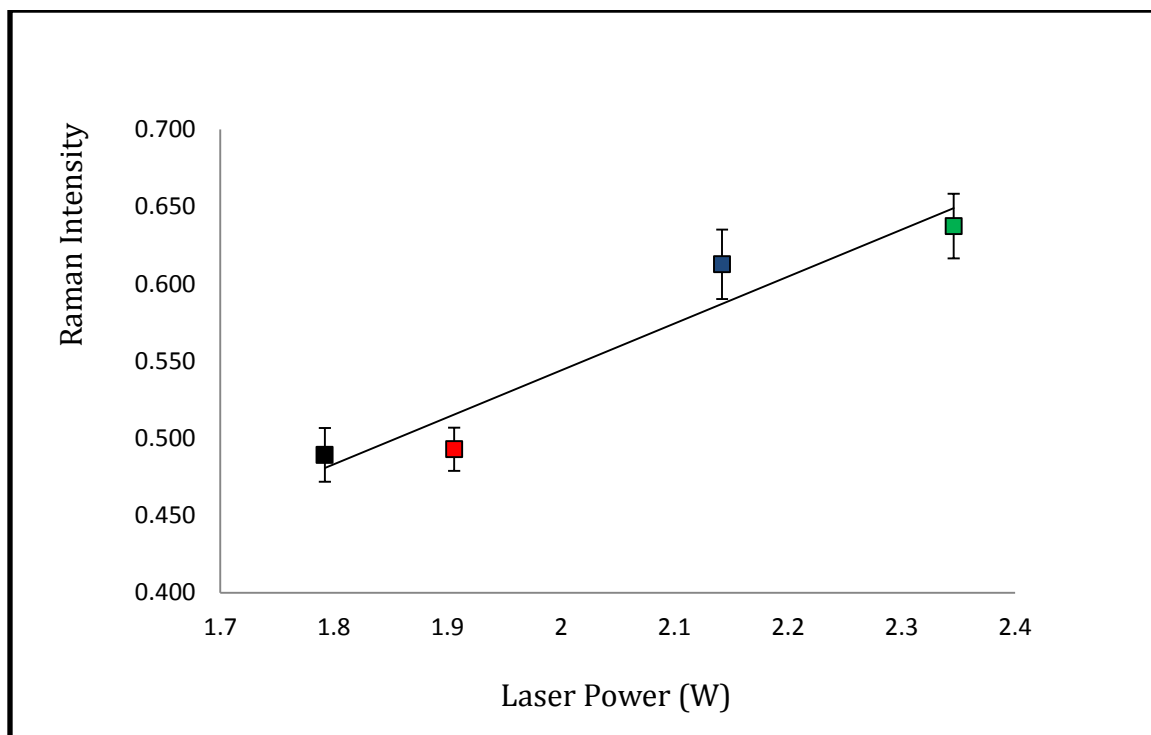
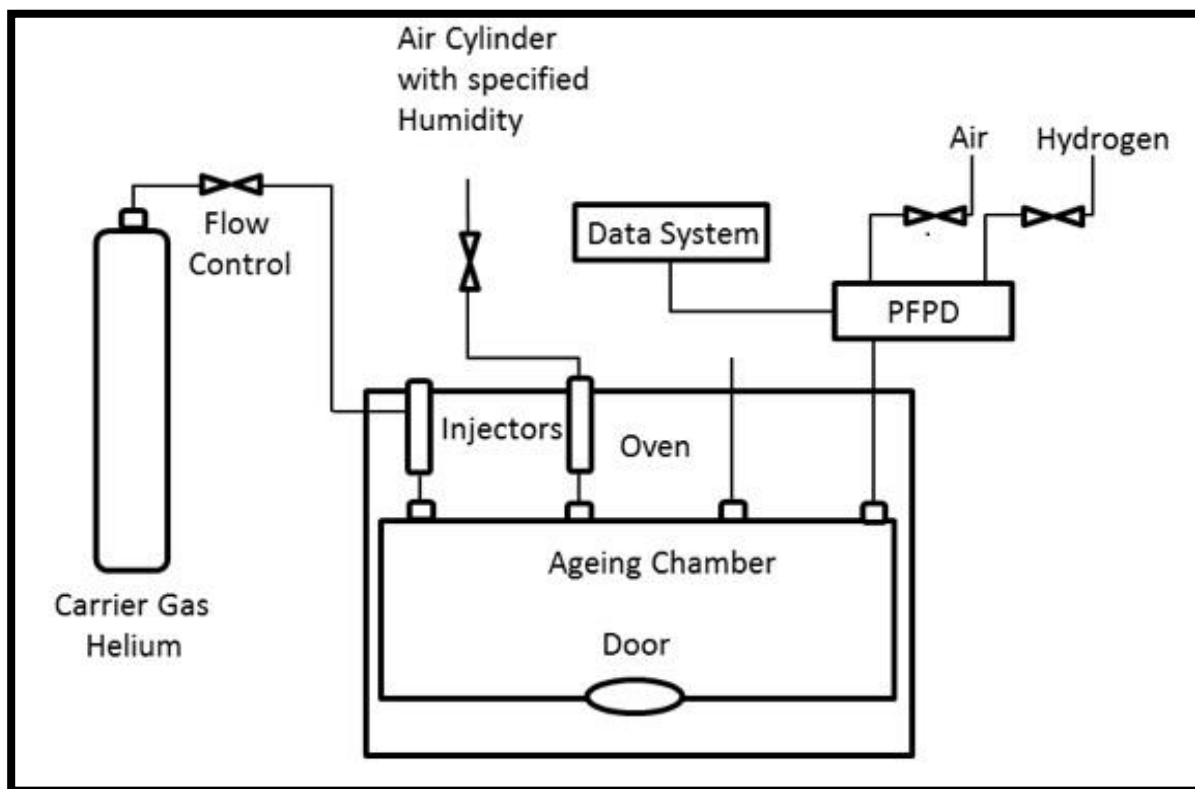


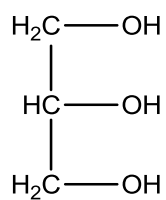
Figure 3-5. Raman spectra of a single sample of Chinawood Oil measured at different laser powers. Tests 1-4, 2 hr aged, T=100°C.



**Figure 3-6.** Variation of the Raman intensity of the major peak in the spectrum ( $\sim 3000\text{ cm}^{-1}$ ) showed using different laser power. Error bars ( $n=3$ ) are shown at 95% confidence (two-tailed) based upon the Student  $t$  value.

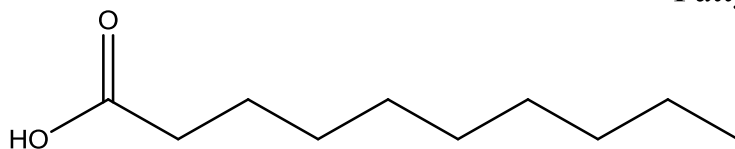


**Figure 3-7.** Schematic diagram of environmental chamber that was used for the accelerated ageing experiment.<sup>22</sup>



Glycerol

Fatty Acid



Triglyceride

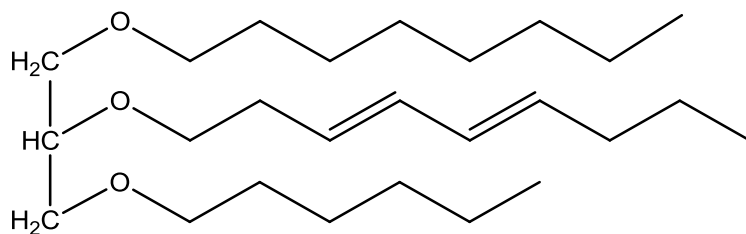
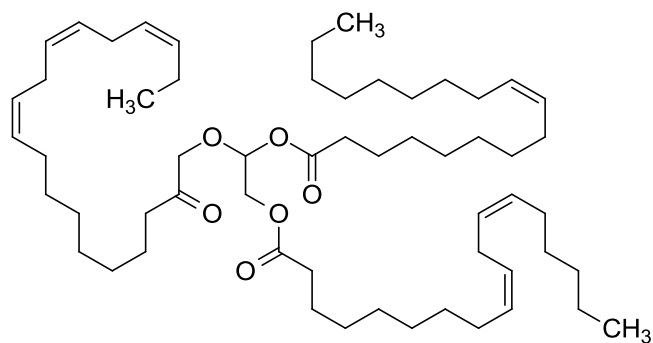


**Figure 3-8.** Structure of glycerol, general structure of a fatty acid, and general structure of a triglyceride.<sup>37</sup>



**Table II.** Percentage fatty acid composition of Linseed Oil and Chinawood Oil.

<b>Fatty acids</b>	<b>Linseed Oil (%)</b>	<b>Chinawood Oil (%)</b>
Palmitic acid (16:0)	5	4
Stearic acid (18:0)	3	1
Oleic acid (cis18:1)	23	8
Linoleic acid (cis, cis 18:2)	21	4
Linolenic acid (cis, cis, cis 18:3)	48	3
Eleosteric acid (cis, trans, trans 18:3)	-	80



LINSEED OIL

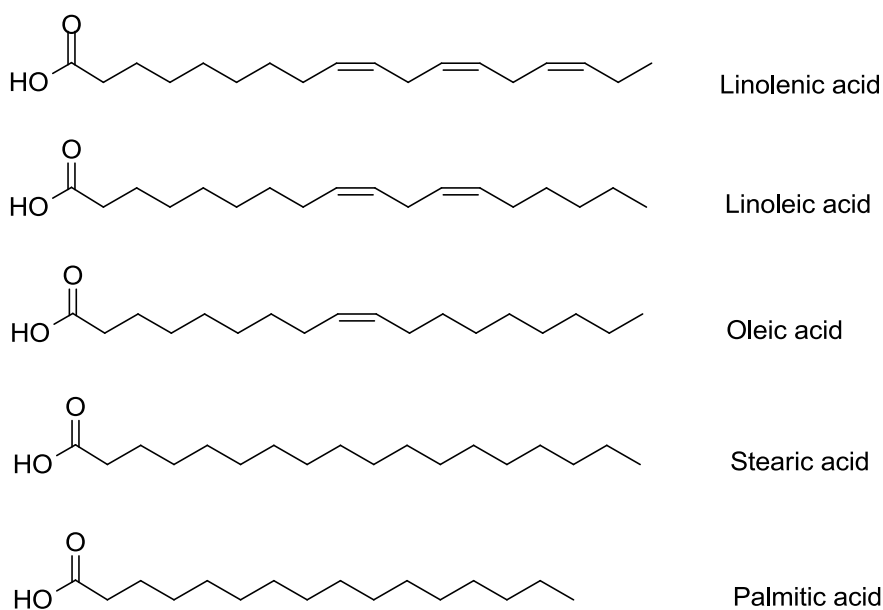


**Figure 3-9.** An example of the possible triglyceride structure that are present in Linseed Oil; chemical structure of the major fatty acid components that form this triglyceride.<sup>23,37</sup>

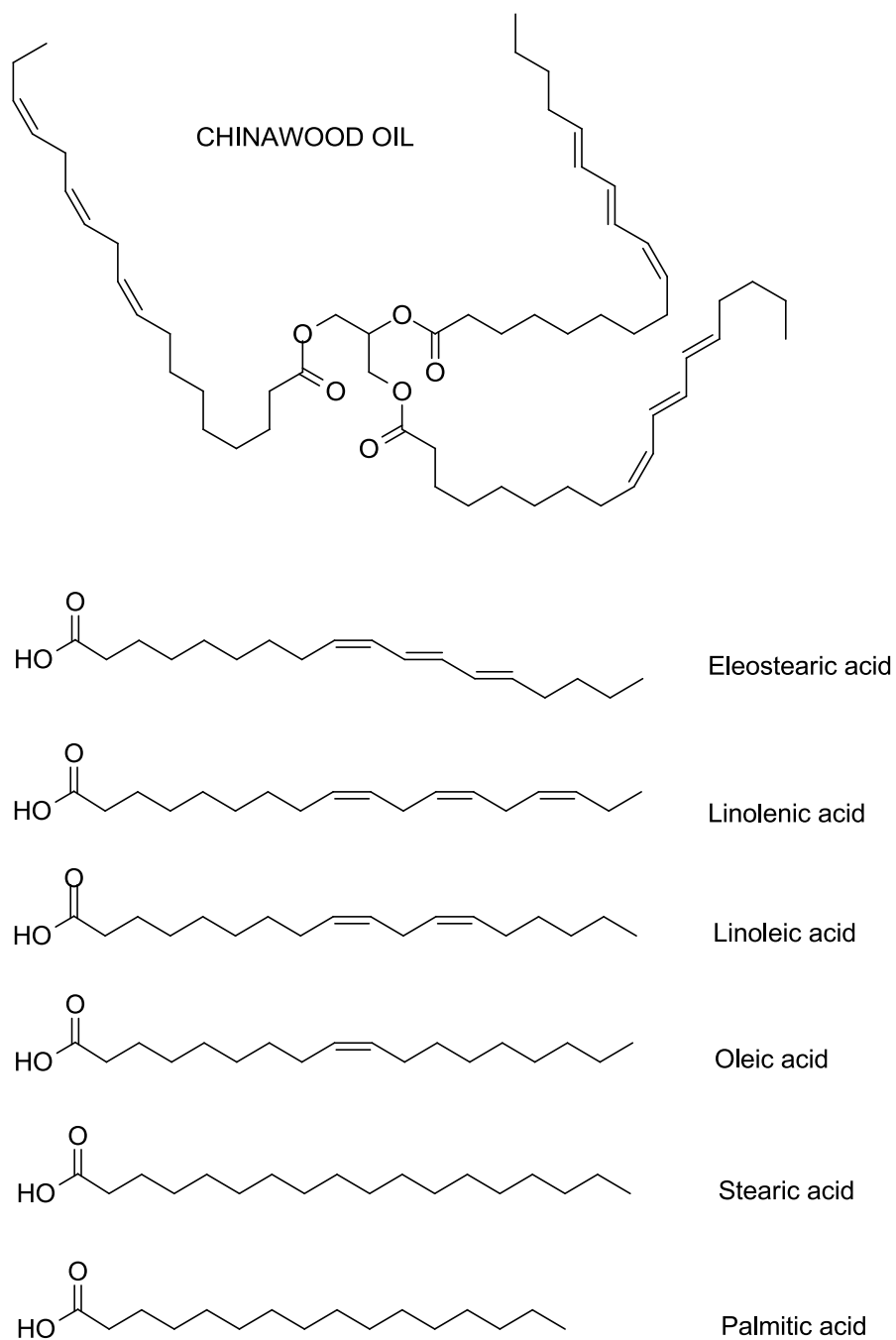
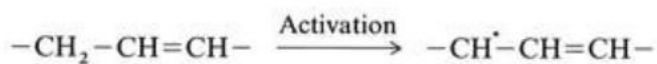
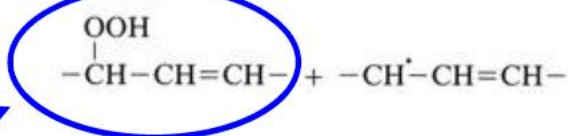
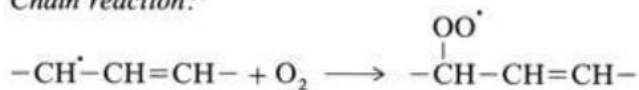


**Figure 3-10.** An example of the possible triglyceride structure of Chinawood Oil; chemical structures of the major fatty acid components that form this triglyceride.<sup>23, 37</sup>



Chain reaction:



hydroperoxide

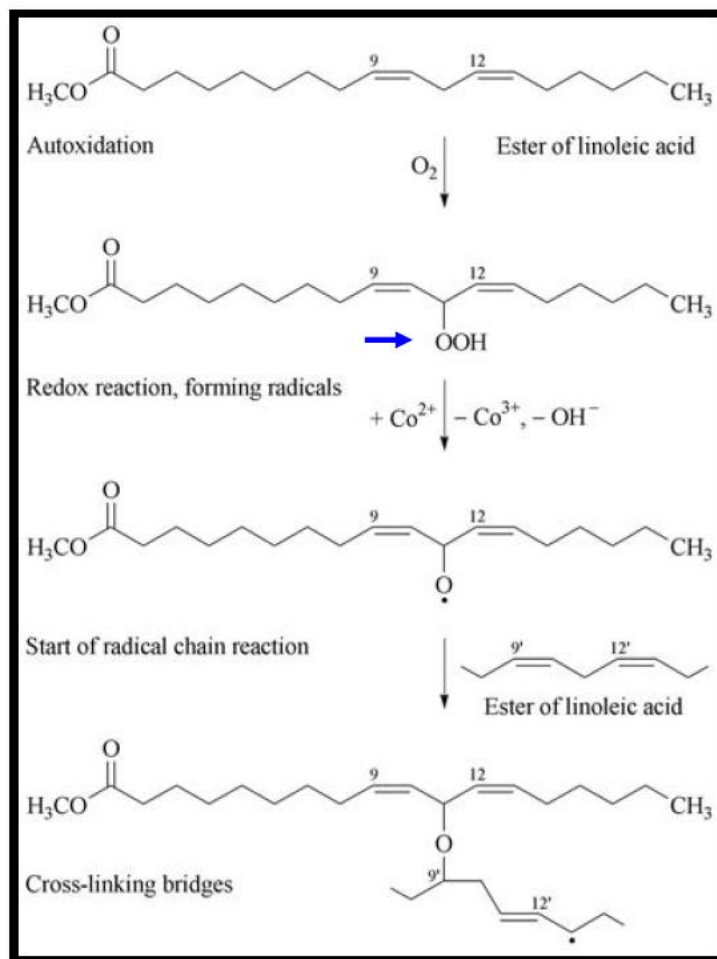
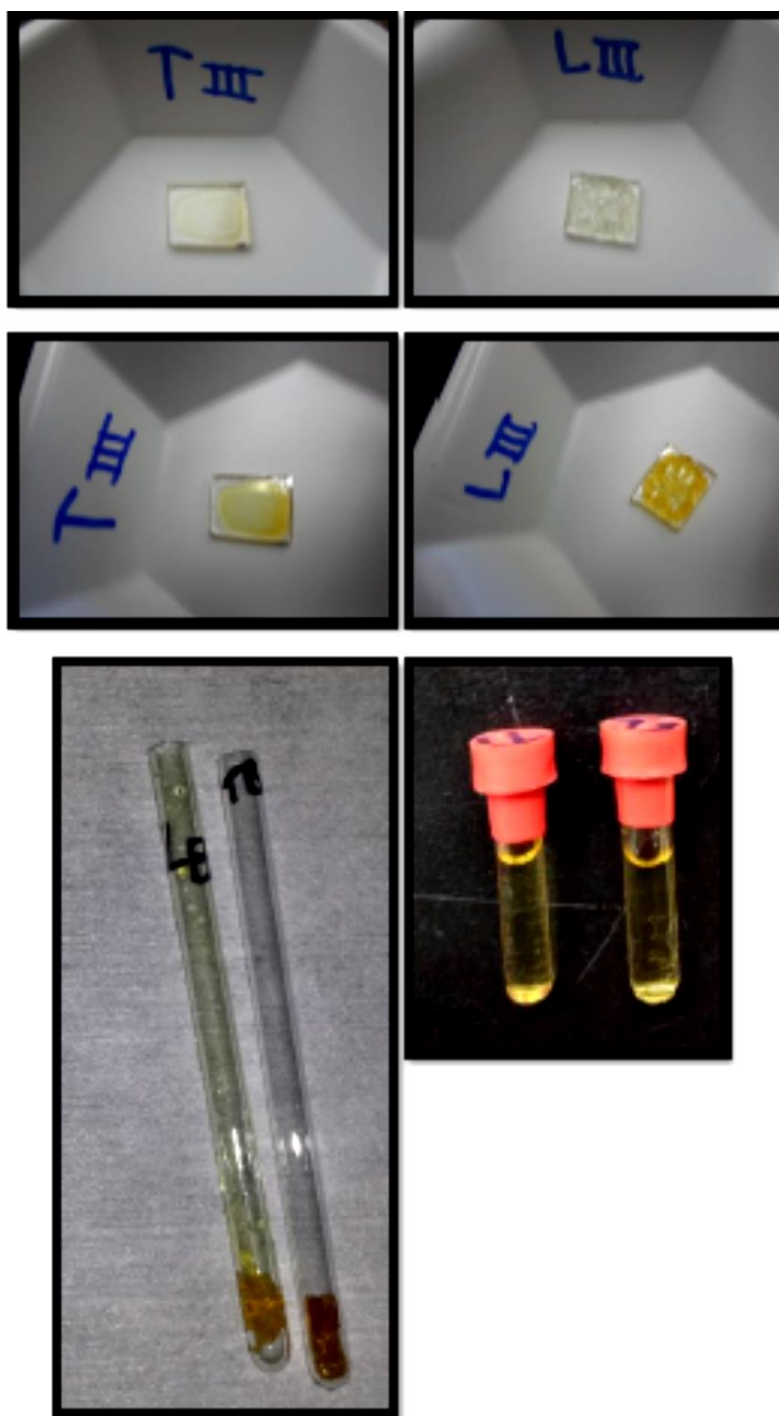
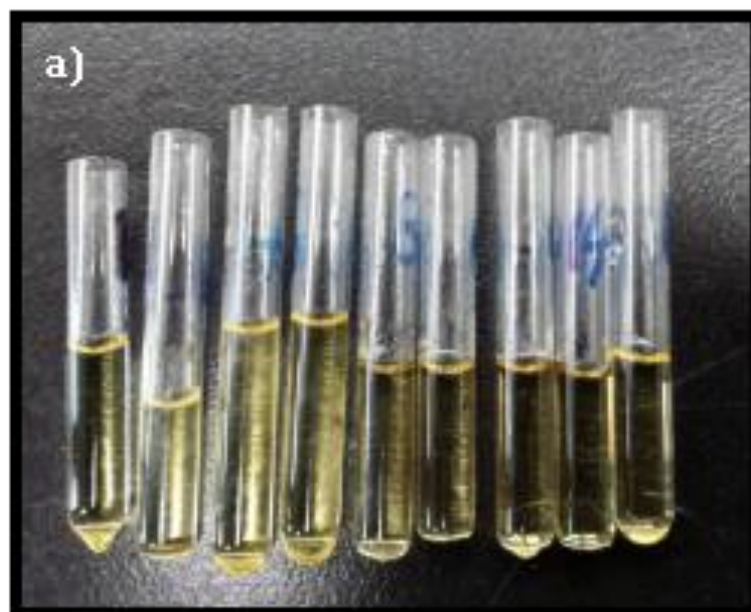


Figure 3-11. Formation of hydroperoxides and cross-linking reaction for a drying oil with non-conjugated double bonds.<sup>23,24</sup>



**Figure 3-12.** Photographs of slides with Linseed Oil and Chinawood Oil in which can be appreciated the different textures of the oils before and after the ageing process. NMR tubes with the aged samples are shown below.



**Figure 3-13.** Color development for samples of Linseed Oil aged with (a) UV light (centered at 254 nm, 15 W) and (b) Heat (90 to 210°C).

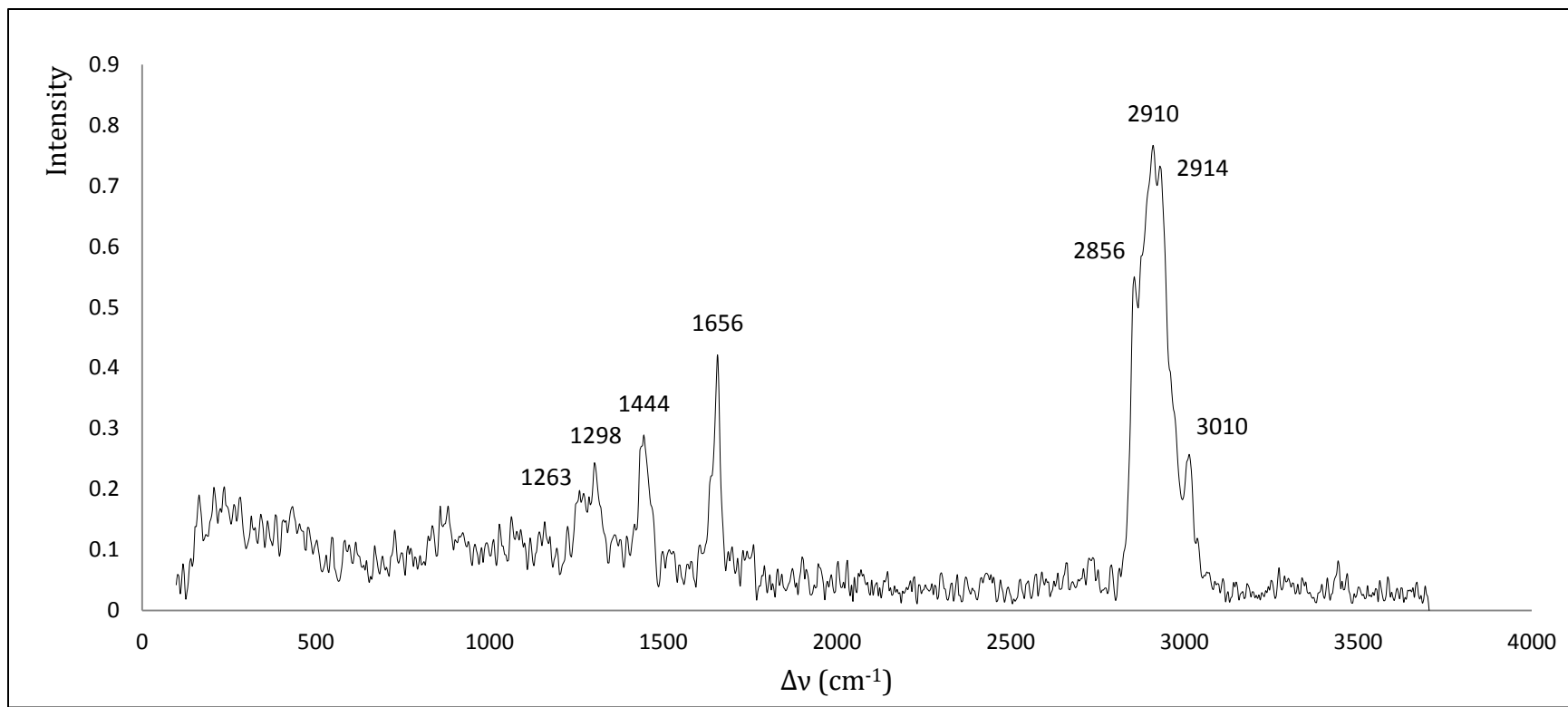


Figure 3-14. FT-Raman spectrum of pristine Linseed Oil after drying.

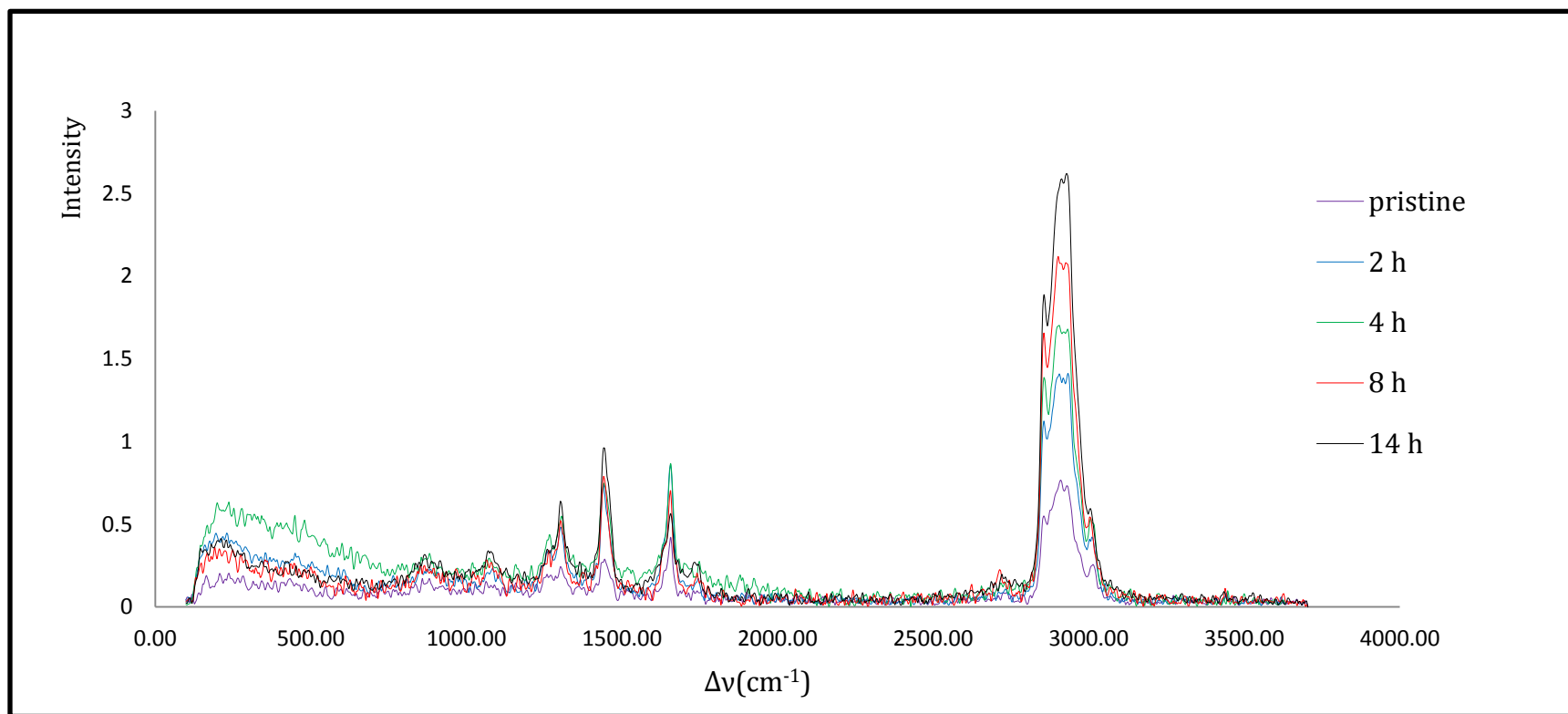


Figure 3-15. FT-Raman spectra of pristine and artificially aged samples of Linseed Oil.



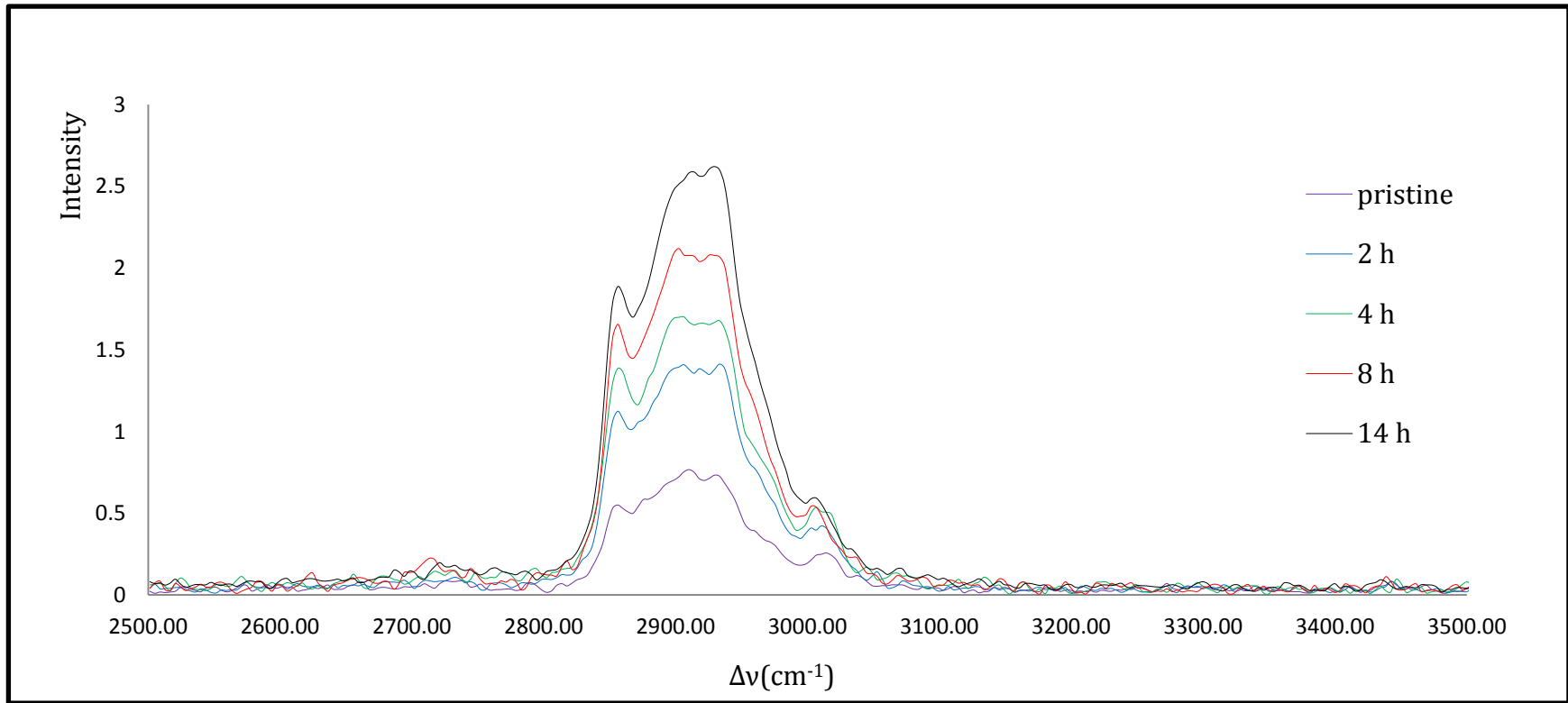
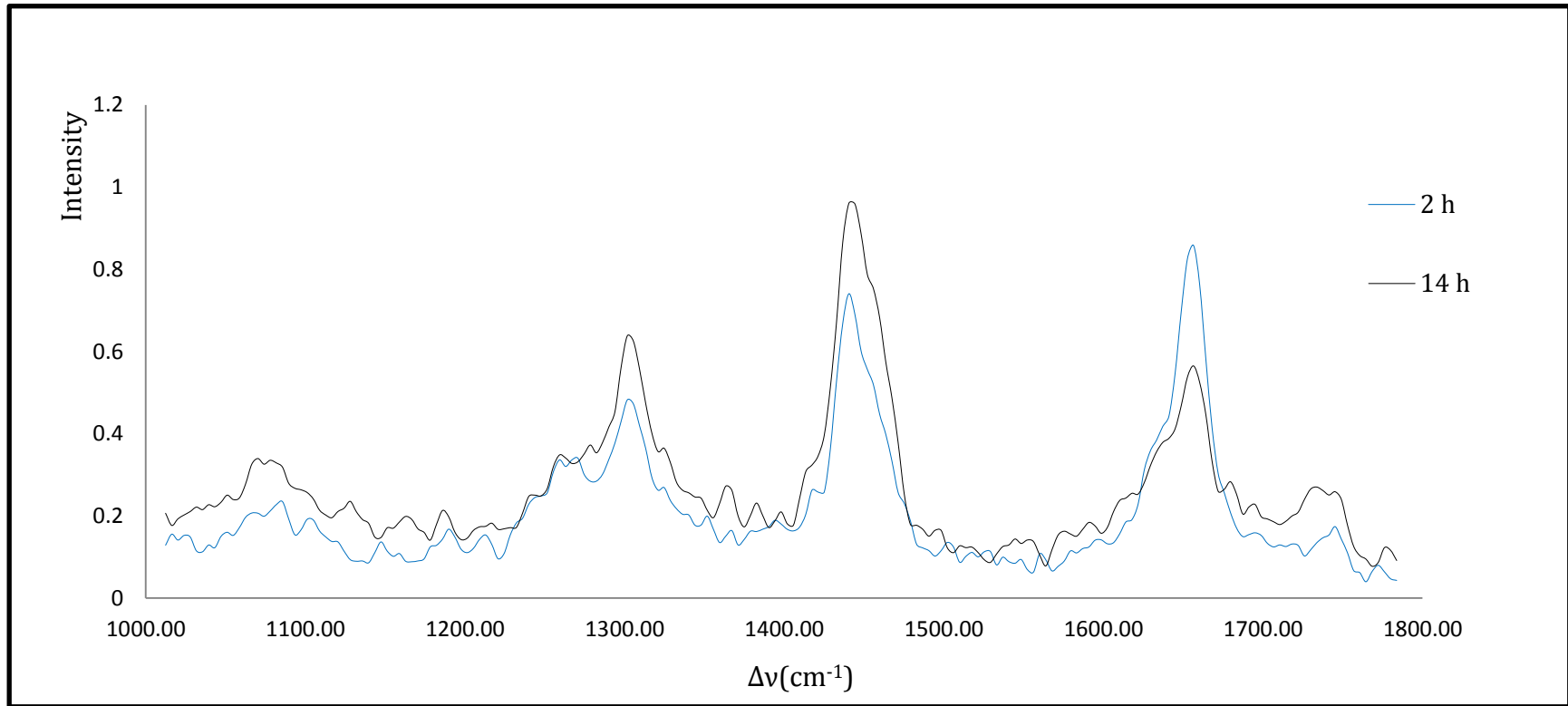


Figure 3-16. FT-Raman spectra of pristine and artificially aged samples of Linseed Oil. Detail of the Raman shift 3010  $\text{cm}^{-1}$ .



**Figure 3-17.** FT-Raman spectra of pristine and artificially aged samples of Linseed Oil. Raman shifts are noted at 1265 and 1655  $\text{cm}^{-1}$ .



**Figure 3-18.** Photographs of: (a) NMR tubes sealed with glass, and (b) sealed NMR tubes in closed vials with the aged samples.

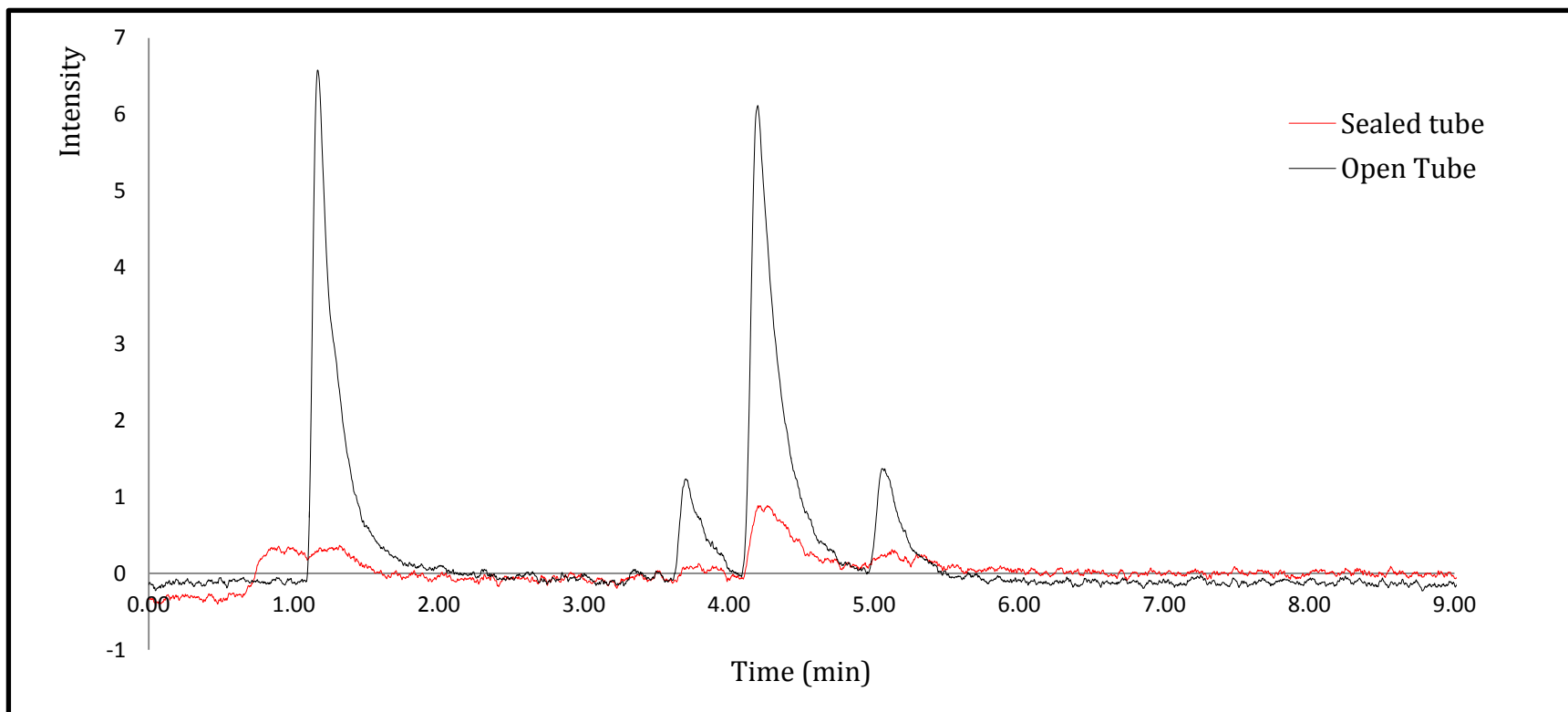


**Figure 3-19.** Chromatograms obtained by GC-TCD. Data were corrected with a blank and smoothed by ensemble averaging with a 51 point "boxcar".

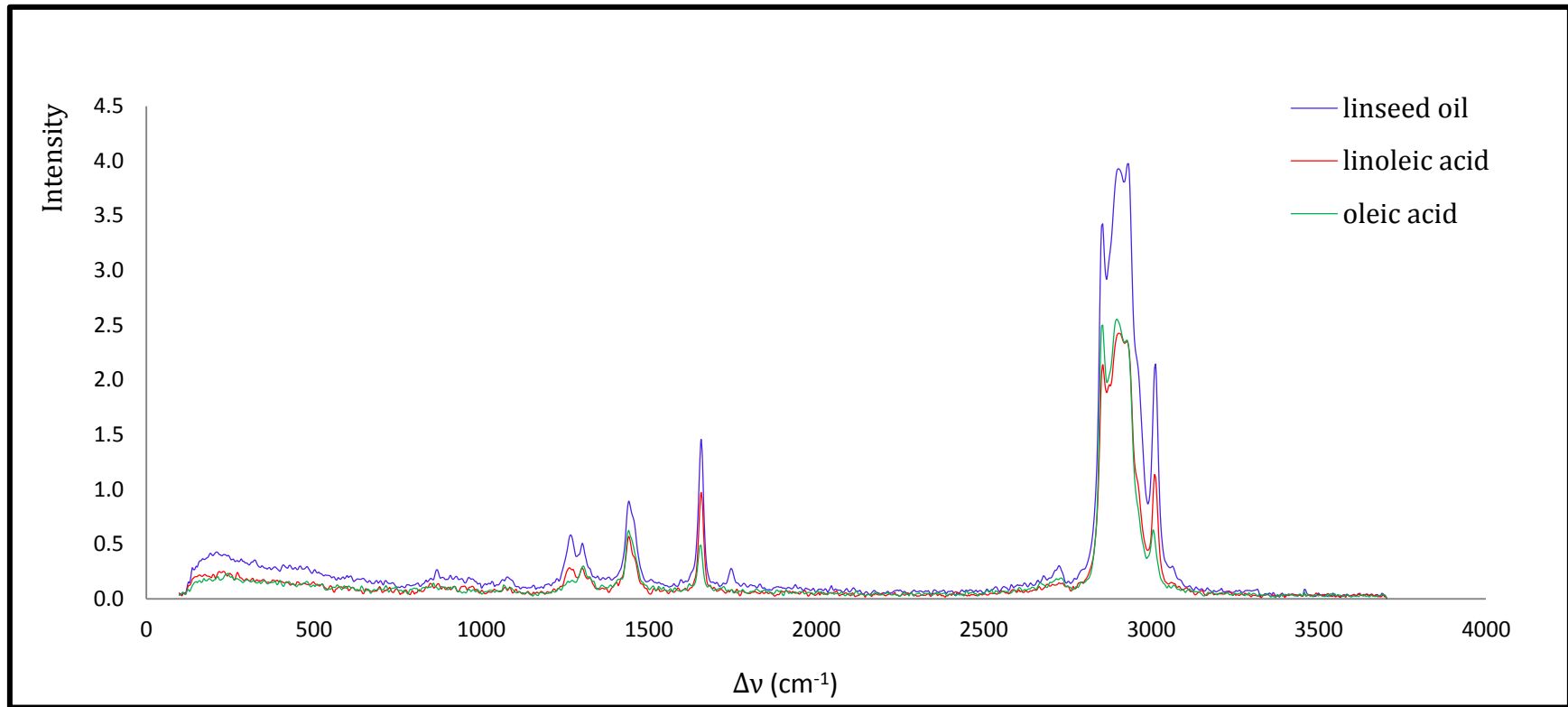


**Figure 3-20.** FT-Raman spectra of pristine Linseed Oil, Linoleic Acid and Oleic Acid after treatment at 50°C in the Ageing Chamber.

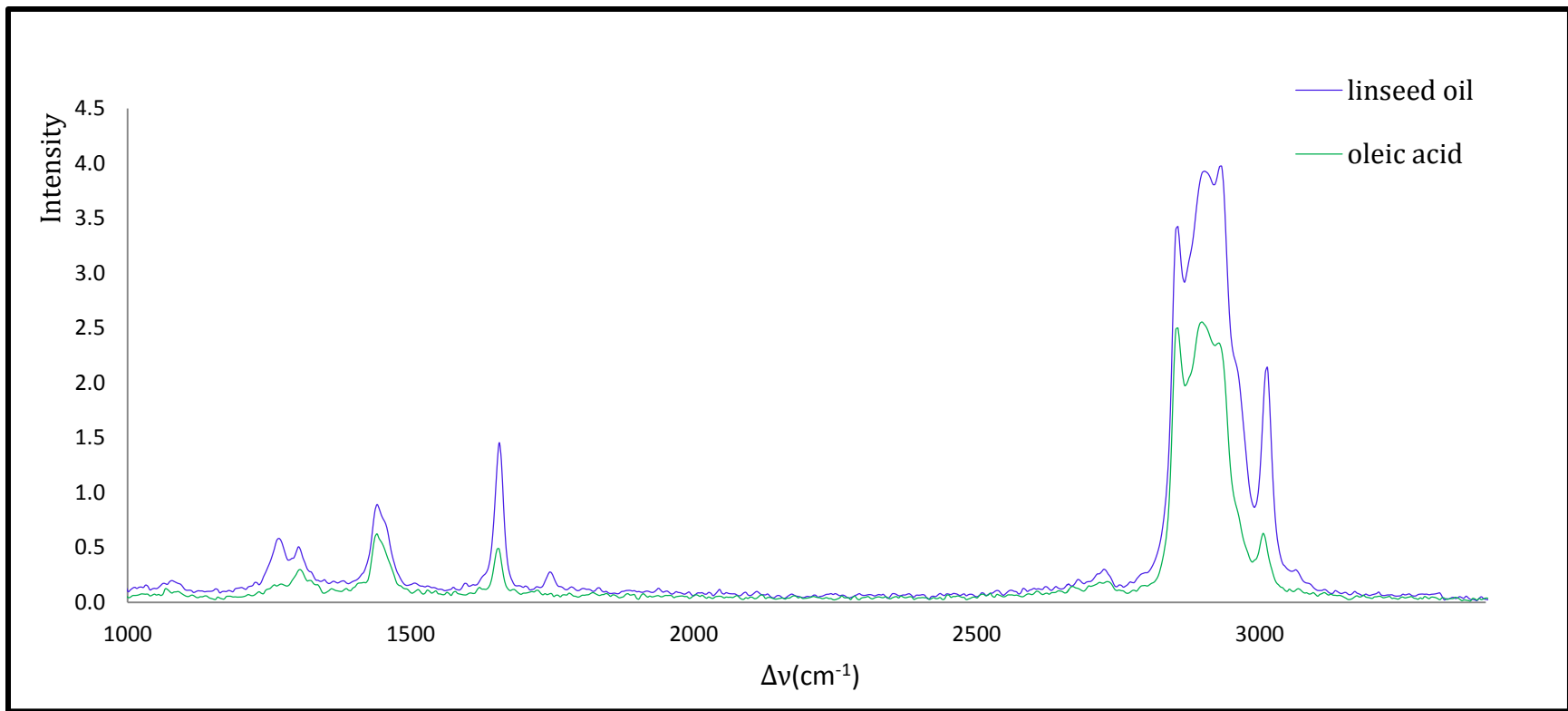


**Figure 3-21.** FT-Raman spectra comparison of pristine Linseed Oil and Oleic Acid.

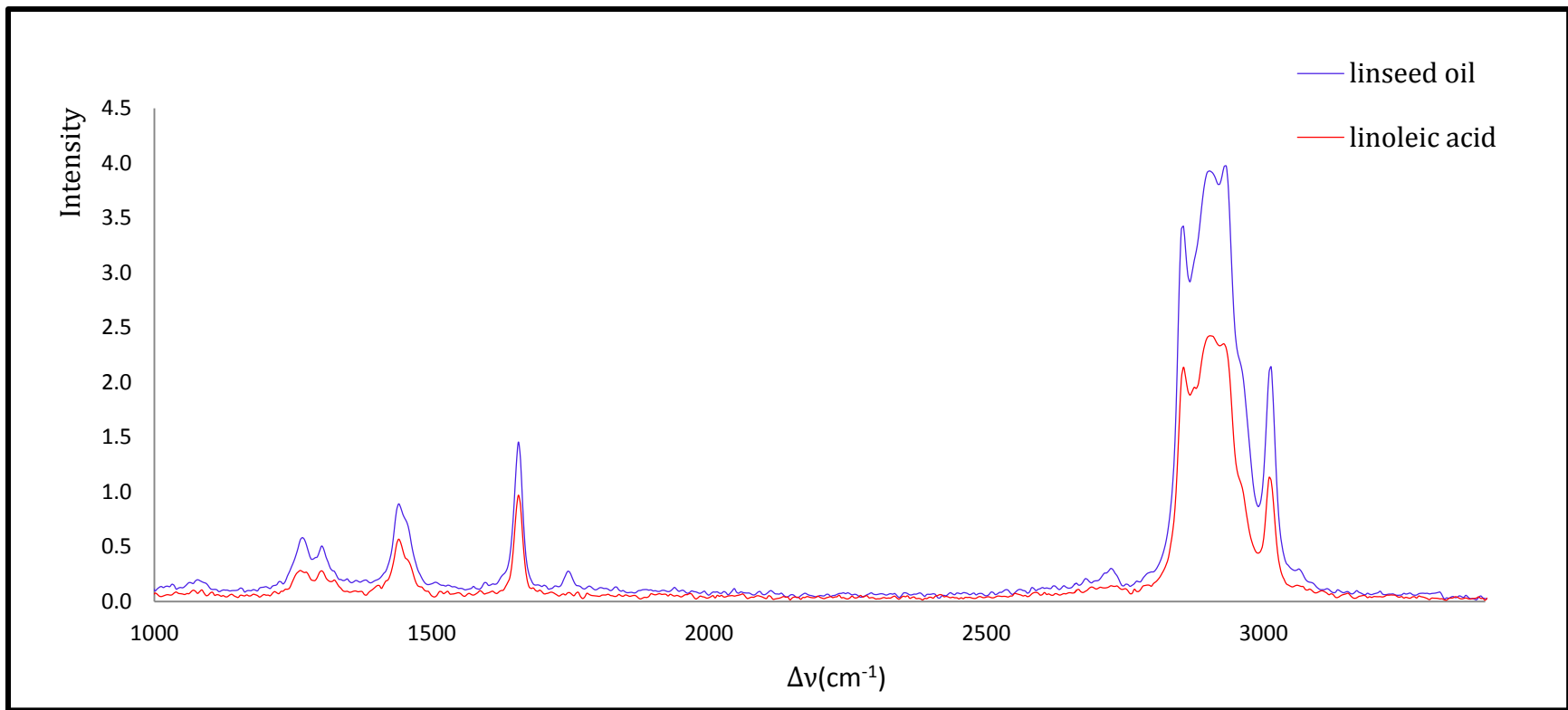


Figure 3-22. FT-Raman spectra comparison of pristine Linseed Oil and Linoleic Acid.

**Table III.** Intensities, relative intensities and retention times of the unknown volatile compounds present in the vial's headspace for both sealed and unsealed tubes.

Signal	Retention time (min)	Intensity			Retention	Selectivity	
		(I <sub>1</sub> )	(I <sub>2</sub> )	[I <sub>2</sub> /I <sub>1</sub> ]*100 (%)	Factor (k)	factor (α)	Resolution (R)
<b>A</b>	0.630*	-	0.3383	-	2.15	11.1	-
<b>B</b>	1.07*	6.580	0.2903	4.0	4.35	5.48	0.80
<b>C</b>	3.06	1.230	0.06291	5.0	14.3	1.67	3.13
<b>D</b>	4.09	6.117	0.8815	14.0	19.5	1.23	1.49
<b>E</b>	4.97	1.367	0.2480	18.0	23.9	1.00	1.28

(\*): these signals were not baseline resolved.



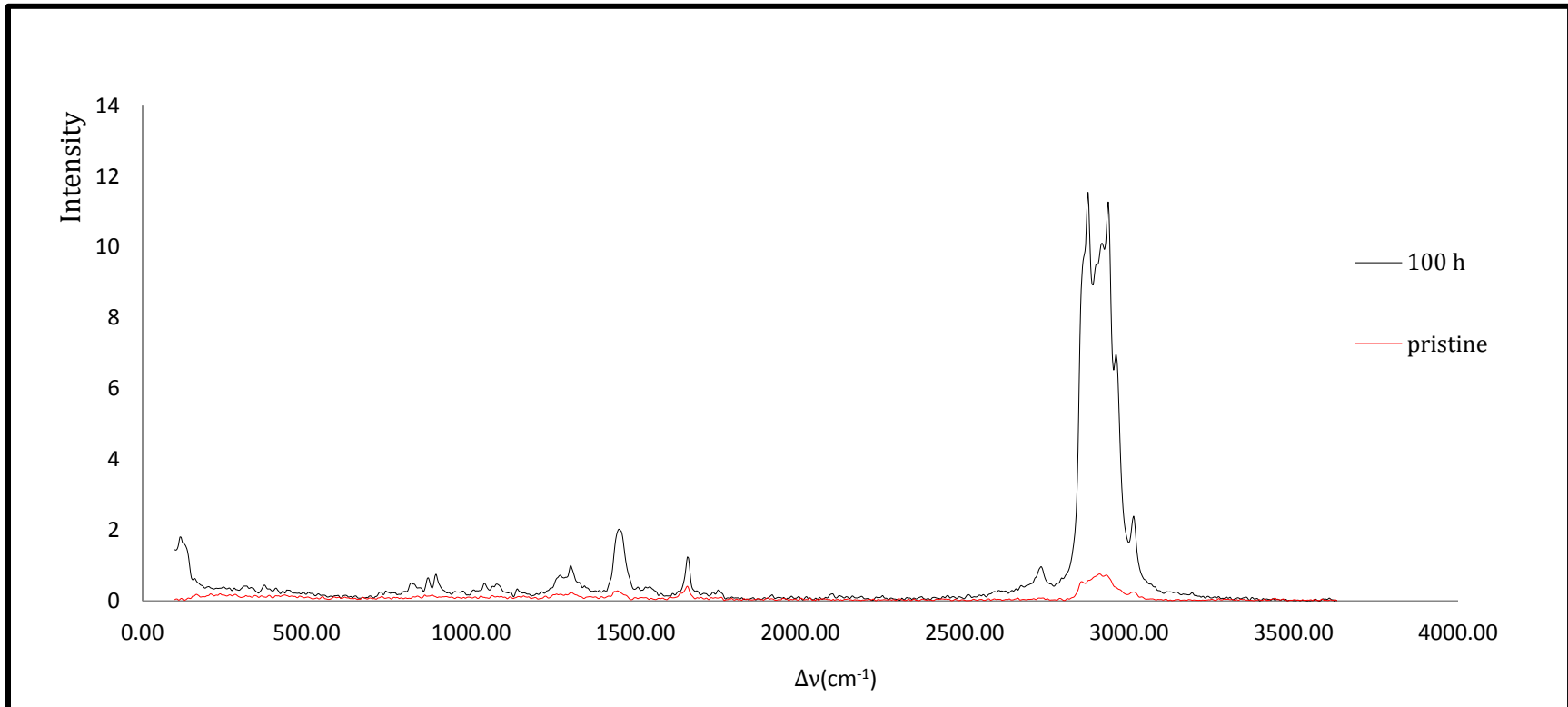


Figure 3-23. FT-Raman spectra comparison of pristine Linseed Oil and the sample aged for 100 hr. at 50°C.

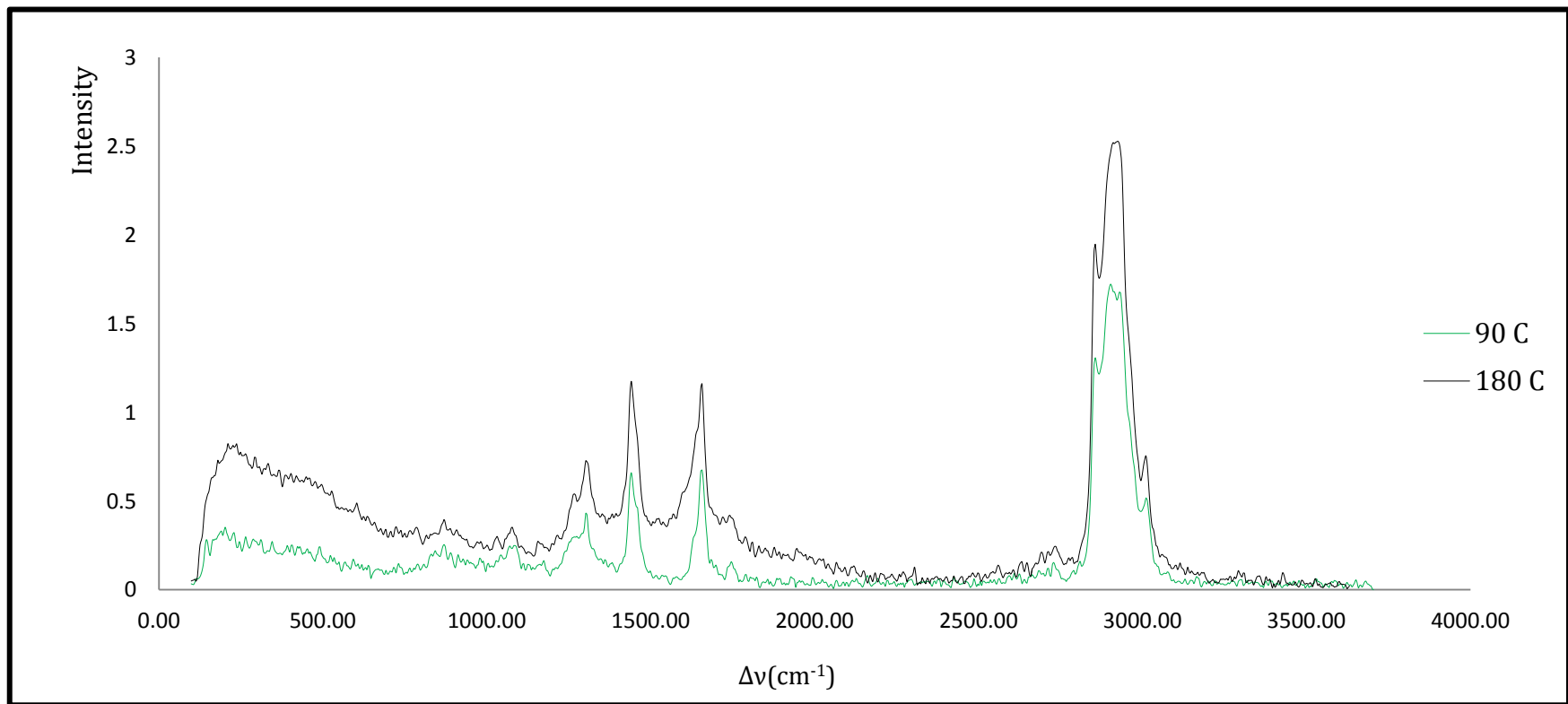


Figure 3-24. Raman spectra comparison of Linseed Oil samples aged the same time at different temperatures.

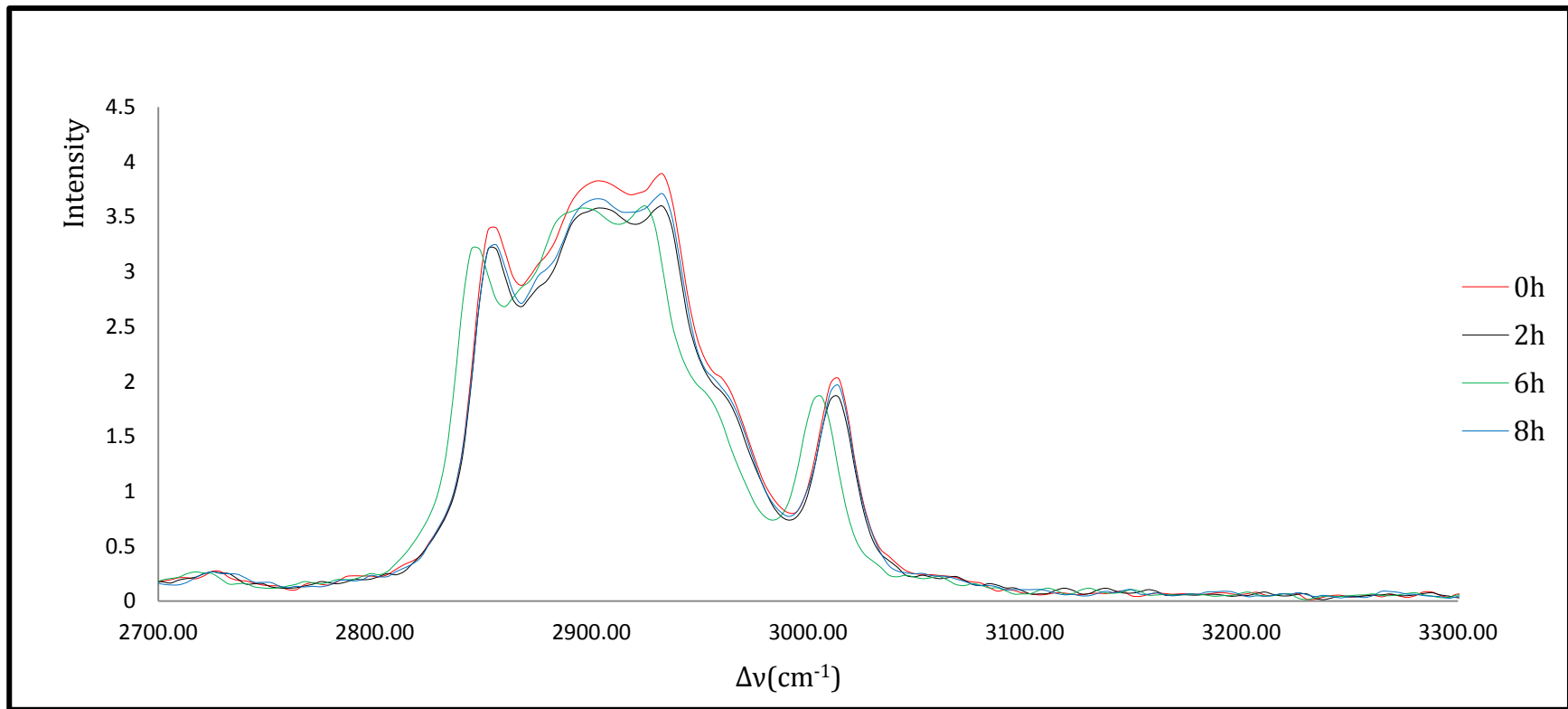


Figure 3-25. FT- Raman spectra of pristine and artificially aged (with UV-light at different times) samples of Linseed Oil.

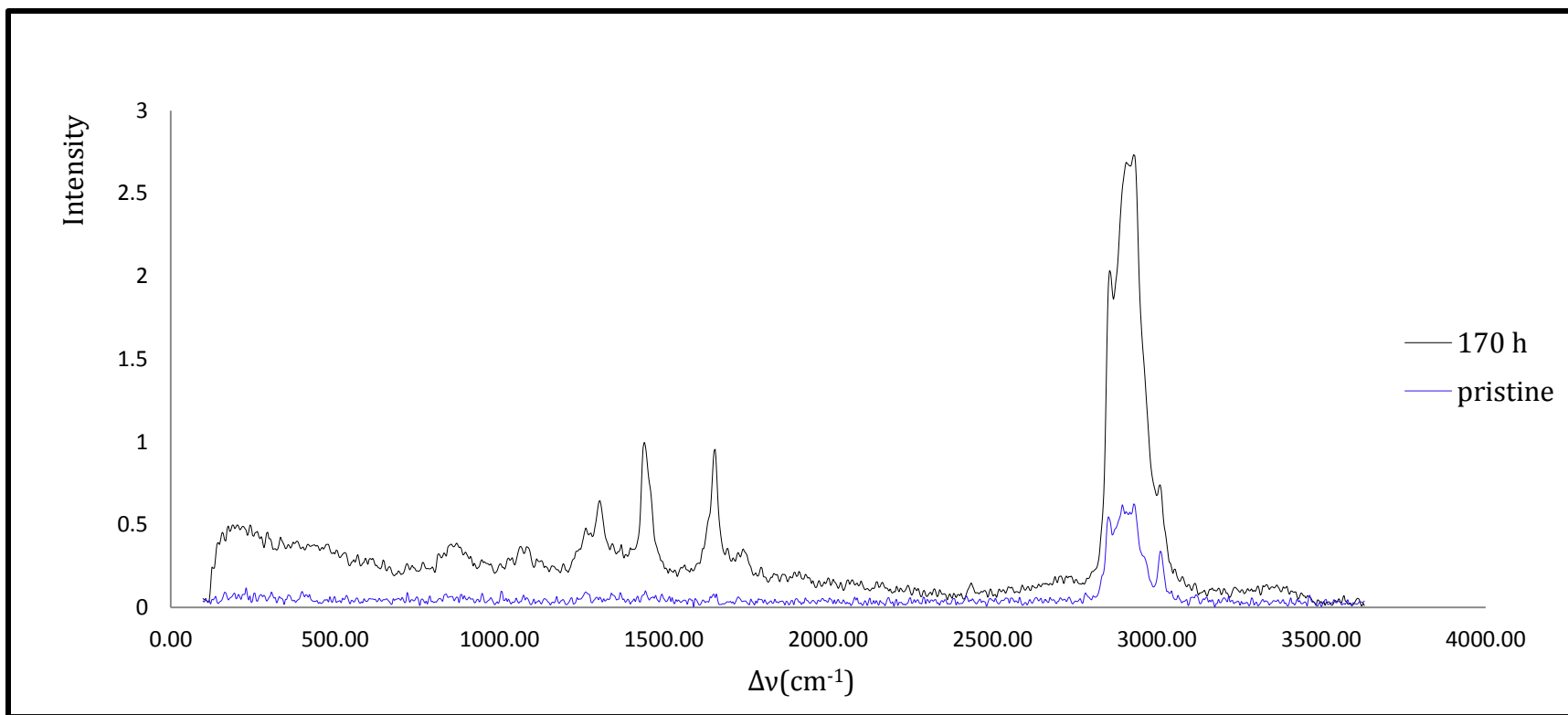


Figure 3-26. FT-Raman spectra comparison of pristine Linseed Oil sample and the 170 hr, UV-light aged samples.

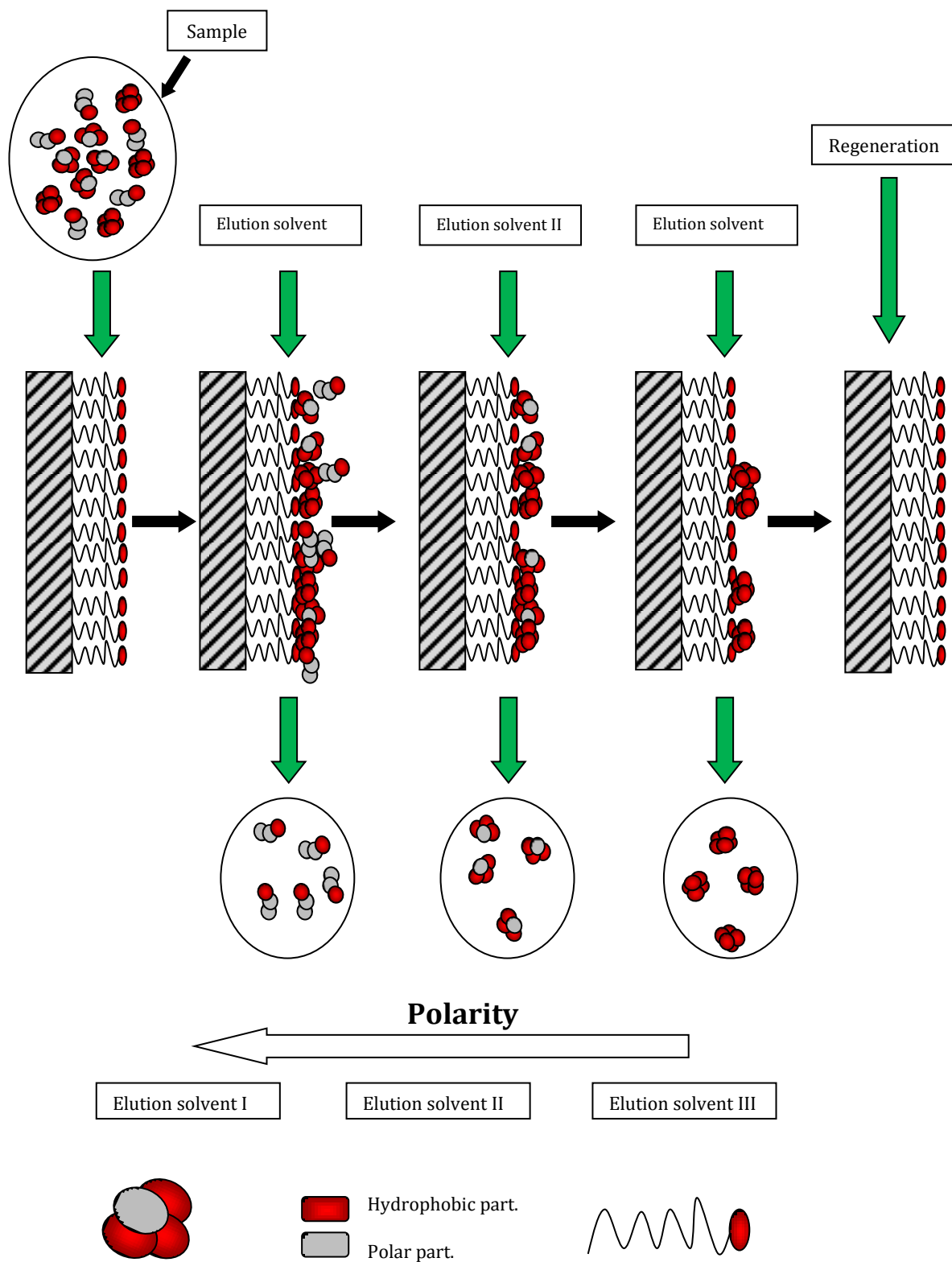
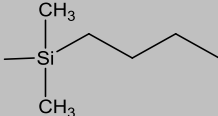
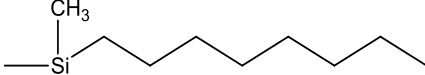
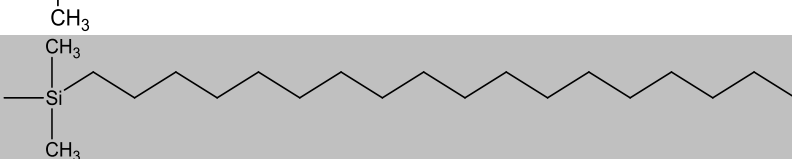
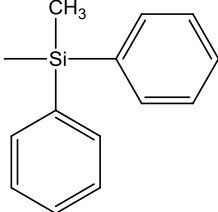
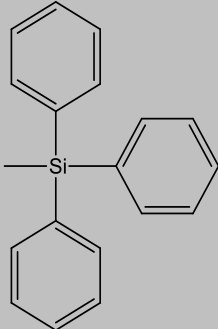
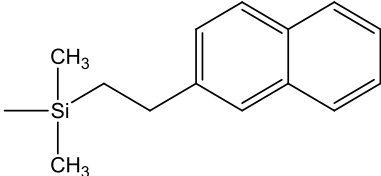
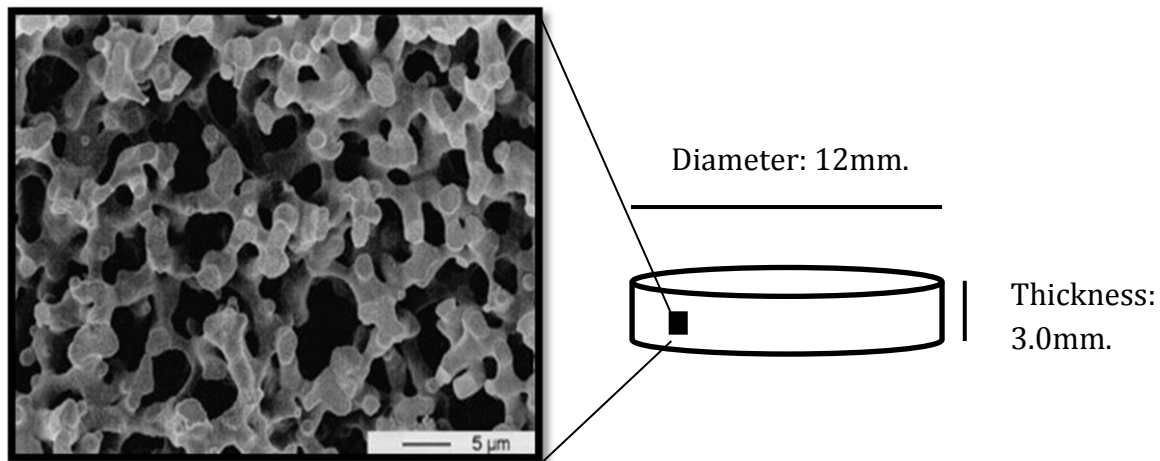


Figure 3-27. Schematic diagram of the chromatographic separation in a RP column.

**Table IV.** Stationary phase ligands that are commonly used in RP-LC.

Ligand.	Chemical structure.
<b>butyl</b>	
<b>octyl</b>	
<b>octadecyl</b>	
<b>biphenyl</b>	
<b>triphenyl</b>	
<b>naphthylethyl</b>	



Bed volume: 0.34mL.

Channel size: average pore radius: 600 - 750 nm

pH stability range: 1-14.

Temperature stability range: 4 to 40°C.

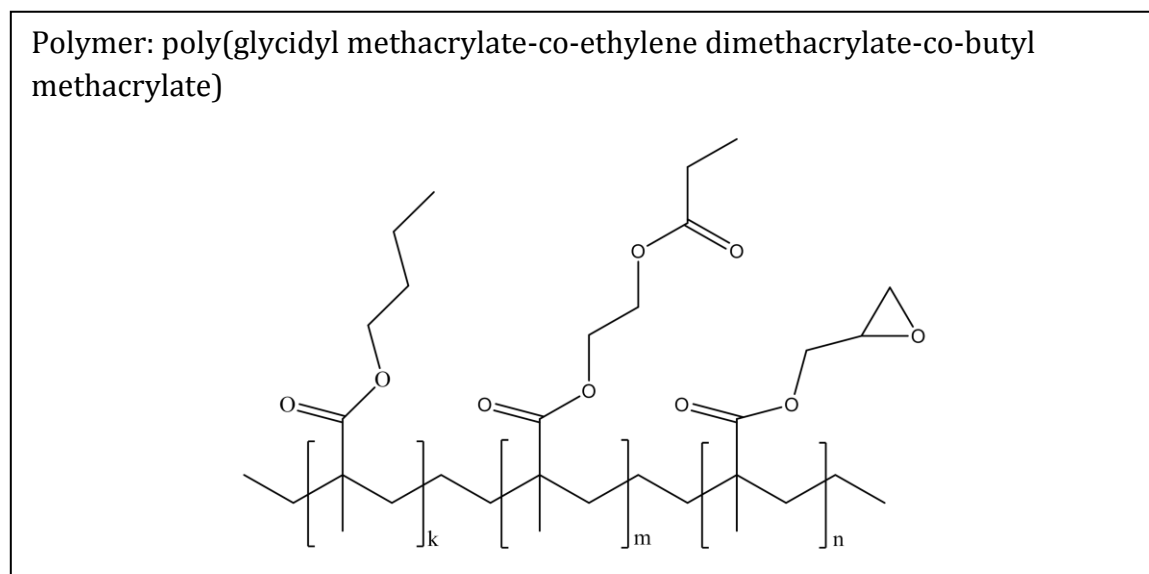
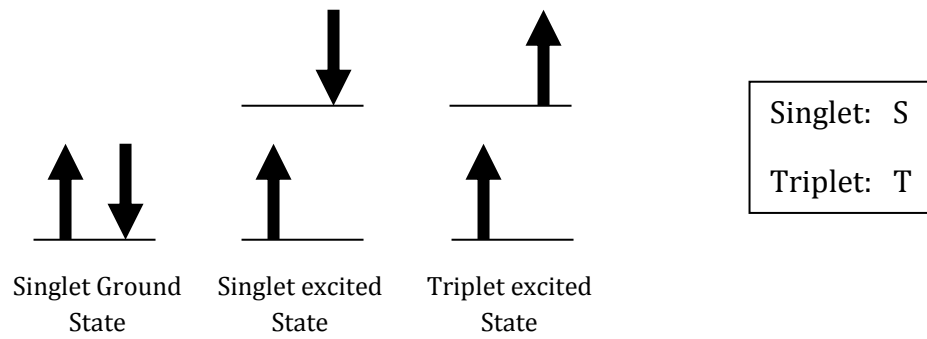


**Figure 3-28.** Schematic diagram and microscopic detail of the structure of a monolith column.<sup>82</sup> Composition and working conditions of the CIM® RP-SDVB DISK monolith column.<sup>83</sup>

A)



B)

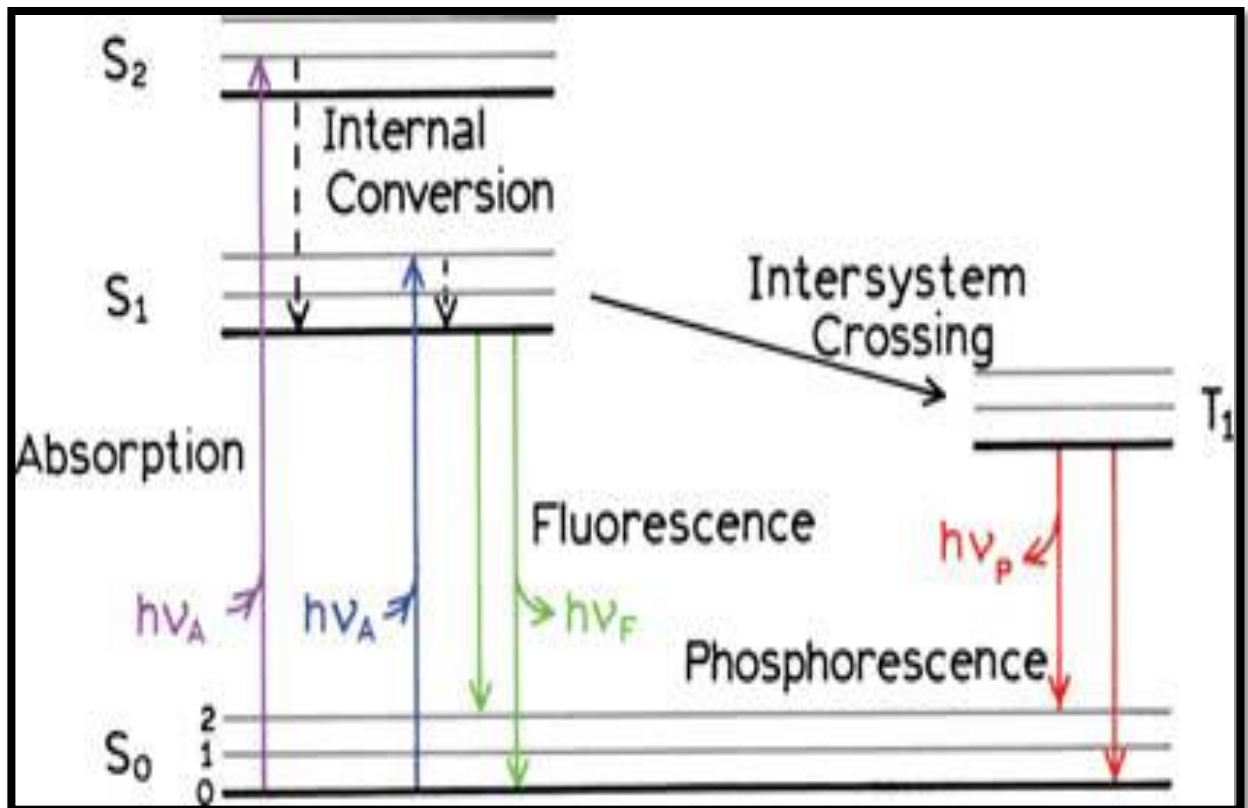


Figure 3-29. A) Diagram of Singlet and Triplet excited states. B) Jablonski diagram.<sup>64</sup>



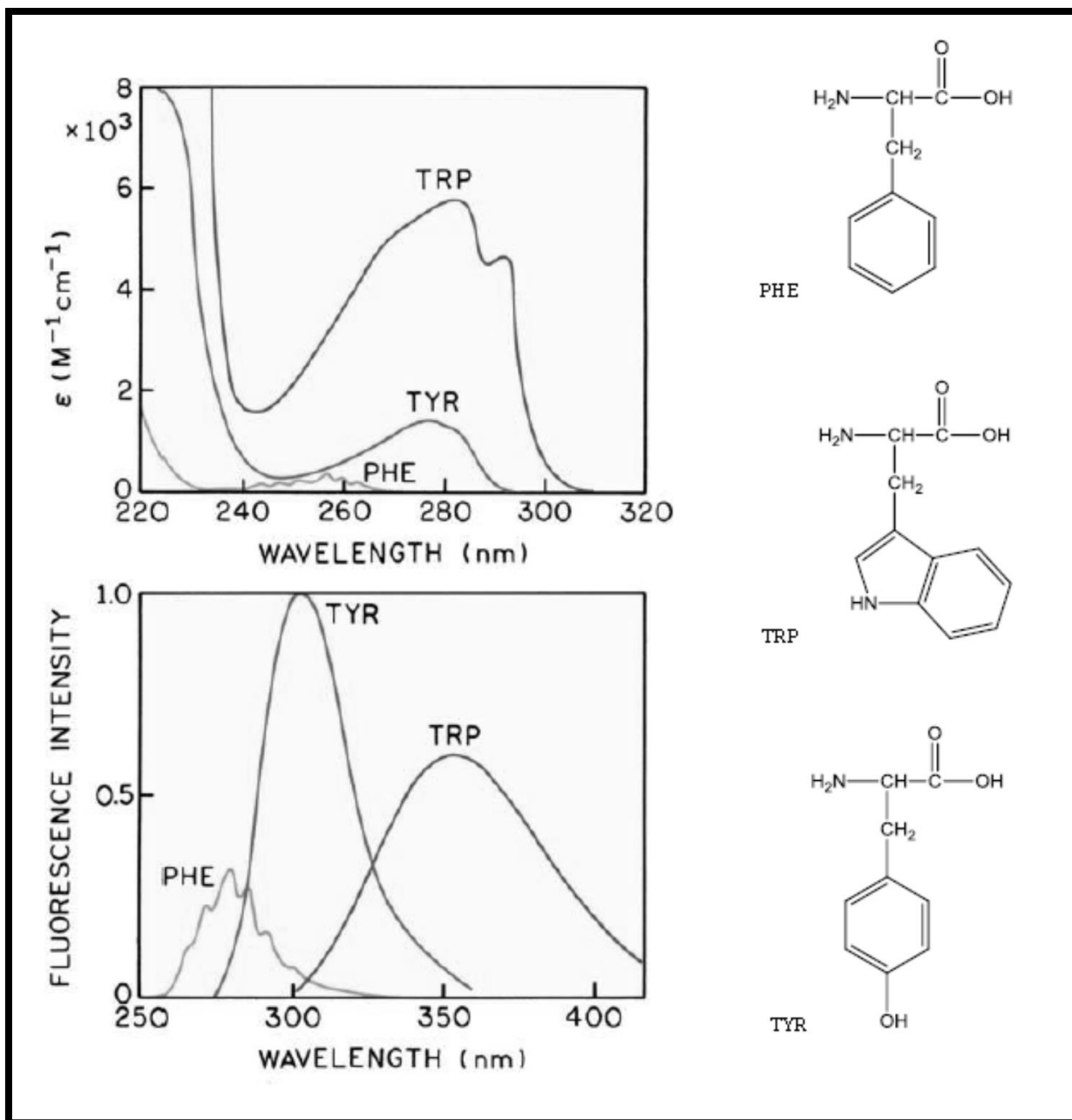
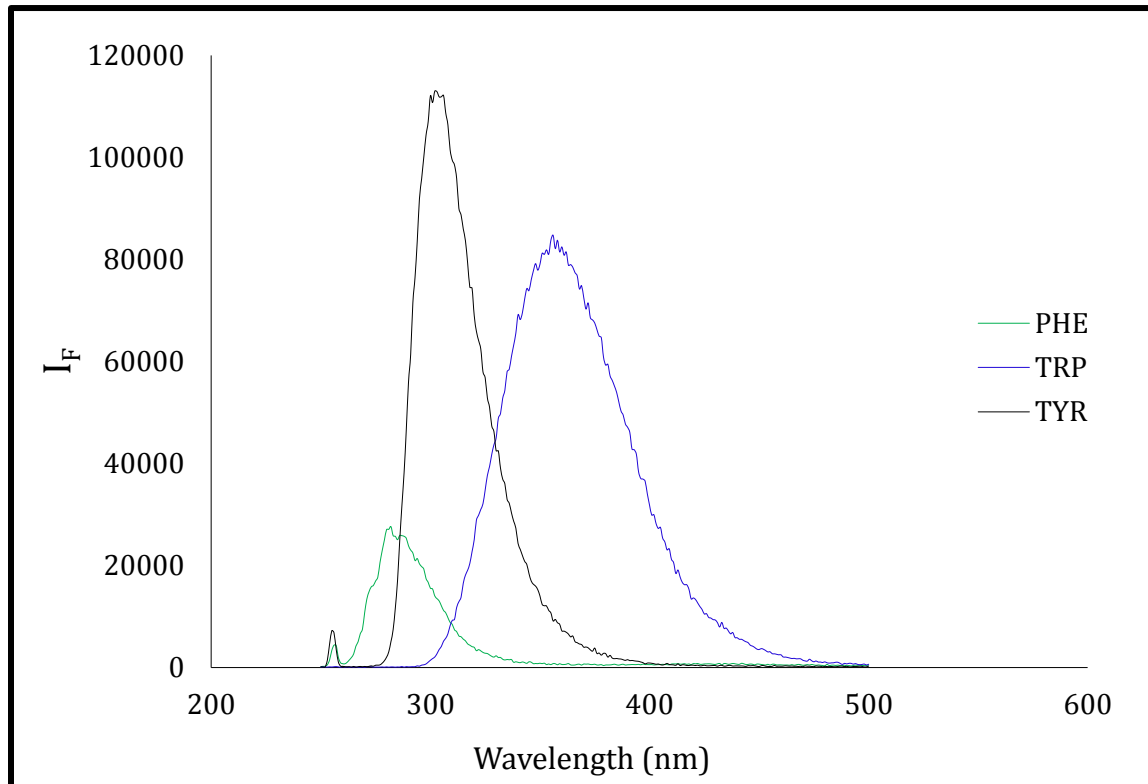


Figure 3-30. Chemical structures and characteristic absorbance and emission spectra of TRP, TYR and PHE.<sup>64</sup>

**Table V.** Basic matrix for a seven factor Plackett-Burman design.<sup>63</sup>

EXPERIMENTS	FACTORS							Response
	A	B	C	D	E	F	G	
1	+	+	+	-	+	-	-	Y <sub>1</sub>
2	-	+	+	+	-	+	-	Y <sub>2</sub>
3	-	-	+	+	+	-	+	Y <sub>3</sub>
4	+	-	-	+	+	+	-	Y <sub>4</sub>
5	-	+	-	-	+	+	+	Y <sub>5</sub>
6	+	-	+	-	-	+	+	Y <sub>6</sub>
7	+	+	-	+	-	-	+	Y <sub>7</sub>
8	-	-	-	-	-	-	-	Y <sub>8</sub>
	E <sub>A</sub>	E <sub>B</sub>	E <sub>C</sub>	E <sub>D</sub>	E <sub>E</sub>	E <sub>F</sub>	E <sub>G</sub>	



**Figure 3-31.** PHE, TRP, and TYR emission spectra obtained with  $\lambda_{ex} = 257$  nm (1 mM aqueous solutions, pH = 7.00).

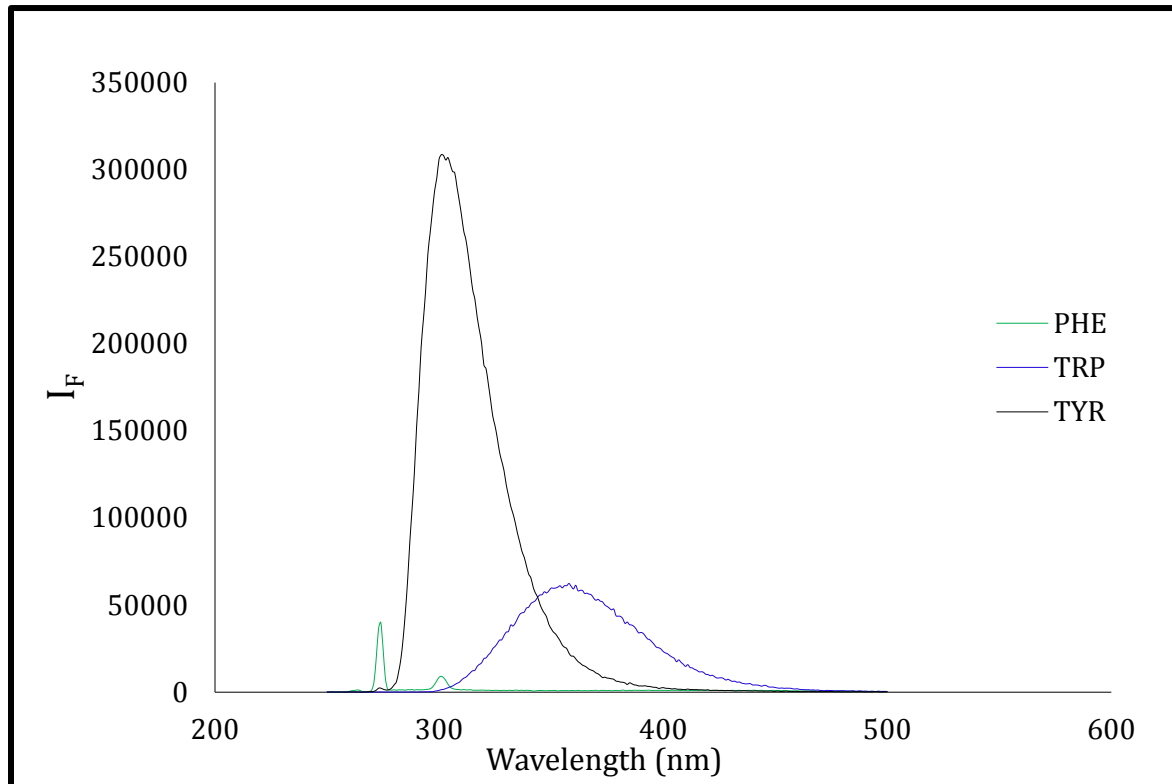


**Figure 3-32.** PHE, TRP, and TYR emission spectra obtained with  $\lambda_{ex}$ = 274nm (1 mM aqueous solutions, pH = 7.00).

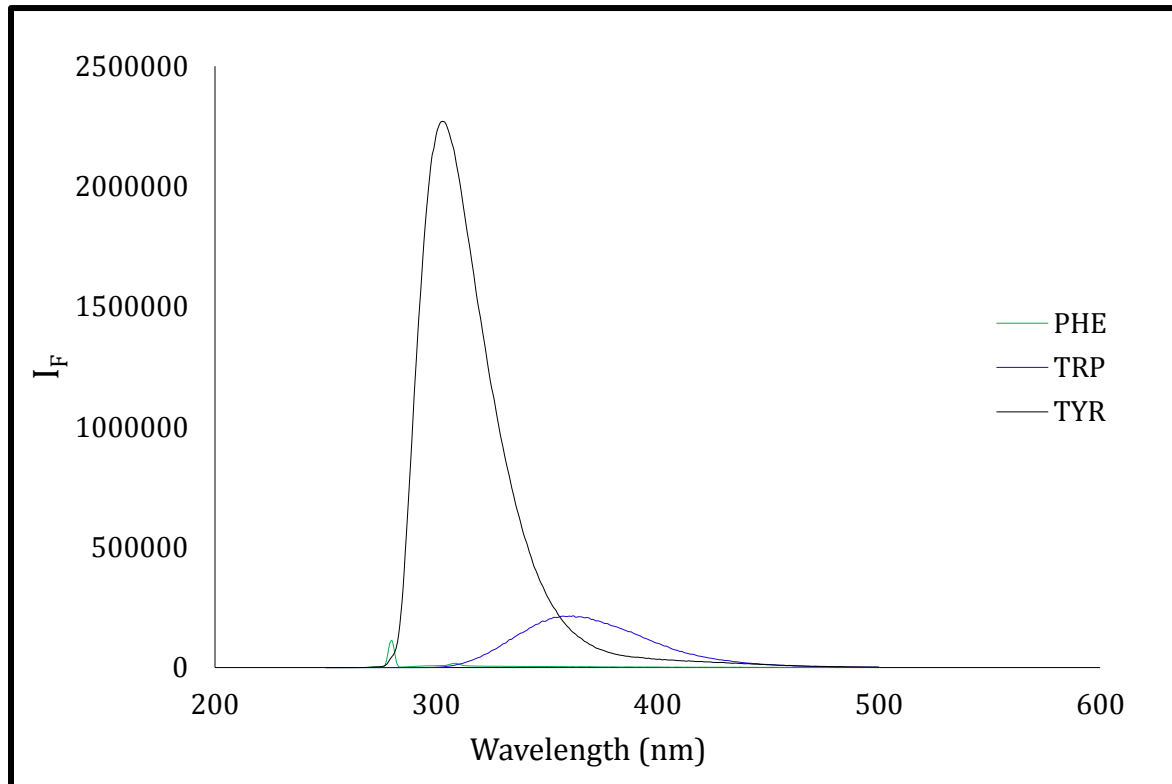


**Figure 3-33.** PHE, TRP, and TYR emission spectra obtained with  $\lambda_{ex} = 280\text{nm}$  (1 mM aqueous solutions, pH = 7.00).

**Table VI.** Absorption and emission wavelengths determined experimentally with the FluoroLog-3 Spectrofluorometer and comparison with theoretical values<sup>59</sup>.

Amino Acid	$\lambda_{ex}$ (nm) <sup>59</sup>	$\lambda_{ex}$ (nm) Experim.	% $\Delta$	$\lambda_{ex}$ (nm) <sup>59</sup>	$\lambda_{ex}$ (nm) Experim.	% $\Delta$
<b>PHE</b>	260	257	1.2	282	282	0.0
<b>TRP</b>	295	280	5.4	353	349	1.1
<b>TYR</b>	275	274	0.4	304	303	0.3

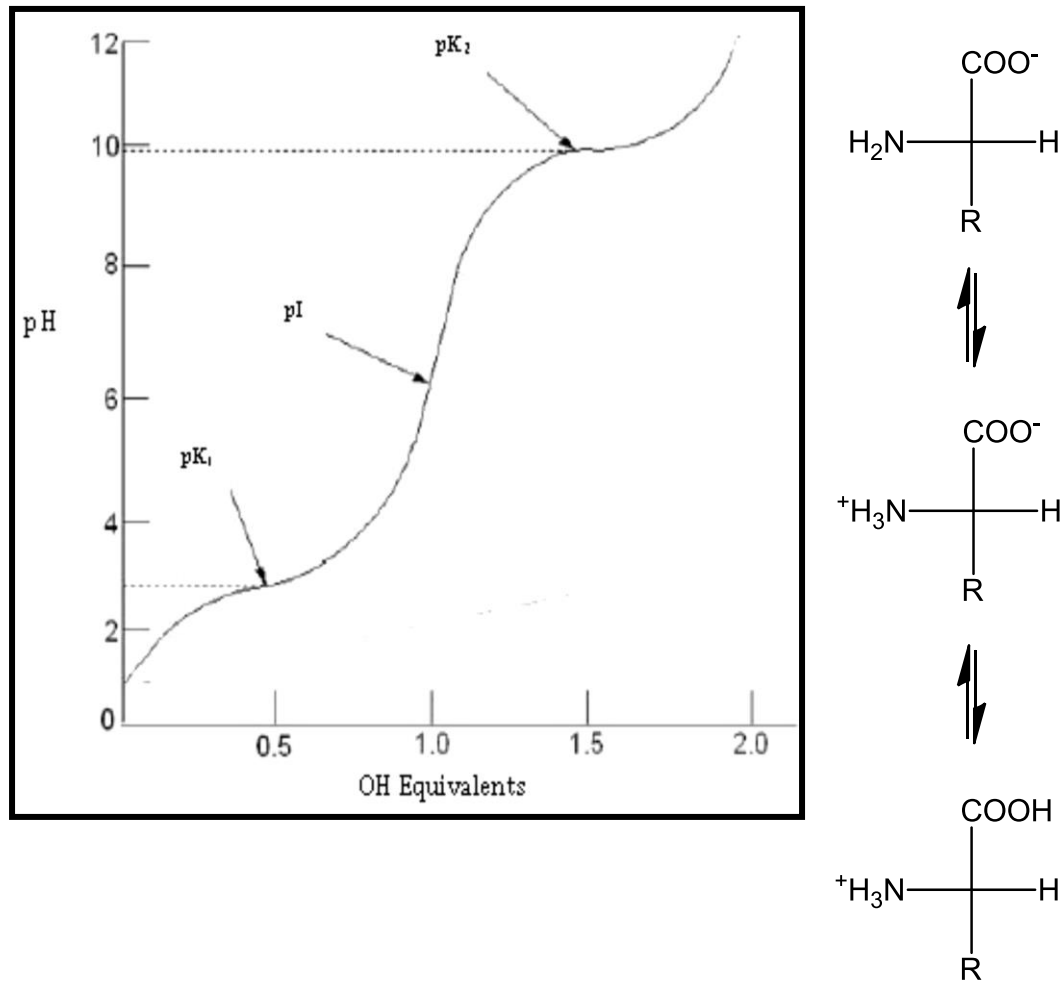


Figure 3-34. Titration of a diprotic amino acid.

**Table VII.** Amino acid pK<sub>a</sub> values.<sup>59</sup>

<b>Amino Acid</b>	<b>pK<sub>1</sub></b>	<b>pI</b>	<b>pK<sub>2</sub></b>	<b>pK<sub>3</sub></b>
<b>PHE</b>	1.83	5.48	9.24	-
<b>TRP</b>	2.38	6.11	9.39	-
<b>TYR</b>	2.20	5.65	9.11	10.1



**Table VIII.** Plackett-Burman design for seven factors.

	[AA] ( $\mu\text{M}$ )	$V_{\text{inj}}$ ( $\mu\text{L}$ )	$v$ ( $\text{mL}/\text{min}$ )	Org	%	pH	USN
	1	2	3	4	5	6	7
1	20	100	2	M	80	1	OFF
2	5	100	2	AN	20	4	OFF
3	5	35	2	AN	80	1	ON
4	20	35	1	AN	80	4	OFF
5	5	100	1	M	80	4	ON
6	20	35	2	M	20	4	ON
7	20	100	1	AN	20	1	ON
8	5	35	1	M	20	1	OFF
9	5	35	1	AN	20	4	ON
10	20	35	1	M	80	1	ON
11	20	100	1	M	20	4	OFF
12	5	100	2	M	20	1	ON
13	20	35	2	AN	20	1	OFF
14	5	100	1	AN	80	1	OFF
15	5	35	2	M	80	4	OFF
16	20	100	2	AN	80	4	ON

[AA]  $\mu\text{M}$  = concentration of each amino acid in the prepared stock solution.

$V_{\text{inj}}$  ( $\mu\text{L}$ ) = size of the loop

$v$  ( $\text{mL}/\text{min}$ ) = flow rate

Org = Methanol (M) & Acetonitrile (AN)

% = % of the organic solvent (in  $18\text{M}\Omega\text{-cm H}_2\text{O}$ )

pH = 1.00 and 4.00

USN: ultrasonic de-gassing.

**Table IX.** Results of Plackett-Burman study.

<b>Factor</b>	<b>Effect</b>
1	8.00
2	0.00
3	0.00
4	24.0
5	20.0
6	36.0
7	0.00

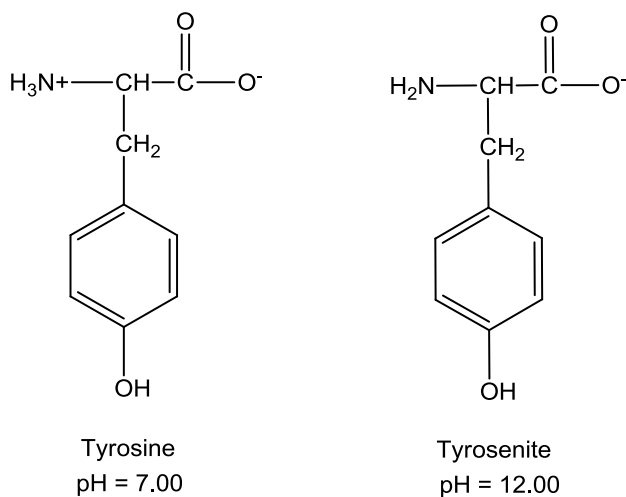
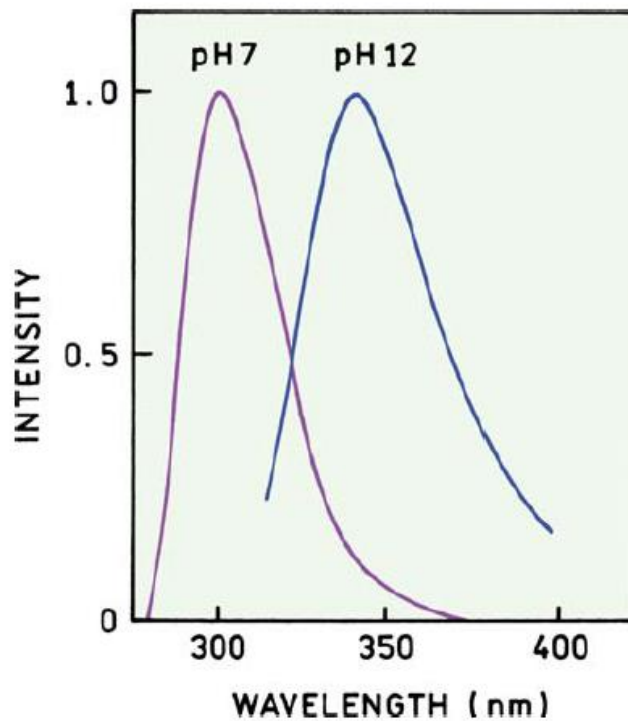


**Figure 3-35.** Emission spectra of TYR at pH= 7.00 and at pH = 9.00. Forms of TYR presents at both pH.<sup>64</sup>

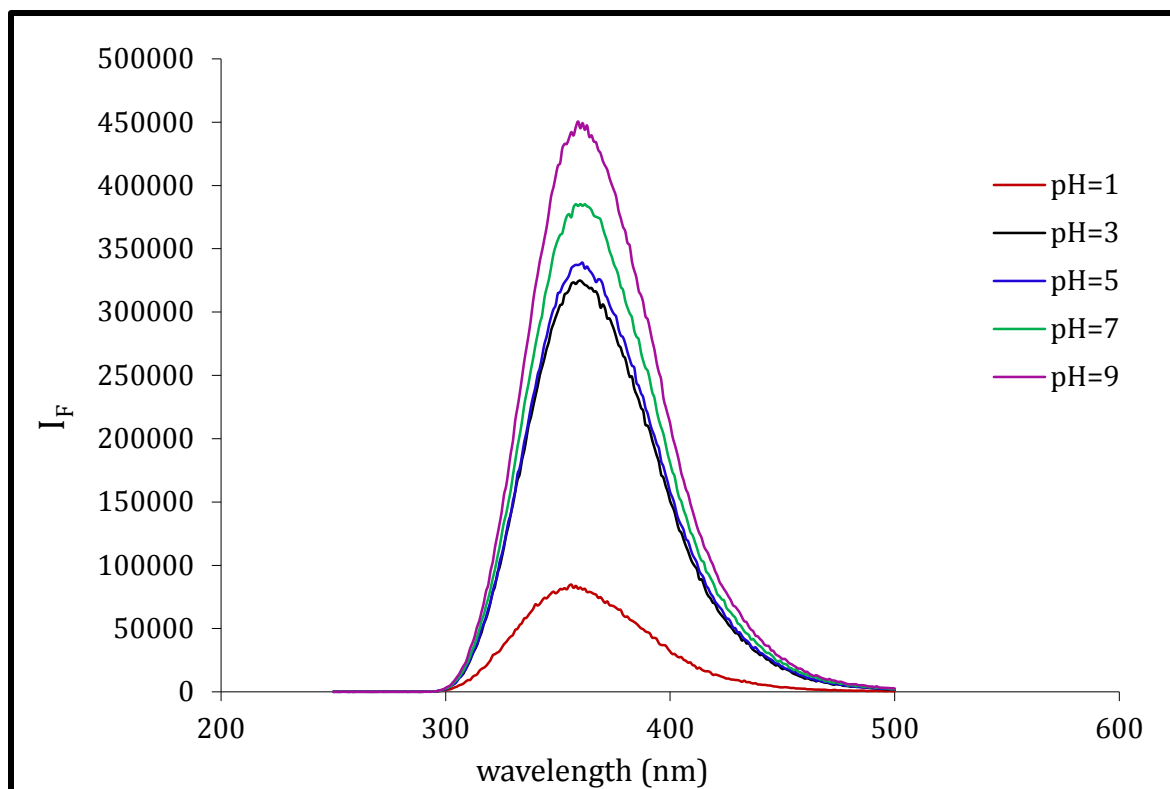


**Figure 3-36.** The fluorescence of TRP varied markedly with solution pH (1 mM aqueous solutions,  $\lambda_{ex}=257$  nm)

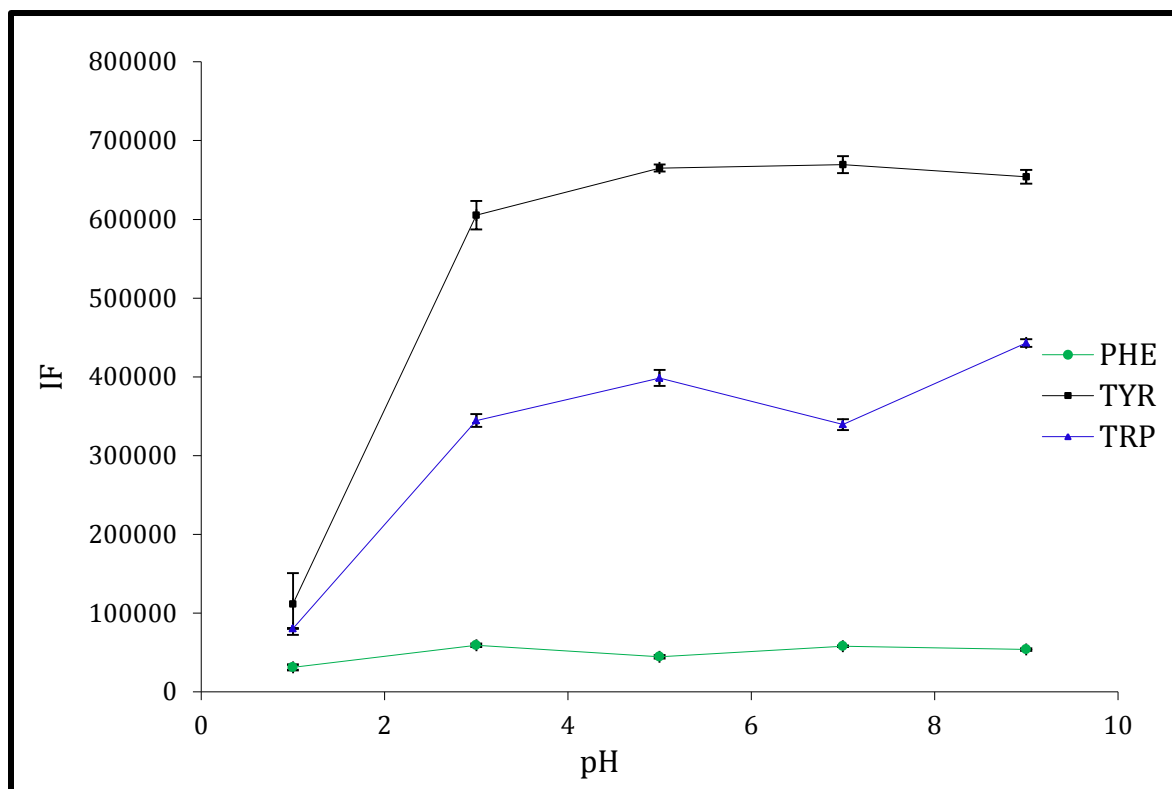


**Figure 3-37.** Relation between intensity of fluorescence and pH for 1mM solutions of PHE, TRP, and TYR. Error bars (n=3) are shown at 95% confidence (two-tailed) based upon the Student t value.

**Table X.** Mobile phases used in this study (% v/v).

Mobile Phase (#)	Methanol	Acetonitrile	Buffer Acetate pH=5.00 ( $\pm 0.01$ )	Buffer Phosphate pH=7.00 ( $\pm 0.01$ )
1		100%		
2	50%	50%		
3		20%	80%	
4		50%	50%	
5		80%	20%	
6	20%			80%
7		20%		80%
8		30%		70%
9		50%		50%
10		80%		20%
11	80%			20%

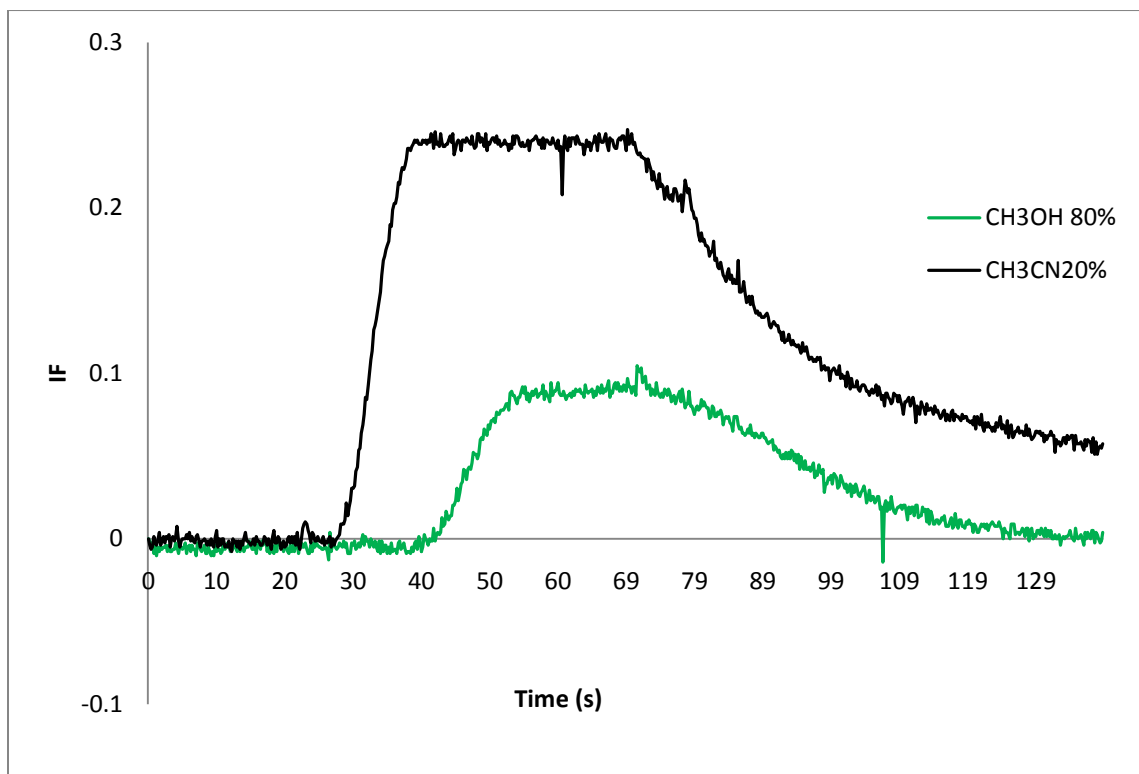


**Figure 3-38.** Comparison of the chromatograms obtained with amino acid mixtures in the Plackett-Burman study for two different mobile phases: 80:20 (v/v) methanol: buffer pH=4.00; and 20:80 (v/v) acetonitrile: buffer pH4.00. Injection loop = 35  $\mu$ L, flow rate = 1.0 mL/m

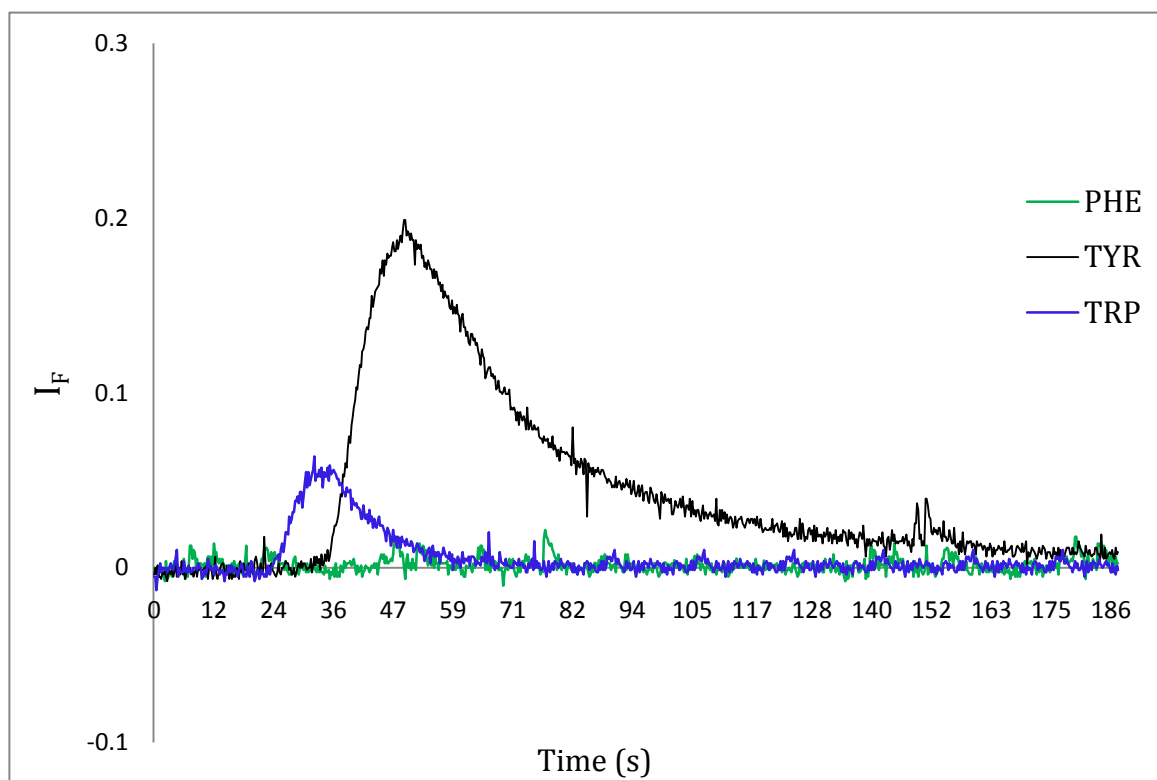


**Figure 3-39.** Comparison of the chromatograms obtained individually for PHE, TRP, and TYR (0.5 mM) with 30:70 (v/v) acetonitrile: phosphate buffer, pH=7.00. Injection loop = 35  $\mu$ L, flow rate = 1.0 mL/min.



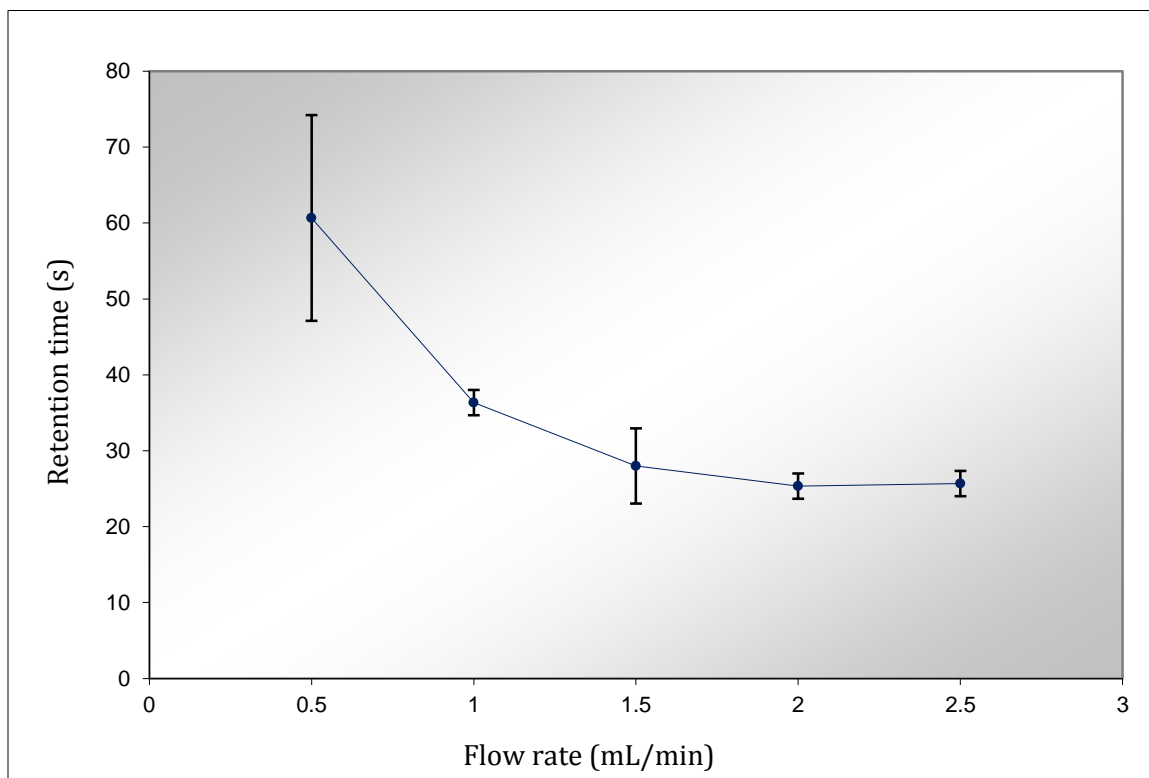


**Figure 3-40.** Effect of mobile phase flow rate on retention time. Error bars (n=3) are shown at 95% confidence (two-tailed) based upon the Student t value.

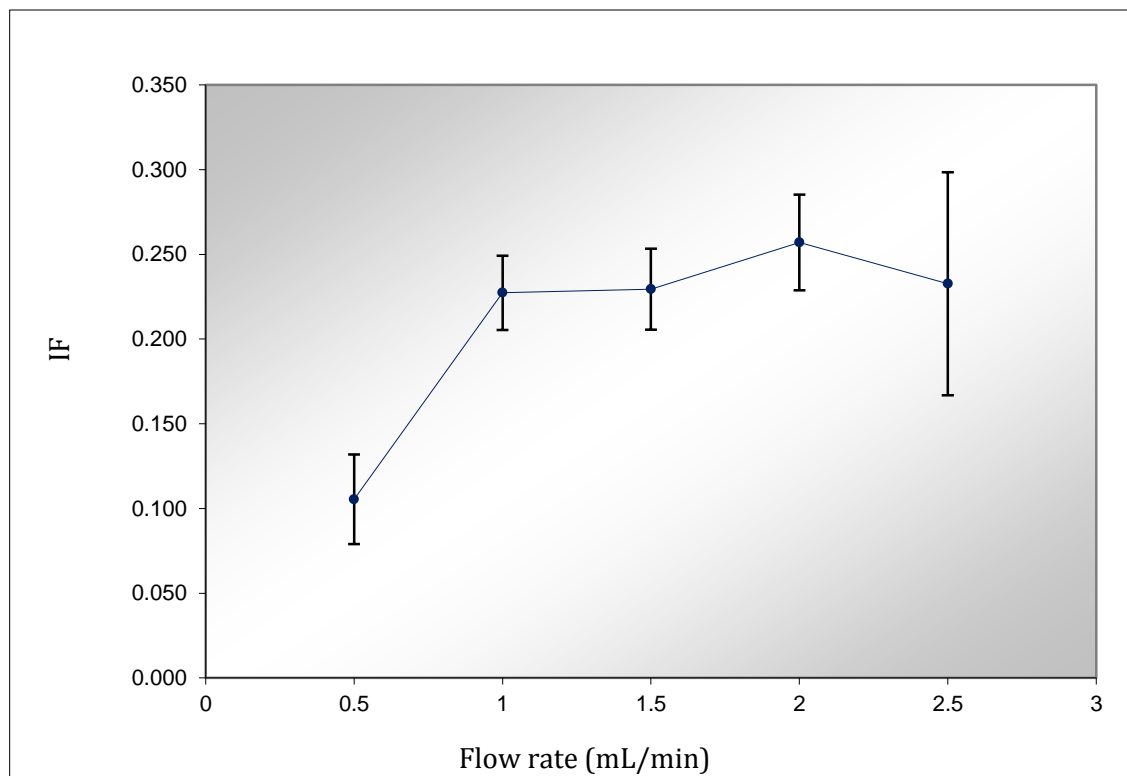


**Figure 3-41.** Effect of the mobile phase flow rate on fluorescence intensity of the solutes. . Error bars (n=3) are shown at 95% confidence (two-tailed) based upon the Student t value.

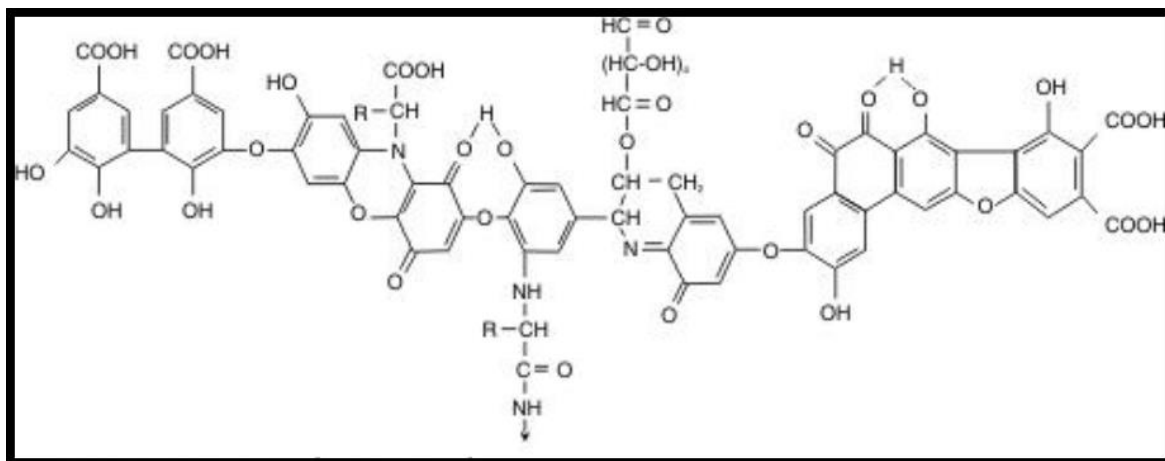
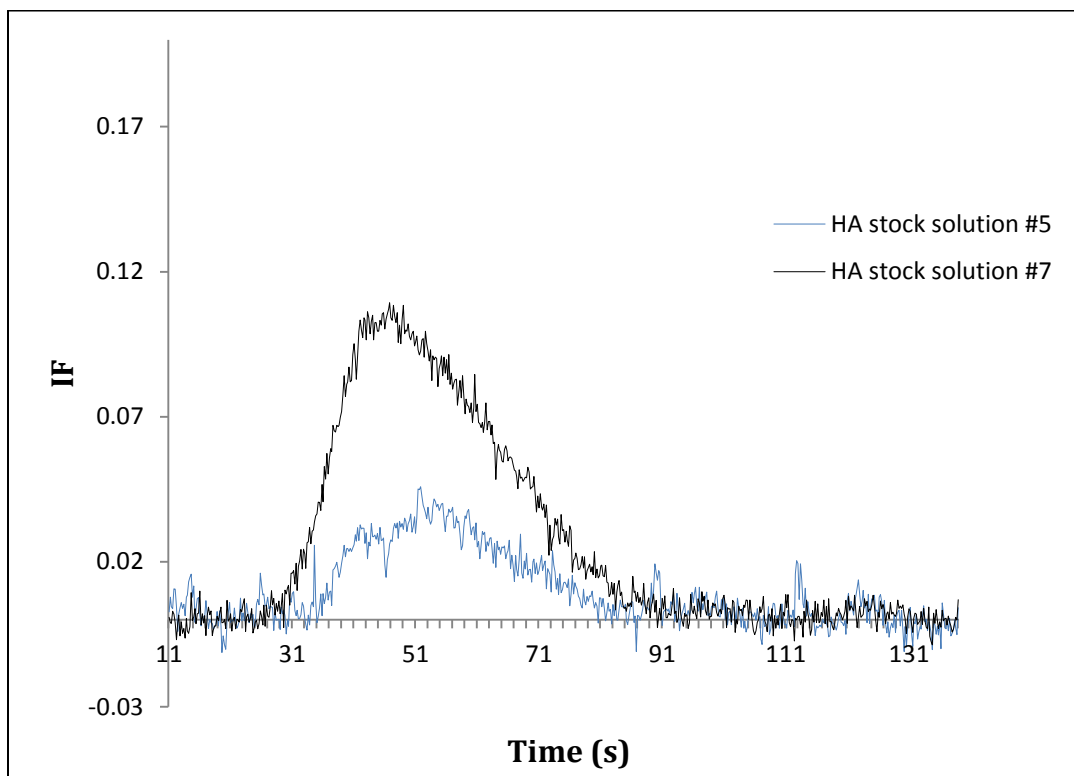


Figure 3-42. Hypothetical structure of a HA according to Stevenson.

**Table XI.** Humic acid stock solutions.

<b>Stock Solution</b>	<b>HA (mg/mL of solution)</b>	<b>Solvent</b>
<b>1</b>	1.6	Pentane
<b>2</b>	1.4	Hexane
<b>3</b>	1.3	Diethylether
<b>4</b>	1.7	Cyclohexane
<b>5</b>	1.3	Buffer pH=3.00
<b>6</b>	1.3	Buffer pH=5.00
<b>7</b>	1.3	Buffer pH=7.00
<b>8</b>	1.3	Buffer pH=9.00
<b>9</b>	1.3	Buffer pH=11.00



**Figure 3-43.** Chromatograms of humic solutions #5 and #7 (Table VIII).  $\lambda_{ex} = 350 \text{ nm}$ ,  $\lambda_{em} = 430 \text{ nm}$ ; 30:70 (v/v) acetonitrile: phosphate buffer pH = 7.00, mobile phase; 1.0 mL/min flow rate; 100  $\mu\text{L}$  injection loop.

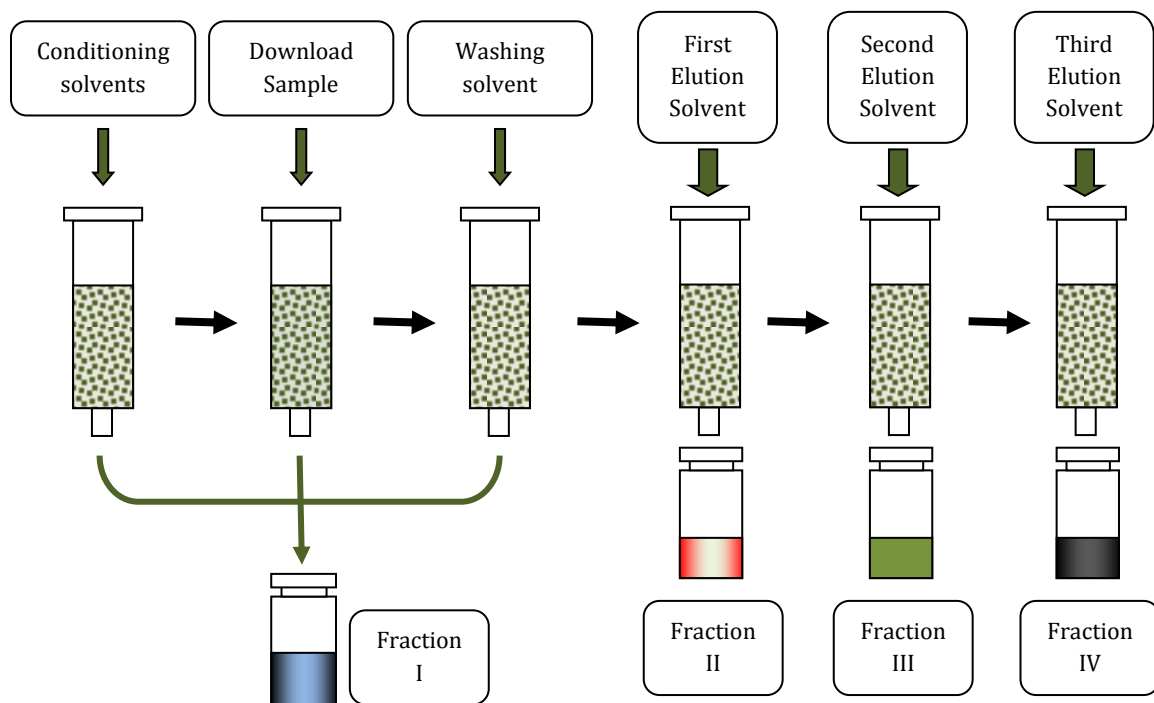


**Figure 3-44.** Scheme of the general procedure followed to obtain the HA fractions.

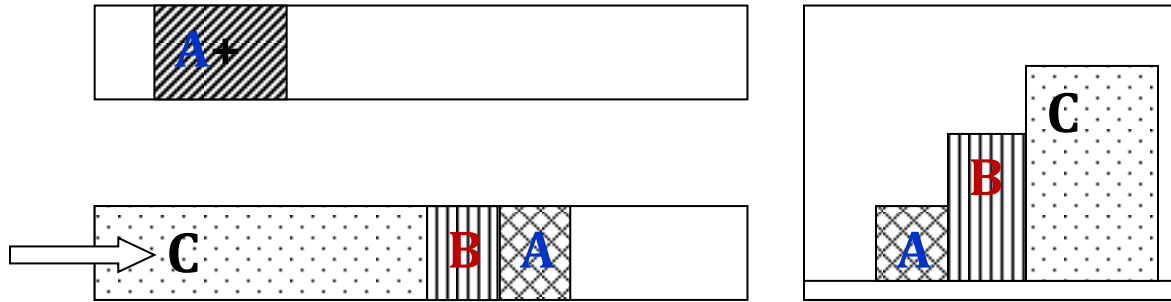


Figure 3-45. Scheme of a displacement development.<sup>81</sup>

**Table XII.** SPE phases used in the preparation of the HA samples.

<b>Retention Mechanism</b>	<b>#</b>	<b>Name</b>	<b>Size</b>
<b>Normal Phase</b>	1	LC-Si (Supelco, St. Louis, MO, USA)	20mL
	2	LC-NH <sub>2</sub> (Supelco, St. Louis, MO, USA)	3mL
<b>Reversed Phase</b>	3	ENVI-8 (Supelco, St. Louis, MO, USA)	3mL
	4	DSC-18 (Supelco, St. Louis, MO, USA)	3mL
	5	PoraPak™ RDX (Waters, Milford, MA, USA)	6mL
<b>Ion- Exchange</b>	6	LC-NH <sub>2</sub> (Supelco, St. Louis, MO, USA)	3mL
	7	LC-SCX (Supelco, St. Louis, MO, USA)	3mL
	8	LC-WCX (Supelco, St. Louis, MO, USA)	3mL



Normal Phase	<p style="text-align: center;">LC-NH<sub>2</sub></p>	<p style="text-align: center;">LC-Si</p>	
Reversed-Phase	<p style="text-align: center;">ENVI-8</p>	<p style="text-align: center;">DSC-18</p>	<p style="text-align: center;">Monomers</p> <p style="text-align: center;">Porapak- RDX : poly(divinylbenzene -vinylpyrrolidone) copolymer</p>
Ion-Exchange	<p style="text-align: center;">LC-WCX</p>	<p style="text-align: center;">LC-SCX</p>	

Figure 3-45. Matrix active groups present in the SPE columns.

**Table X.** HA samples; conditioning, washing and elution solvents used in the SPE clean-up.

<b>SPE columns.</b>	<b>HA samples.</b>	<b>Conditioning solvent. (in order of use)</b>	<b>Washing solvent.</b>	<b>Elution solvents. (in order of use)</b>
<b>LC-Si</b>				
	1-4	Solvent of the sample.	Solvent of the sample.	Ethyl acetate/ Dimethylformamide/ Methanol.
<b>LC-NH<sub>2</sub></b>				
<b>ENVI-8</b>				
<b>DSC-18</b>	5-9	Methanol/ H <sub>2</sub> O 18MΩ-cm/ Solvent of the sample.	Solvent of the sample.	Methanol/ Dimethylformamide/ Ethyl acetate
<b>PoraPak™ RDX</b>				
<b>LC-NH<sub>2</sub></b>				
<b>LC-SCX</b>	5-9	Methanol/ H <sub>2</sub> O 18MΩ-cm/ Solvent of the sample.	Solvent of the sample.	Buffer with pH> than the pH of the solvent of the sample.
<b>LC-WCX</b>				

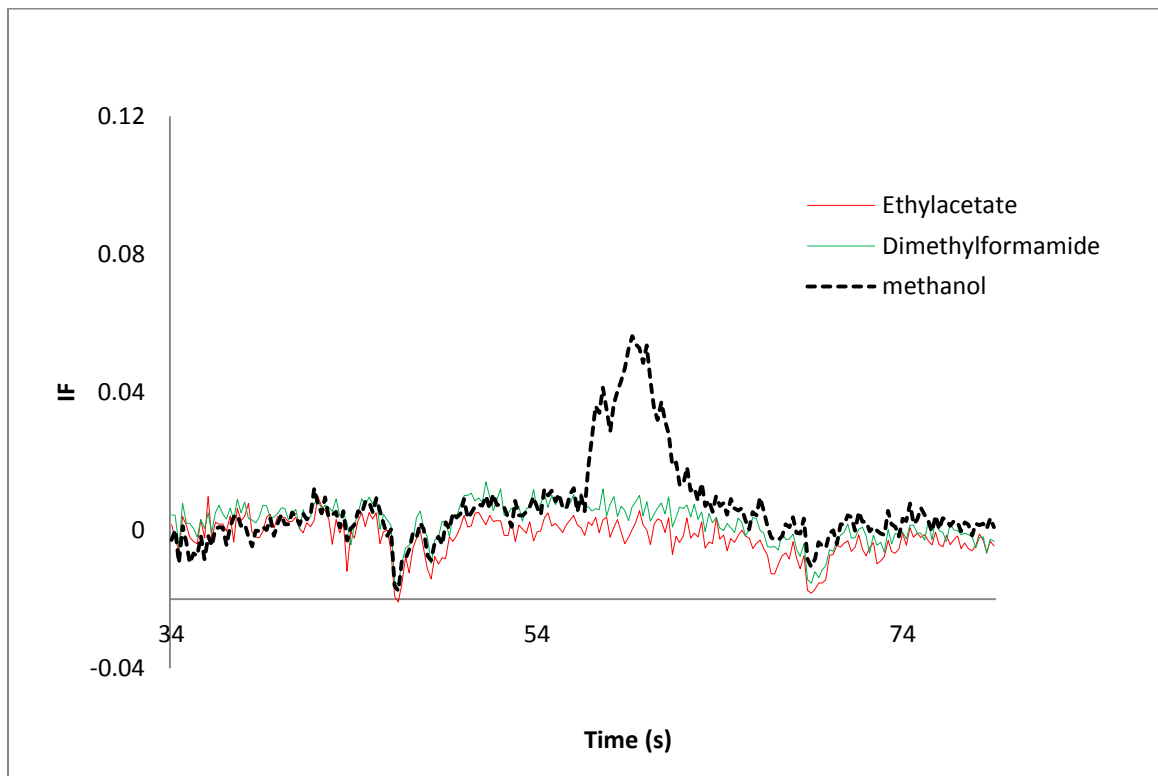


**Figure 3-46.** Chromatograms of humic acid fractions from LC-NH2. Fraction #1= ethylacetate, fraction #2= dimethylformamide, fraction #3 methanol.  $\lambda_{\text{ex}} = 350 \text{ nm}$ ,  $\lambda_{\text{em}} = 430 \text{ nm}$ ; acetonitrile and buffer phosphate pH=7.00 (1:2 v/v) mobile phase; 1.0 mL/min flow rate; 100  $\mu\text{L}$  injection loop.

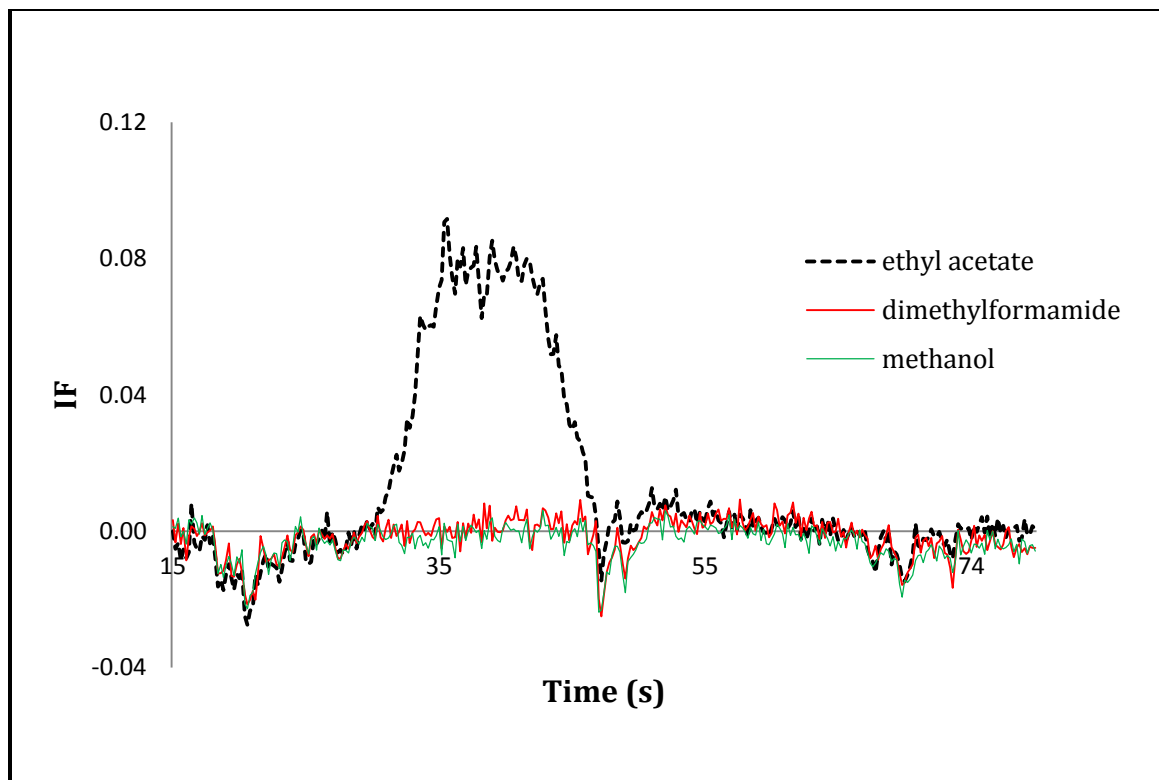


**Figure 3-47.** Chromatograms of humic acid fractions from ENVI-8. Fraction #1= methanol, fraction #2= dimethylformamide, fraction #3 ethylacetate.  $\lambda_{\text{ex}}=350$  nm,  $\lambda_{\text{em}}=430$  nm; acetonitrile and buffer phosphate pH=7.00 (1:2 v/v) mobile phase; 1.0 mL/min flow rate; 100  $\mu\text{L}$  injection loop.

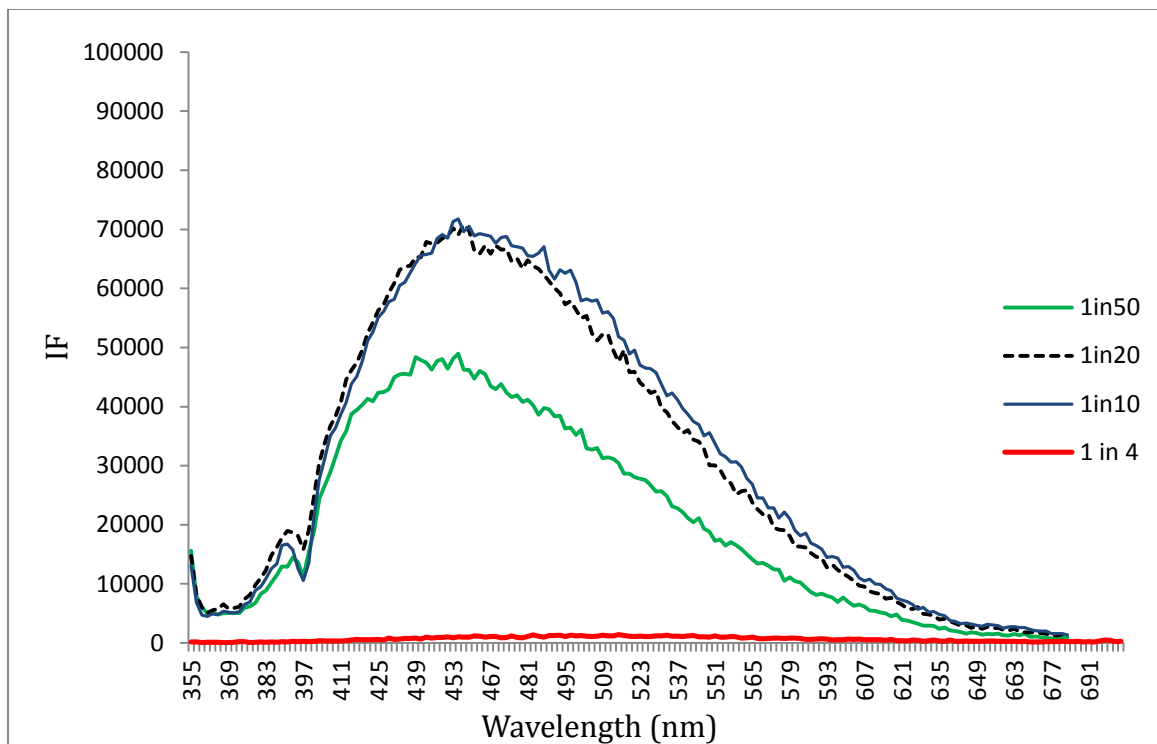


**Figure 3-48.** Spectrum of four humic acid dilutions from HA (1.3 mg/mL in acetonitrile and buffer phosphate pH=7 (30:70 v/v)).  $\lambda_{ex} = 350$  nm.

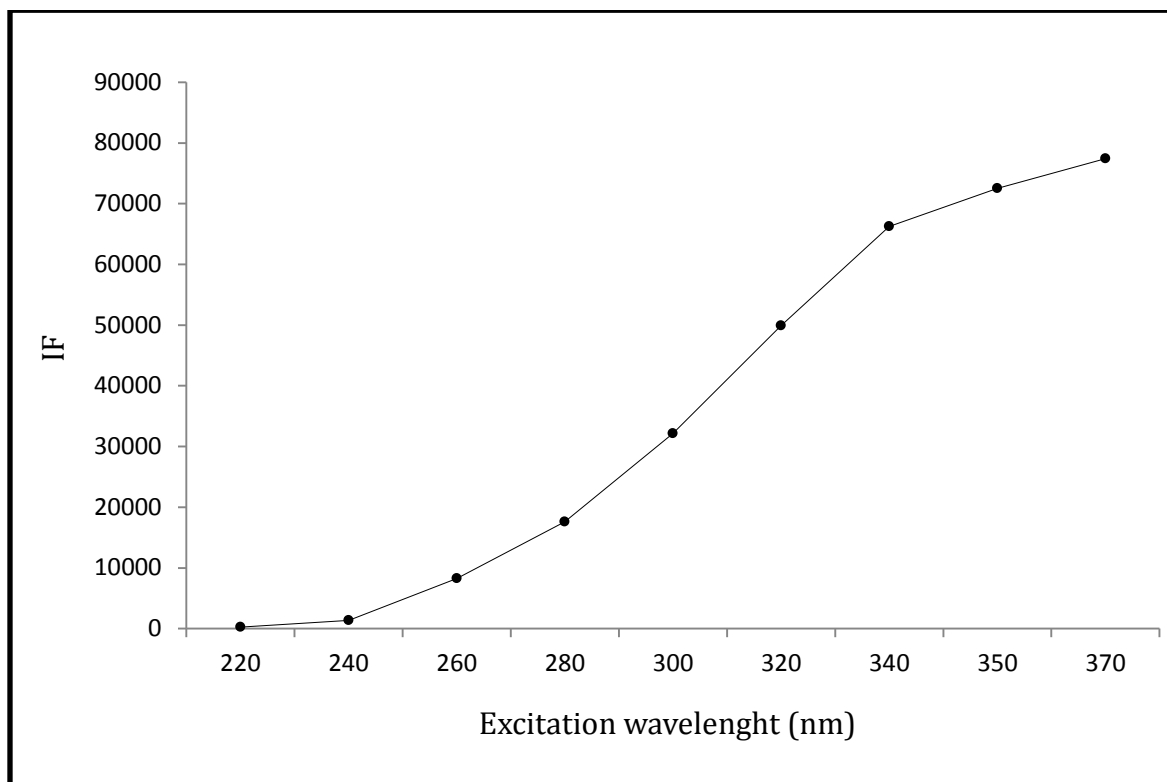


**Figure 3-49.** Variation of the fluorescence intensity with excitation wavelength for the HA solution of concentration 0.13 mg/mL.

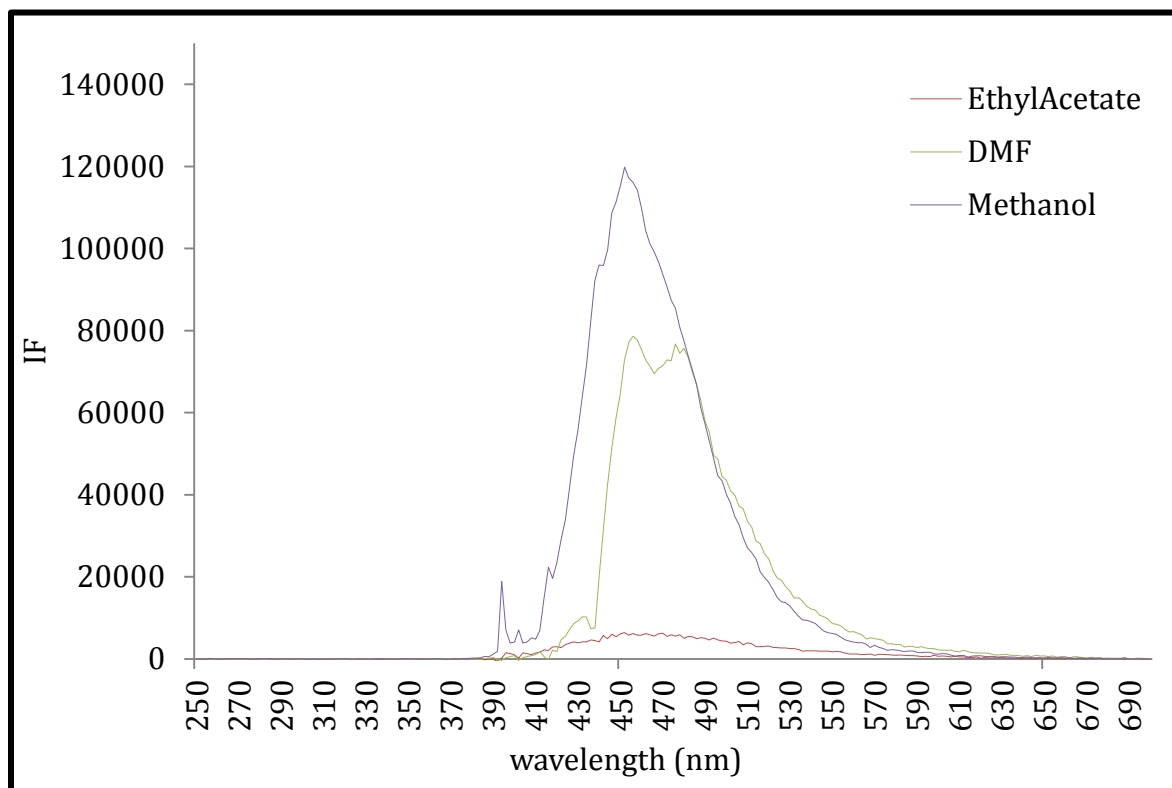
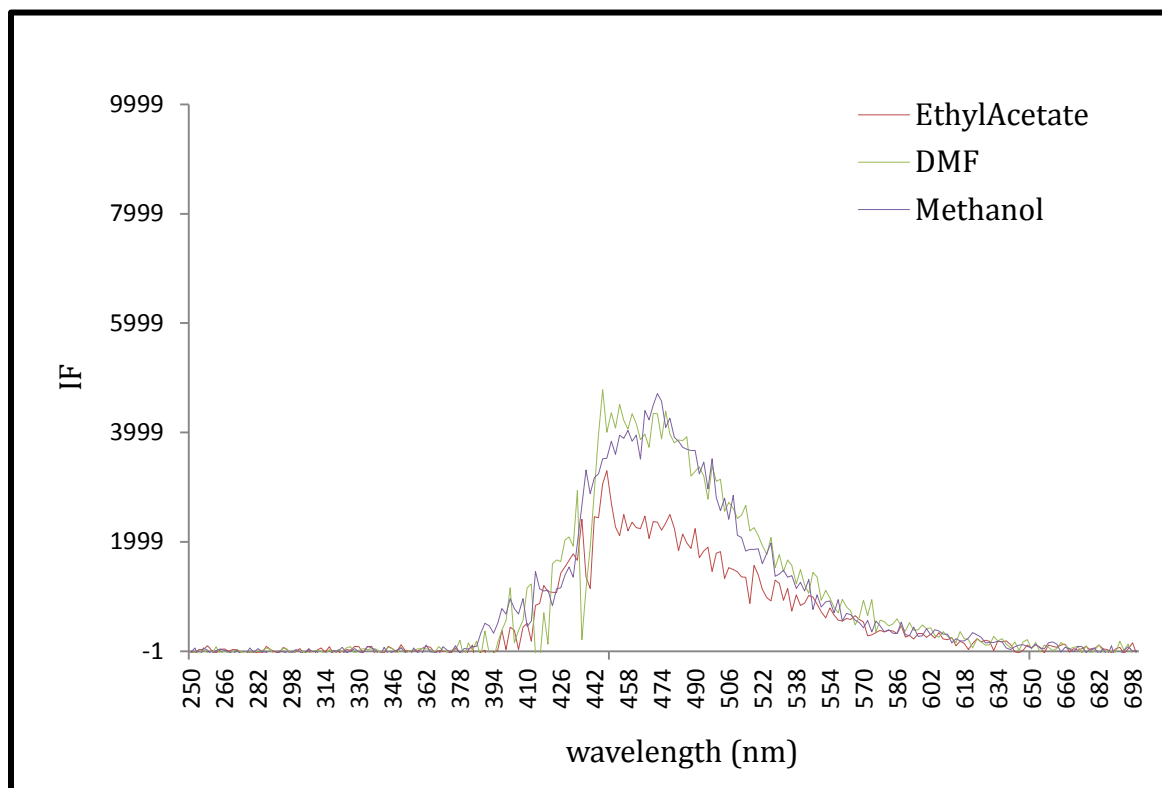


Figure 3-50. Spectrum of HA fractions #1, #2 and #3 from LC-Si (Normal phase, diethyl ether)



**Figure 3-51.** Spectrum of HA fractions #1, #2 and #3 from LC-NH2 (Normal phase, Diethyl ether).



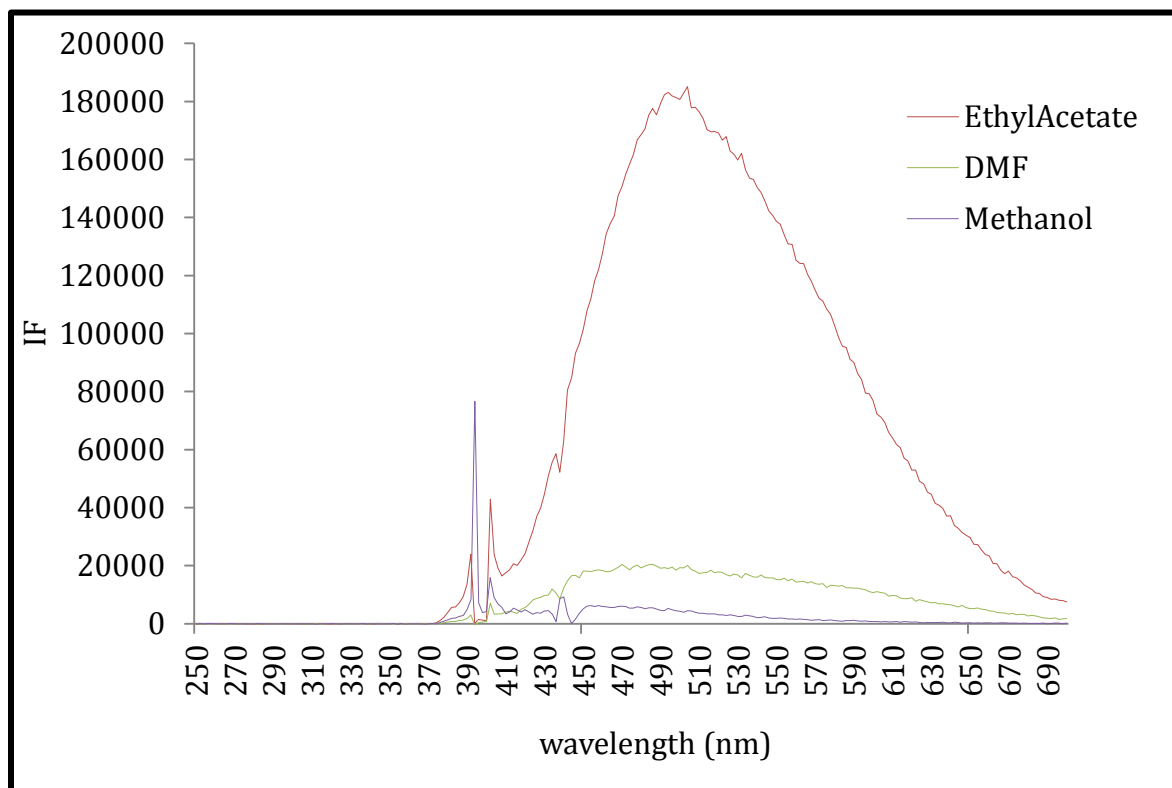


Figure 3-52. Spectrum of HA fractions #1, #2 and #3 from ENVI-8 (pH=9.0)

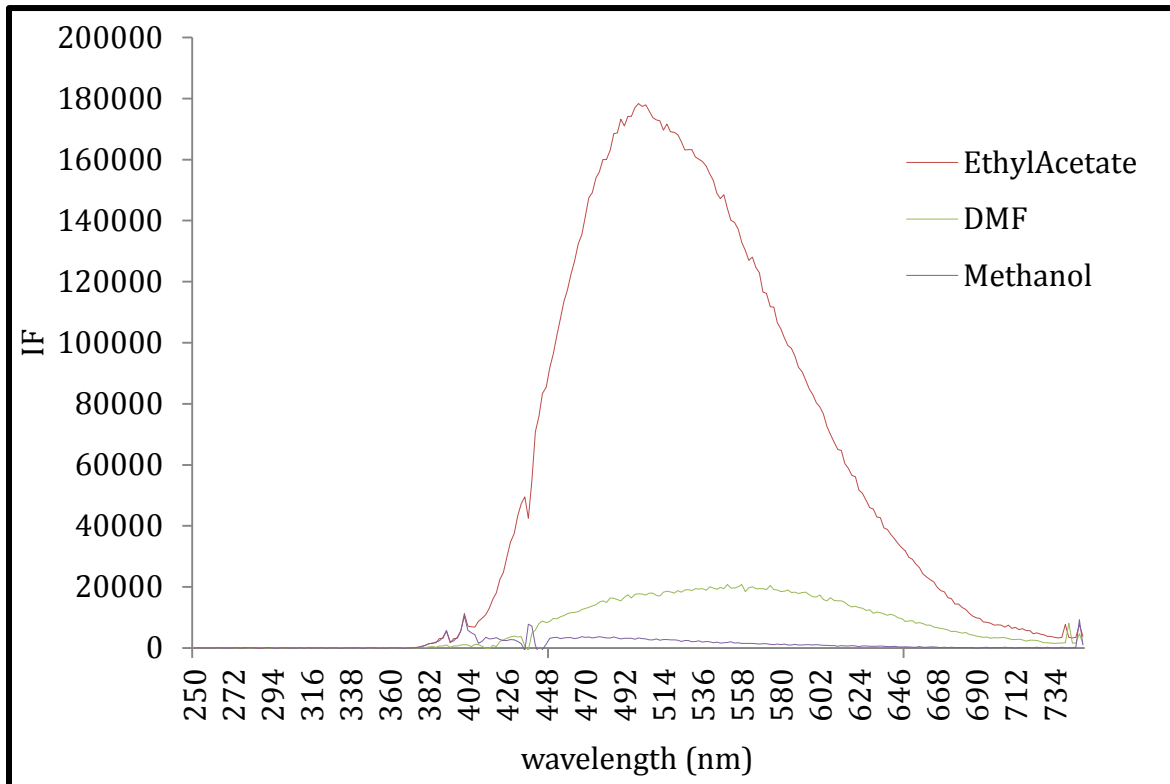
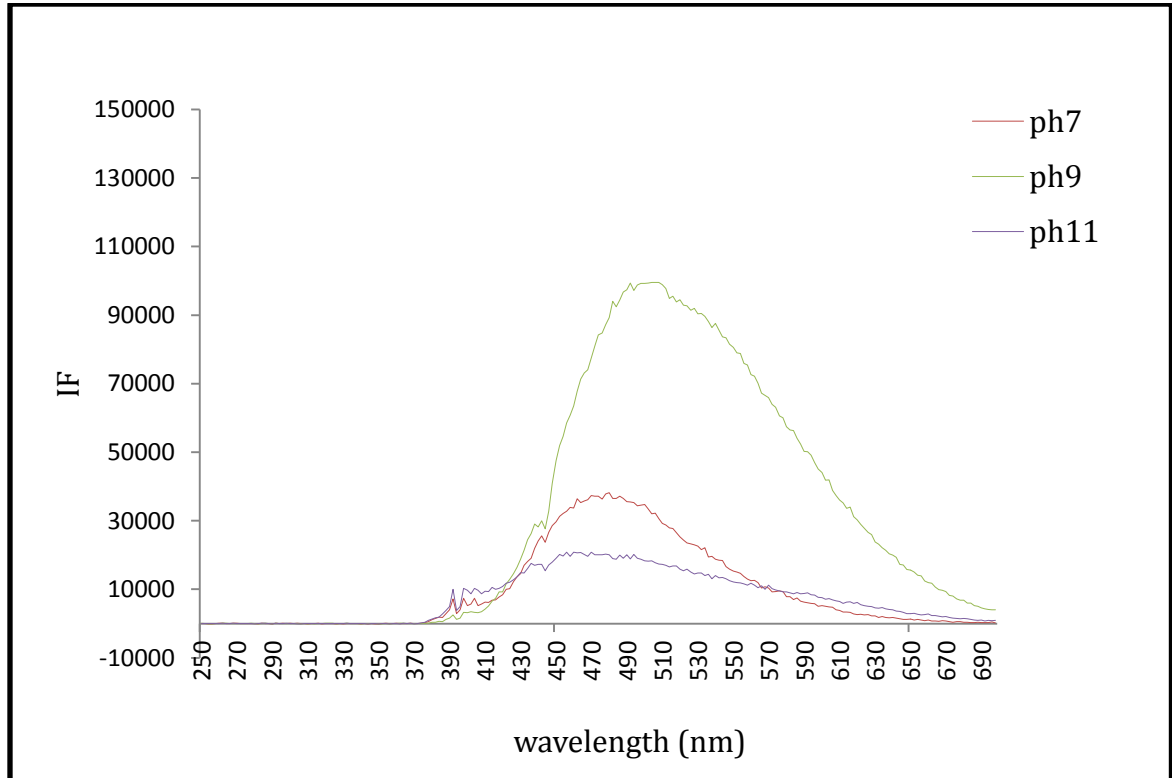


Figure 3-53. Spectrum of HA fractions #1, #2 and #3 from DSC-18 (pH=7.0)



**Figure 3-54.** Spectrum of HA fractions #1, #2 and #3 from LC-WCX (pH=7.0)

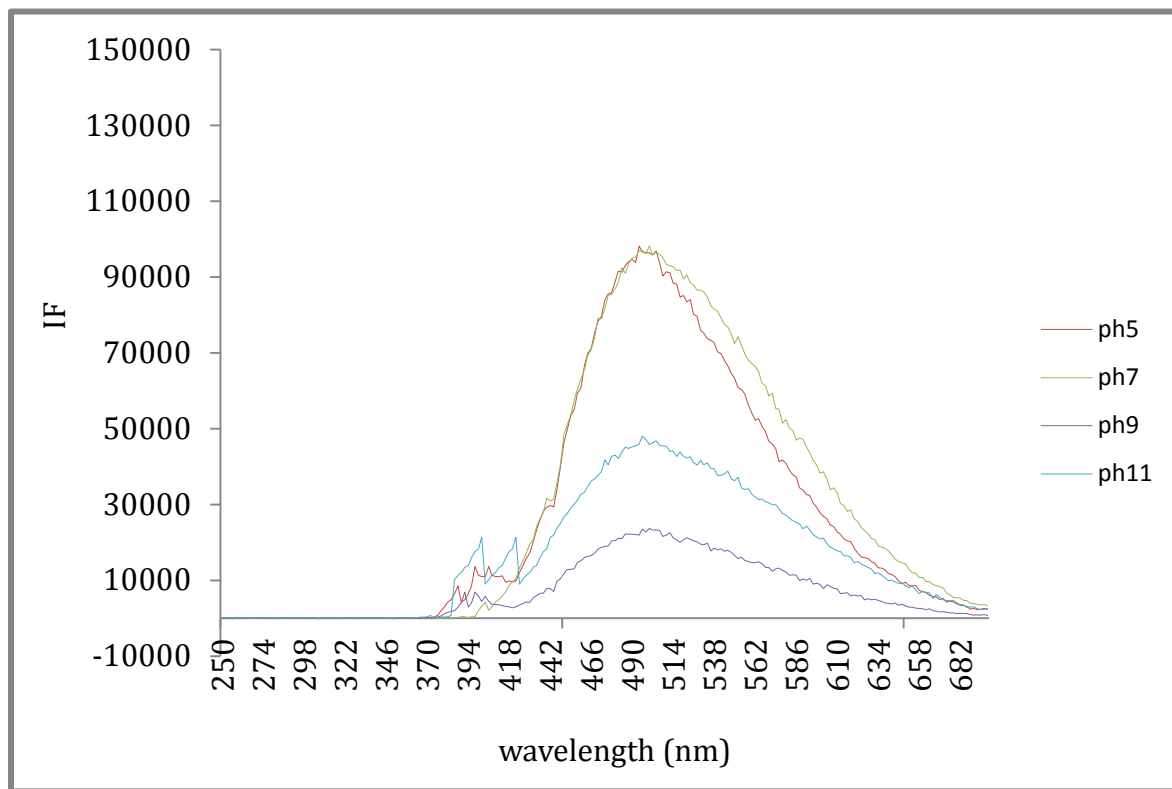
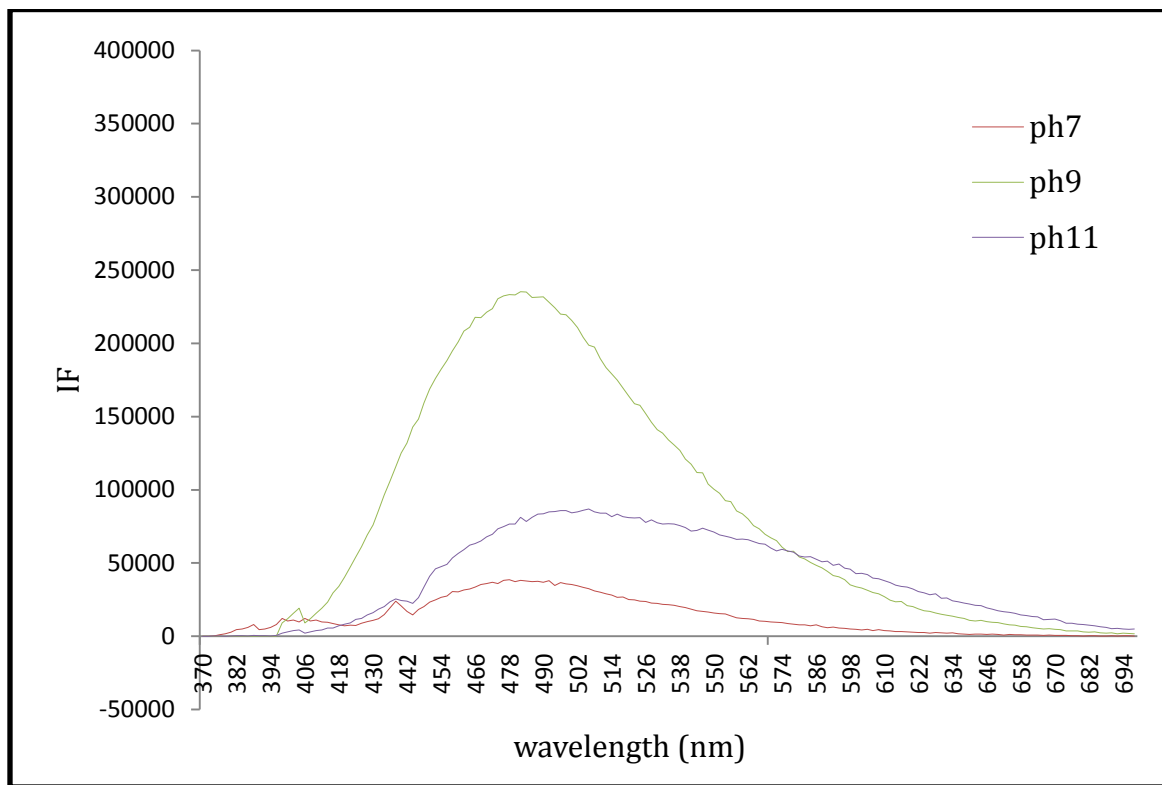


Figure 3-55. Spectrum of HA fractions #1, #2 and #3 from LC-SCX (pH=7.0)



**Figure 3-56.** Spectrum of HA fractions #1, #2 and #3 from LC-NH2 (II) (pH=7.0)

**Table XIV.** Maximum emission wavelength obtained experimentally in FluoroLog®-3 Spectrofluorometer

<b>SPE</b>	<b><math>\lambda_{em}</math> (maximum) (nm)</b>	<b><math>\lambda_{em}</math> (maximum) (nm) Corrected by calibration</b>
<b>LC-Si</b>	452	405
<b>LC-NH<sub>2</sub></b>	470	423
<b>ENVI-8</b>	504	457
<b>DSC-18</b>	500	453
<b>LC-NH<sub>2</sub> (II)</b>	486	439
<b>LC-SCX</b>	494	447
<b>LC-WCX</b>	490	443

### 3.4 References

1. Ferraro, J. R., *Introductory Raman Spectroscopy*. Elsevier Science: 2003.
2. McCreery, R. L., *Raman Spectroscopy for Chemical Analysis*. Wiley: 2005.
3. Skoog, D. A.; Holler, F. J.; Crouch, S. R., *Principles of Instrumental Analysis*. Thomson Brooks/Cole: 2007.
4. Vandenabeele, P.; Wehling, B.; Moens, L.; Edwards, H.; De Reu, M.; Van Hooydonk, G., Analysis with micro-Raman spectroscopy of natural organic binding media and varnishes used in art. *Anal. Chim. Acta* **2000**, *407* (1-2), 261-274.
5. Schoenemann, A.; Edwards, H. G. M., Raman and FTIR microspectroscopic study of the alteration of Chinese tung oil and related drying oils during ageing. *Anal. Bioanal. Chem.* **2011**, *400* (4), 1173-1180.
6. Marengo, E.; Liparota, M. C.; Robotti, E.; Bobba, M.; Gennaro, M. C., The state of conservation of painted surfaces in the presence of accelerated ageing processes monitored by use of FT-Raman spectroscopy and multivariate control charts. *Anal. Bioanal. Chem.* **2005**, *381* (4), 884-895.
7. Manzano, E.; Garcia-Atero, J.; Dominguez-Vidal, A.; Ayora-Canada, M. J.; Capitan-Vallvey, L. F.; Navas, N., Discrimination of aged mixtures of lipidic paint binders by Raman spectroscopy and chemometrics. *J. Raman Spectrosc.* **2012**, *43* (6), 781-786.
8. Lazzari, M.; Chiantore, O., Drying and oxidative degradation of linseed oil. *Polym. Degrad. Stab.* **1999**, *65* (2), 303-313.
9. Feller, R. L., *Accelerated aging: photochemical and thermal aspects*. Getty Conservation Institute: 1994.
10. Bonaduce, I.; Carlyle, L.; Colombini, M. P.; Duce, C.; Ferrari, C.; Ribechini, E.; Selleri, P.; Tine, M. R., New insights into the ageing of linseed oil paint binder: a qualitative and quantitative analytical study. *PLoS One* **2012**, *7* (11), e49333.
11. Burgio, L.; Clark, R. J. H., Library of FT-Raman spectra of pigments, minerals, pigment media and varnishes, and supplement to existing library of Raman spectra of pigments with visible excitation. *Spectrochim. Acta, Part A* **2001**, *57A* (7), 1491-1521.
12. Vandenabeele, P.; Edwards, H. G. M.; Moens, L., A Decade of Raman Spectroscopy in Art and Archaeology. *Chem. Rev. (Washington, DC, U. S.)* **2007**, *107* (3), 675-686.
13. Mallégol, J.; Gardette, J.-L.; Lemaire, J., Long-term behavior of oil-based varnishes and paints. Fate of hydroperoxides in drying oils. *Journal of the American Oil Chemists' Society (JAOCS)* **2000**, *77* (3), 249-255.
14. Megahed, M. G., Effect of microwave heating of linseed oil on the formation of primary and secondary oxidation products. *Agric. Biol. J. North Am.* **2011**, *2* (4), 673-679.
15. Leona, M. V. D., R.; Berrie, B.; Casadio, F.; Ernst, R. R.; Faber, K. T.; Sgamellotti, A.; Trentelman, K.; Whitmore, P., Chemistry and materials research at the interface between science and art, report of a workshop cosponsored by the National Science Foundation and the Andrew W. Mellon Foundation., **2009**.
16. Kendhammer, L., thesis Lisa. **2013**.

17. Thomas, A., Fats and Fatty Oils. In *Ullmann's Encyclopedia of Industrial Chemistry*, Wiley-VCH Verlag GmbH & Co. KGaA: 2000.
18. Poth, U., Drying Oils and Related Products. In *Ullmann's Encyclopedia of Industrial Chemistry*, Wiley-VCH Verlag GmbH & Co. KGaA: 2000.
19. O'Neill, L. A.; Rybicka, S. M.; Robey, T., Yellowing of drying oil films. *Chem. Ind. (London, U. K.)* **1962**, 1796-97.
20. Hess, P. S.; O'Hare, G. A., Oxidation of linseed oil. Temperature effects. *Ind. Eng. Chem.* **1950**, *42*, 1424-31.
21. Faulkner, R. N., The autoxidation of methyl elaeostearate. *Journal of Applied Chemistry* **1958**, *8* (7), 448-458.
22. Juita; Dlugogorski, B. Z.; Kennedy, E. M.; Mackie, J. C., Low temperature oxidation of linseed oil: a review. *Fire Sci. Rev.* **2012**, *1* (1), 3/1-3/36.
23. Juita; Dlugogorski, B. Z.; Kennedy, E. M.; Mackie, J. C., Oxidation reactions and spontaneous ignition of linseed oil. *Proc. Combust. Inst.* **2011**, *33* (Pt. 2), 2625-2632.
24. Haslbeck, F.; Grosch, W.; Firl, J., Formation of hydroperoxides with unconjugated diene systems during autoxidation and enzymic oxygenation of linoleic acid. *Biochim. Biophys. Acta, Lipids Lipid Metab.* **1983**, *750* (1), 185-93.
25. Haslbeck, F.; Grosch, W., Autoxidation of phenyl linoleate and phenyl oleate: HPLC analysis of the major and minor monohydroperoxides as phenyl hydroxystearates. *Lipids* **1983**, *18* (10), 706-13.
26. Sims, R. P. A., Possible mechanism in thermal polymerization of drying oils. I. Catalysis and inhibition studies. *J. Am. Oil Chem. Soc.* **1955**, *32*, 94-8.
27. Kumarathasan, R.; Rajkumar, A. B.; Hunter, N. R.; Gesser, H. D., Autoxidation and yellowing of methyl linolenate. *Progress in Lipid Research* **1992**, *31* (2), 109-126.
28. Chen, Z.; Hoggard, P. E., The effect of dissolved transition metal complexes on the rate of yellowing of linseed oil. *J. Am. Oil Chem. Soc.* **1999**, *76* (2), 277-280.
29. Juita; Dlugogorski, B. Z.; Kennedy, E. M.; Mackie, J. C., Identification and Quantitation of Volatile Organic Compounds from Oxidation of Linseed Oil. *Ind. Eng. Chem. Res.* **2012**, *51* (16), 5645-5652.
30. Juita; Dlugogorski, B. Z.; Kennedy, E. M.; Mackie, J. C., Mechanism of Formation of Volatile Organic Compounds from Oxidation of Linseed Oil. *Ind. Eng. Chem. Res.* **2012**, *51* (16), 5653-5661.
31. Nelson, D. L.; Cox, M. M., *Lehninger Principles of Biochemistry*. W. H. Freeman: 2012.
32. Montero, L.; Herrero, M.; Ibanez, E.; Cifuentes, A., Separation and characterization of phlorotannins from brown algae *Cystoseira abies-marina* by comprehensive two-dimensional liquid chromatography. *Electrophoresis* **2014**, *35* (11), 1644-1651.
33. Ahn, S.; Lee, H.; Lee, S.; Chang, T., Characterization of Branched Polymers by Comprehensive Two-Dimensional Liquid Chromatography with Triple Detection. *Macromolecules (Washington, DC, U. S.)* **2012**, *45* (8), 3550-3556.
34. Elsner, V.; Laun, S.; Melchior, D.; Koehler, M.; Schmitz, O. J., Analysis of fatty alcohol derivatives with comprehensive two-dimensional liquid chromatography coupled with mass spectrometry. *J. Chromatogr. A* **2012**, *1268*, 22-28.



35. Le Masle, A.; Angot, D.; Gouin, C.; D'Attoma, A.; Ponthus, J.; Quignard, A.; Heinisch, S., Development of on-line comprehensive two-dimensional liquid chromatography method for the separation of biomass compounds. *J. Chromatogr. A* **2014**, *1340*, 90-98.
36. Brudin, S. S.; Shellie, R. A.; Haddad, P. R.; Schoenmakers, P. J., Comprehensive two-dimensional liquid chromatography: Ion chromatography × reversed-phase liquid chromatography for separation of low-molar-mass organic acids. *J. Chromatogr. A* **2010**, *1217* (43), 6742-6746.
37. Bushey, M. M.; Jorgenson, J. W., Automated instrumentation for comprehensive two-dimensional high-performance liquid chromatography of proteins. *Anal. Chem.* **1990**, *62* (2), 161-7.
38. Cohen, S. A.; Schure, M. R.; Editors, *Multidimensional Liquid Chromatography; Theory and Application in Industrial Chemistry and the Life Sciences*. John Wiley & Sons, Inc.: 2008; p 456 pp.
39. Bedani, F.; Schoenmakers, P. J.; Janssen, H.-G., Theories to support method development in comprehensive two-dimensional liquid chromatography - A review. *J. Sep. Sci.* **2012**, *35* (14), 1697-1711.
40. Dugo, P.; Favoino, O.; Luppino, R.; Dugo, G.; Mondello, L., Comprehensive Two-Dimensional Normal-Phase (Adsorption)–Reversed-Phase Liquid Chromatography. *Analytical Chemistry* **2004**, *76* (9), 2525-2530.
41. Schoenmakers, P. J.; Vivo-Truyols, G.; Decrop, W. M., A protocol for designing comprehensive two-dimensional liquid chromatography separation systems. *Journal of chromatography. A* **2006**, *1120* (1-2), 282-90.
42. Murphy, R. E.; Schure, M. R.; Foley, J. P., Effect of Sampling Rate on Resolution in Comprehensive Two-Dimensional Liquid Chromatography. *Anal. Chem.* **1998**, *70* (8), 1585-1594.
43. Li, X.; Carr, P. W., Effects of first dimension eluent composition in two-dimensional liquid chromatography. *Journal of chromatography. A* **2011**, *1218* (16), 2214-21.
44. Jandera, P., Programmed elution in comprehensive two-dimensional liquid chromatography. *Journal of chromatography. A* **2012**, *1255*, 112-29.
45. Hooker, T. F.; Jeffery, D. J.; Jorgenson, J. W., Two-dimensional separations in high-performance capillary electrophoresis. *Chem. Anal. (N. Y.)* **1998**, *146* (High-Performance Capillary Electrophoresis), 581-612.
46. Ghabbour, E. A.; Davies, G.; Chemistry, R. S. o., *Humic Substances: Structures, Models and Functions*. Royal Society of Chemistry: 2001.
47. Stevenson, F. J., *Humus Chemistry: Genesis, Composition, Reactions*. Wiley: 1982.
48. Stevenson, F. J., *Humus Chemistry: Genesis, Composition, Reactions*. Wiley: 1994.
49. MacCarthy, P., The principles of humic substances: an introduction to the first principle. *Spec. Publ. - R. Soc. Chem.* **2001**, *273* (Humic Substances), 19-30.
50. Fanali, S.; Haddad, P. R.; Poole, C.; Schoenmakers, P.; Lloyd, D. K., *Liquid Chromatography: Fundamentals and Instrumentation*. Elsevier Science: 2013.

51. Tomaz, C. T.; Queiroz, J. A., Chapter 6 - Hydrophobic Interaction Chromatography. In *Liquid Chromatography*, Fanali, S.; Haddad, P. R.; Poole, C. F.; Schoenmakers, P.; Lloyd, D., Eds. Elsevier: Amsterdam, 2013; pp 121-141.
52. Unger, K. K.; Lamotte, S.; Machtejevas, E., Chapter 3 - Column Technology in Liquid Chromatography. In *Liquid Chromatography*, Fanali, S.; Haddad, P. R.; Poole, C. F.; Schoenmakers, P.; Lloyd, D., Eds. Elsevier: Amsterdam, 2013; pp 41-86.
53. Jinno, K., Retention behavior of large polycyclic aromatic hydrocarbons in reversed-phase liquid chromatography. *Adv. Chromatogr. (N. Y.)* **1989**, *30*, 123-65.
54. Jinno, K.; Tanigawa, E., Retention prediction of small peptides in reversed-phase liquid chromatography. *Chromatographia* **1988**, *25* (7), 613-617.
55. Svec, F., Porous polymer monoliths: Amazingly wide variety of techniques enabling their preparation. *Journal of Chromatography A* **2010**, *1217* (6), 902-924.
56. Svec, F., Quest for organic polymer-based monolithic columns affording enhanced efficiency in high performance liquid chromatography separations of small molecules in isocratic mode. *Journal of Chromatography A* **2012**, *1228* (0), 250-262.
57. Zhu, G.; Zhang, L.; Yuan, H.; Liang, Z.; Zhang, W.; Zhang, Y., Recent development of monolithic materials as matrices in microcolumn separation systems. *J. Sep. Sci.* **2007**, *30* (6), 792-803.
58. Guiochon, G., Monolithic columns in high-performance liquid chromatography. *Journal of Chromatography A* **2007**, *1168* (1-2), 101-168.
59. Lakowicz, J. R., *Principles of fluorescence spectroscopy*. Springer: New York ; Berlin.
60. Coble, P. G., Characterization of marine and terrestrial DOM in seawater using excitation-emission matrix spectroscopy. *Marine Chemistry* **1996**, *51* (4), 325-346.
61. Chen, H.; Zheng, B.-h.; Zhang, L., Linking fluorescence spectroscopy to diffuse soil source for dissolved humic substances in the Daning River, China. *Environ. Sci.: Processes Impacts* **2013**, *15* (2), 485-493.
62. Mopper, K.; Feng, Z.; Bentjen, S. B.; Chen, R. F., Effects of cross-flow filtration on the absorption and fluorescence properties of seawater. *Mar. Chem.* **1996**, *55* (1/2), 53-74.
63. Plackett, R. L.; Burman, J. P., The Design of Optimum Multifactorial Experiments. *Biometrika* **1946**, *33* (4), 305-325.
64. Stowe, R. A.; Mayer, R. P., Efficient screening of process variables. *Ind. Eng. Chem.* **1966**, *58* (2), 36-40.
65. Zhang, T.; Lu, J.; Ma, J.; Qiang, Z., Fluorescence spectroscopic characterization of DOM fractions isolated from a filtered river water after ozonation and catalytic ozonation. *Chemosphere* **2008**, *71* (5), 911-921.
66. Trubetskoj, O. A.; Richard, C.; Guyot, G.; Voyard, G.; Trubetskaya, O. E., Analysis of electrophoretic soil humic acids fractions by reversed-phase high performance liquid chromatography with on-line absorbance and fluorescence detection. *J. Chromatogr. A* **2012**, *1243*, 62-68.
67. Rodríguez, F. J.; Schlenger, P.; García-Valverde, M., A comprehensive structural evaluation of humic substances using several fluorescence techniques before and after ozonation. Part I: Structural characterization of humic substances. *Science of The Total Environment* **2014**, *476-477* (0), 718-730.

68. Mobed, J. J.; Hemmingsen, S. L.; Autry, J. L.; McGown, L. B., Fluorescence Characterization of IHSS Humic Substances: Total Luminescence Spectra with Absorbance Correction. *Environ. Sci. Technol.* **1996**, *30* (10), 3061-3065.
69. Kalbitz, K.; Geyer, S.; Geyer, W., A comparative characterization of dissolved organic matter by means of original aqueous samples and isolated humic substances. *Chemosphere* **2000**, *40* (12), 1305-1312.
70. Chen, J.; LeBoeuf, E. J.; Dai, S.; Gu, B., Fluorescence spectroscopic studies of natural organic matter fractions. *Chemosphere* **2003**, *50* (5), 639-647.
71. Trubetskaya, O.; Trubetskoj, O.; Richard, C., Hydrophobicity of electrophoretic fractions of different soil humic acids. *J. Soils Sediments* **2014**, *14* (2), 292-297.
72. Peuravuori, J.; Koivikko, R.; Pihlaja, K., Characterization, differentiation and classification of aquatic humic matter separated with different sorbents: synchronous scanning fluorescence spectroscopy. *Water Research* **2002**, *36* (18), 4552-4562.
73. Peuravuori, J.; Pihlaja, K., Molecular size distribution and spectroscopic properties of aquatic humic substances. *Anal. Chim. Acta* **1997**, *337* (2), 133-150.
74. Świetlik, J.; Sikorska, E., Application of fluorescence spectroscopy in the studies of natural organic matter fractions reactivity with chlorine dioxide and ozone. *Water Research* **2004**, *38* (17), 3791-3799.
75. Woelki, G.; Friedrich, S.; Hanschmann, G.; Salzer, R., HPLC fractionation and structural dynamics of humic acids. *Fresenius' J. Anal. Chem.* **1997**, *357* (5), 548-552.
76. Robards, K.; Haddad, P. R.; Jackson, P. E., *Principles and Practice of Modern Chromatographic Methods*. Academic Press: 1994.

## CHAPTER 4. CONCLUSIONS

The goal of this thesis was two-fold. First, to characterize the ageing of varnishes that are commonly used in Art Conservation by employing an ageing chamber and FT-Raman Spectroscopy. Second, to develop and optimize a RP-LC method as the second dimension of a LCxLC instrument that will be used to characterize HAs. We treated each of these in turn but they are not unrelated. The Raman method that was developed for studying the ageing of varnishes may also be applied off-line to individual fractions collected from the LCxLC system as a means to characterize them more fully. The power of FT-Raman for detailed molecular structure characterization as epitomized by the work that was done with the aged varnishes would provide another powerful tool to study the fractions obtained from the LCxLC system.

Thermal studies of the varnishes were initially conducted at several levels of temperature over a range of time periods. The temperatures ranged from 25°C to 210°C while the time periods ranged from 2 to 170 hr. The first question addressed was to verify by GC the integrity of the sample tubes that were used in the ageing chamber. We then observed that for pristine samples (*i.e.*, not subjected to ageing experiments), the same features as those found in the literature were obtained so the Raman shifts could be accurately identified for the aged varnishes. The correlation between the changes in band intensity, broadening, and distortion with the ageing process was demonstrated. The primary decomposition process that was observed in the ageing process was the loss of cis double bonds and the initiation of a polymerization process. This proposed mechanism was demonstrated by the observation of changes in specific vibrational bands (at 1265, 1298,

1444, 1657, 1737, 2856, 2910, 2914 and 3010  $\text{cm}^{-1}$ ) in the spectra. Thus one can conclude that the ageing process could be successfully studied using the methods developed in this thesis. One could also correlate the drastic variation in the color of the samples when they were exposed to heat or to UV light to support the proposed mechanism of varnish decomposition.

Future work involves studying additional factors in ageing experiments (*e.g.*, atmospheric gases such as nitrogen oxides, water vapor, sulfur oxides, etc.) and to extend the methodology to other varnishes that are commonly used in Art Conservation (*e.g.*, Dammar, Mastic, etc.) as well as to mixtures of varnishes as well as other additives that are used in artistic varnishes. Additionally, kinetic treatment of the reactions involved in the ageing process (*i.e.*, reaction orders, rate constants) could also be studied. Finally, the characterization of authentic aged varnishes from artistic objects is the ultimate goal of future studies.

In the second part of this study, a RP-LC method using a C4 monolithic disk was developed and optimized to characterize HAs. The instrument was designed, constructed, and then tested for mixtures of amino acids, a standard HA sample, and sub-fractions of the HA standard. Method factors that were optimized included injection volume, flow rate, mobile phase composition, and detector conditions. A Plackett-Burman experimental design was applied as part of the optimization process as an effective and efficient means to identify the most significant factors in the RP-LC method. The Plackett-Burman experiments were conducted by studying the separation of a model mixture of three amino acids. We found that pH, type of organic solvent, and percentage of organic solvent in the mobile phase were the most significant factors to control. We studied an HA standard solution

using the optimized RP-LC conditions and then fractionated the HA standard by SPE chromatography to isolate sub-samples to simplify further studies. The presence of HA's characteristic broad fluorescence signal was corroborated by the use of a high-resolution spectrofluorimeter. The differences between the maximum emission wavelengths obtained for the fractions lead us to conclude that the separation was successfully achieved.

Future work entails additional improvement of the RP-LC instrument and methodology. The development of a quality control regime based upon the model amino acid mixture would also be worthy of further study. Alternative detectors such as UV absorption and amperometry could be examined as well, the latter as a means to identify quinones in the samples. The next logical step would be to design an effective interface for integrating the RP-LC method into the LCxLC system. The application of the LCxLC system to other interesting complex mixtures of organic compounds, supported by FT Raman characterization, will be the subject of further inquiry.